Graduate School ETD Form 9
(Revised 01/14)

# PURDUE UNIVERSITY
## GRADUATE SCHOOL
## Thesis/Dissertation Acceptance

This is to certify that the thesis/dissertation prepared

By Jiayang Liu

Entitled
Electrochemical Behaviors of Micro-arc Oxidation Coated Magnesium Alloy

For the degree of Master of Science in Mechanical Engineering

Is approved by the final examining committee:

Jing Zhang

Jie Chen

Jiliang Li

Sungsoo Na

To the best of my knowledge and as understood by the student in the *Thesis/Dissertation Agreement. Publication Delay, and Certification/Disclaimer (Graduate School Form 32)*, this thesis/dissertation adheres to the provisions of Purdue University's "Policy on Integrity in Research" and the use of copyrighted material.

Approved by Major Professor(s): Jing Zhang

Approved by: Jie Chen 07/31/2014

Head of the Department Graduate Program Date

# ELECTROCHEMICAL BEHAVIORS OF MICRO-ARC OXIDATION COATED MAGNESIUM ALLOY

A Thesis

Submitted to the Faculty

of

Purdue University

by

Jiayang Liu

In Partial Fulfillment of the

Requirements for the Degree

of

Master of Science in Mechanical Engineering

August 2014

Purdue University

Indianapolis, Indiana

## ACKNOWLEDGMENTS

I would like to appreciate my graduate committee chair with my deepest gratitude, Dr. Jing Zhang, for his great guidance, caring, advice and supports. I really appreciate his concentration on my experiments and patience in reviewing and revising my thesis. I also would like to thank my committee members, Dr. Jie Chen, Dr. Jiliang Li and Dr. Sungsoo Na for serving on the committee and giving me abun- dant suggestions for my thesis work. Also I want to thank Dr. Jian Xie and Dr. Yadong Liu for electrochemical experiment assistance and providing the knowledge of corrosion science.

I acknowledge the IUPUI international development fund for the financial support in this study.

I would like to thank Dr. Yeon-Gil Jung at Changwon National University in Korea for the scanning electron micrographs and X-ray diffraction analyse. I would like to thank Dr. Tiean-Min Gabriel Chu and Dr. Ding Li for assistance in sample polishing. I also would like to thank Dr. Mangilal Agarwal for using the optical microscope.

I would like to appreciate Dr. Chengyun Ning at South China University of Technology in China and his students Yuanjun Guo and Wenming Xiong for supplying the coated magnesium samples for this research.

Thanks to my lab mates and friends, Xingye Guo, Yi Zhang, Linmin Wu, Dr. Qi Liu, and Lujie Ye, for their suggestion and help.

# TABLE OF CONTENTS

Page

# LIST OF TABLES

Table Page

Table Page

# LIST OF FIGURES

Figure Page

Figure Page

# ABSTRACT

Liu, Jiayang. M.S.M.E., Purdue University, August 2014. Electrochemical Behaviors of Micro-arc Oxidation Coated Magnesium Alloy. Major Professor: Jing Zhang, Department of Mechanical Engineering.

In recent years, magnesium alloys, due to their high strength and biocompatibility, have attracted significant interest in medical applications, such as cardiovascular stents, orthopedic implants, and devices. To overcome the high corrosion rate of magnesium alloys, coatings have been developed on the alloy surface. Most coating methods, such as anodic oxidation, polymer coating and chemical conversion coating, cannot produce satisfactory coating to be used in human body environment. Recent studies demonstrate that micro-arc oxidation (MAO) technique can produce hard, dense, wear-resistant and well-adherent oxide coatings for light metals such as aluminum, magnesium, and titanium. Though there are many previous studies, the understanding of processing conditions on coating performance remains elusive. Moreover, previous tests were done in simulated body fluid. No test has been done in a cell culture medium, which is much closer to human body environment than simulated body fluid.

In this study, the effect of MAO processing time (1 minute, 5 minutes, 15 minutes, and 20 minutes) on the electrochemical behaviors of the coating in both conventional simulated body fluid and a cell culture medium has been investigated. Additionally a new electrolyte (12 g/L $Na_2SiO_3$, 4 g/L NaF and 4 ml/L $C_3H_8O_3$) has been used in the MAO coating process.

Electrochemical behaviors were measured by performing potentiodynamic polarization and electrochemical impedance spectroscopy tests. In addition to the tests in simulated body fluid, the MAO-coated and uncoated samples were immersed in a cell

culture medium to investigate the corrosion behaviors and compare the difference in these two kinds of media.

The results show that in the immersion tests in conventional simulated body fluid, the 20-minute MAO coated sample has the best resistance to corrosion due to the largest coating thickness. In contrast, in the cell culture medium, all MAO coated samples demonstrate a similar high corrosion resistance behavior, independent of MAO processing time. This is probably due to the organic passive layers formed on the coating surfaces.

Additionally, a preliminary finite element model has been developed to simulate the immersion test of magnesium alloy in simulated body fluid. Comparison between the predicted corrosion current density and experimental data is discussed.

# 1. INTRODUCTION

## 1.1 Background

Metallic materials such as cobalt-based alloys, stainless steels and titanium alloys are suitable for use as replacing or repairing impaired load-bearing bone tissues, due to their excellent mechanical properties [1,2]. However, a limitation of these metallic biomaterials which hampers their usage is that toxic meal ions can release through the process of corrosion [3–7]. It can cause inflammation of bones tissue. Furthermore, the elastic moduli of currently used metallic biomaterials do not match the bone tissue of human being. That will lead to the reduction of stimulating new bone growth and remodeling, and decreas of the implants stability [8]. Another drawback for the currently used metallic biomaterials is their remaining as permanent fixtures, which means that they must be removed in another surgical operation after the damaged part heals [9]. Repeating operations heavily aggravate the patients burden and health costs.

In contrast, degradable implanting materials are designed to dissolve in the human body while or after the work pieces finish their tasks so that the second surgical procedure is unnecessary. It can reduce the risk of complications effectively, which commonly occur after a surgery. Furthermore, a degradation rate can be designed for degradable implants so that healing rate can be controlled according to the health requirements.

Magnesium and its alloys are promising and potential biodegradable and biocompatible metallic implants due to the following reasons. First of all, magnesium and its alloys have good biocompatibility, which means that in a bone system, the presence of Mg element can stimulate the growth of bone tissues [1]. Another advantage of Mg and its alloys is the non-toxicity, since $Mg^{2+}$ is an essential element for the human being. The redundant magnesium element can be excreted by urine. The third important ability of magnesium and its alloys is that the mechanical properties, such as density, compressive yield strength and elastic modulus are much closer to those of human natural bone than the other common metallic implants (Table 1.1) [1]. Magnesium is also an essential element for metabolism and exists in human bone tissue [10–12]. The biodegradation is also a key characteristic of magnesium and its alloys which allows the magnesium element to be biodegraded in body fluid through corrosion [13]. Other characteristics such as non-magnetic, available for roentgenoscopy and good machinability make the magnesium and its alloys become an ideal biocompatible and biodegradable material for implants. In summary, magnesium and its alloy have become more and more attractive in biomedical field due to their biocompatible and biodegradable characteristics. Therefore, magnesium and its alloys could replace existing materials for implanting, facilitate healing, and reduce the health costs.

Table 1.1. Summary of the mechanical properties of common implant materials and natural bone [1]

| Properties | Natural bone | Mg alloy | Co-Cr alloy | Ti alloy | Stainless steel |
|---|---|---|---|---|---|
| Density ($g/cm^3$) | 1.8-2.1 | 1.74-2.0 | 8.3-9.2 | 4.4-4.5 | 7.9-8.1 |
| Elastic Modulus (GPa) | 3-20 | 41-45 | 230 | 110-117 | 189-205 |
| Compressive yield strength (MPa) | 130-180 | 65-100 | 450-1000 | 758-117 | 170-310 |
| Fracture toughness ($MPa \times m^{1/2}$) | 3-6 | 15-40 | N/A | 55-115 | 50-200 |

## 1.2 Literature Review

### 1.2.1 Biodegradable and Biocompatible Magnesium Alloys

In the past few years, different types of magnesium alloys, including pure magnesium, have been studied as biomedical materials. Among those alloys, AZ91 and AZ31 are typical kinds of Mg-Al-Zn alloys used in medical applications. Magnesium alloys as biocompatible implants were introduced to trauma and orthopedic surgery in the first half of last century [14]. It was found that a large amount of hydrogen gas accumulated around the implants because the rapid corrosion happened on the surface, which caused researchers to stop using magnesium alloys as the biomaterials [15]. As new high-quality Mg alloys have been developed, magnesium alloys have again attracted attention in biomaterial field. Several biocompatible and biodegradable magnesium alloys have recently been investigated [16–19]. It has been found that some Mg alloys are not suitable to be biomaterials in medical applications because they contain rare earth elements and heavy metal elements, such as Zr and/or Cd, which are harmful to human body [20].

AZ31 magnesium alloy is considered as the most appropriate biocompatible material compared to other Mg alloys due to its low aluminum concentration. The AZ series of magnesium alloys, such as AZ31 magnesium alloy, which mainly contain aluminum, are favorable biomaterials due to their low aluminum content and good mechanical properties. It has been demonstrated that the content of aluminum not only can ameliorate the mechanical behavior of material, but also improve the corrosion resistance [21]. It has been showed that a high aluminum concentration, which is mainly formed as $Mg_{17}Al_{12}$ and precipitates at the grain boundaries, can increase the tendency for pitting corrosion [22]. Higher aluminum concentration is harmful for the osteoblasts and neurons [23]. Hence, it is very important to control the amount of aluminum released from magnesium alloys.

### 1.2.2 Approaches to Improve Corrosion Resistance

Magnesium is a very reactive element and has a very high corrosion rate when it is immersed in a physiological electrolyte [24]. This constraint restricts the application of the magnesium alloys from being used as suitable implants [25]. The most important aspect in reducing the corrosion rate of biodegradable magnesium alloys is to decrease hydrogen evolution and alkalization. The decrease implies that the human body can gradually consume the corrosion products with enough time [25].

The degradable and corrosive properties of magnesium and its alloys must be controlled in order to use this material in practical applications. Various approaches have been studied to develop magnesium alloys by adding alloying elements and applying protective coatings which could decrease corrosion rates. The materials should be non-toxic and biocompatible.

It is not easy to add alloying elements in magnesium due to its low solubility in many elements. Hence, providing an effective coating on magnesium alloys has become the most effective approach to enhance the corrosion resistance of Mg alloys. The coating should provide protection to the substrate by creating a barrier between the metal and conductive solution. Also the coating should be uniform and perfectly adhered. Several coating approaches have been studied recently to improve the ability to resist corrosion of magnesium alloys, such as polymer coating [26], anodic oxidation [27, 28], chemical conversion coating [29], and plasma iodization [30].

The micro-arc oxidation technique (MAO) is one of the most popular approaches due to its remarkable ability of improvement on corrosion resistance by producing a dense, thick, hard oxide coating on Mg alloys [31, 32]. Furthermore, the MAO technique can form a uniform film which can strongly adhere on the surfaces of the substrate with very complicated geometries [33, 34]. The MAO coating can also provide a high degree of hardness and sustain at high temperatures. To use this kind of coating approach and decrease the influence from pores, a proper selection of the MAO processing parameters, such as electrolytic solutions, MAO duration, pulse frequency, and applied voltage are required. Based on a literature review, it is generally believed that a compact MAO coating with fewer defects, stable composition and greater thickness would greatly provide an effective corrosion protection to the substrate of magnesium alloy. Therefore, understanding the MAO processing parameters is the key to improving the properties of magnesium alloys.

An ideal coated alloy sample can be implanted in human body with a controlled duration. Much research has been conducted to validate the corrosion properties of MAO coated AZ31 Mg alloys and other Mg alloys by immersing in simulated body fluid, as well as sodium chloride. Wang et al. tested the MAO-coated AZ31 Mg alloy immersed in an alkaline electrolyte [35]. The results show that the coating is porous, and includes MgO and $Mg_2SiO_4$ phases. Srinivansan also studied the phosphate-based coated AM50 magnesium alloy in NaCl solution [36]. The SBF contains closely equal amount of ions in human body fluid. However, there is no study of the effect of a cell culture medium in human body. The cell culture medium is much closer to the human body environment than simulated body fluid.

In this study, a new electrolyte (the composition of electrolyte for MAO process is 12 g/L $Na_2SiO_3$, 4 g/L NaF and 4 ml/L $C_3H_8O_3$) was used in fabricating the MAO coating. The corrosion behavior of coated samples in such electrolyte has not previously been studied.

Moreover, few previous studies, provide systematical understanding of the effect of coating processing conditions on the resultant alloy structures, and more importantly, their degradation behaviors in physiological environments. Using AZ31 magnesium alloy in simulated body fluid and cell culture medium as a model system, a specific goal of this project is to understand how to regulate the magnesium alloy degradation behaviors through engineering the coating processing conditions (e.g., processing time).Given the project objectives in mind, the specific tasks are described below.

(1) In order to investigate the influence of MAO coating processing time on the coatings, a uncoated sample, 1-minute, 5-minuts, 15-minute and 20-minute MAO

coating processing time samples will be tested by immersing in simulated body fluid and cell culture medium for 7 days.

(2)In order to understand the degradation behaviors of the MAO coatings, immersion tests in conventional simulated body fluid and cell culture medium will be conducted. Potentiodynamic polarization and electrochemical impedance spectroscopy will be used to measure the Nyquist and Tafel curves. To evaluate the quality of the coatings, The microstructure and surface morphology of the coatings will be examined using scanning electron microscope and optical microscope.

(3)A two-dimensional finite element model of uncoated AZ31 magnesium alloy in simulated body fluid will be constructed. Corrosion current density will be compared with the experimental results. The model can be used to study coating processing parameters effects on electrochemical properties.

## 1.3 Goals and Objectives of the Study

The long-term goal of the project is to develop a new generation of biocompatible magnesium alloy based implants with controlled degradation rate in physiological environments. In this study, the electrochemical behaviors of MAO coated AZ31 magnesium alloy in conventional simulated body fluid as well as in a cell culture medium will be examined to determine how MAO processing time influences coating corrosion resistance.

The objectives of the projects are as follows:

(1) Investigation of the effect of MAO processing time on the coating quality. For this purpose, four MAO processing durations (1, 5, 15, and 20 minutes) will be used to coat the AZ31 magnesium alloy samples. The electrochemical behaviors and microstructures of the coated sample and uncoated sample will be characterized.

(2) Comparative study between the conventional simulated body fluid and the cell culture medium as well as their effects on the MAO coated alloys.

(3) Development of a computational model to simulate the electrochemical process of magnesium alloy in simulated body fluid.

## 1.4 Thesis Outline

The thesis focuses on the electrochemical properties of micro-arc oxidation coated magnesium alloys in the conventional simulated body fluid and cell culture medium. In Chapter 2, the detailed characterizations of both uncoated and MAO coated AZ31 magnesium alloys are presented. The MAO process and the coating compositions are introduced. The coating surface and cross-section morphologies using scanning electron microscope (SEM) are also shown. Furthermore, the X-ray diffraction (XRD) results of the coated samples are provided.

In Chapter 3, the electrochemical experiment results of both the uncoated and MAO coated AZ31 magnesium alloys immersed in simulated body fluid are presented. The results of Tafel curves and Nyquist plots can reveal the corrosion rate and corrosion resistance of the tested samples. The potentiodynamic polarization and electrochemical impedance spectroscopy tests are conducted. Moreover, both microscopic and macroscopic images of sample morphologies through the immersion tests are provided. The porosities of the MAO coated samples are calculated.

In Chapter 4, the electrochemical tests are conducted in a cell culture medium. The potentiodynamic polarization and electrochemical impedance spectroscopy tests are conducted. The microscopic and macroscopic images of the samples are provided.

Chapter 5 presents a computational model to simulate the localized corrosion behaviors of uncoated sample immersed in simulated body fluid. The results are compared with the experiment. The model is capable to provide a reasonable analysis of the corrosion mechanisms, and can be used to develop a more advanced model.

Finally, in Chapter 6, the conclusion and future work are presented.

# 2. PREPARATION AND CHARACTERIZATIONS OF MAO COATING

## 2.1 Preparation for the MAO Coating

### 2.1.1 Principle of Micor-arc Oxidation Deposition Process

Micro-arc oxidation (MAO) is a new electrochemical surface coating treatment process that generates oxide coating layer on metals. The formation mechanism of oxide coating involves several electrochemical reactions [25]. Figure 2.1 [25, 37] shows the schematic of the plasma discharge during the MAO process. The substrate metals, such as aluminum, magnesium or titanium and their alloys, are placed into an electrolyte solution within a high pulsed electric field. Under the applied potential, the substrate metals react with the active oxygen ions in the electrolyte solution and produce a dense coating layer. Figure 2.2 shows the equipment used to produce MAO-coated AZ31 magnesium alloys in this work.

### 2.1.2 MAO Sample Preparation

AZ31 magnesium alloy is used in this research. Table 2.1 shows the chemical composition of this alloy. Samples used as the substrates have the dimensions of 20mm $\times$ 5mm $\times$ 0.4mm. Before being immersed in conductive solutions, all uncoated samples were polished on 2400 grit grade SiC papers. An ultrasonic wave cleaner was used to degrease the surfaces of samples, which were rinsed in deionized water for 20 minutes. Finally, all samples were dried in warm air for 2 minutes. The composition of electrolytes for the MAO process is 12 g/L $Na_2SiO_3$, 4 g/L NaF and 4 ml/L $C_3H_8O_3$.

The MAO coating was produced using MAO-20 equipment (Chengdu Pulsetech Electrical Co., China) by Prof. Chengyun Ning (South China University of Tech-

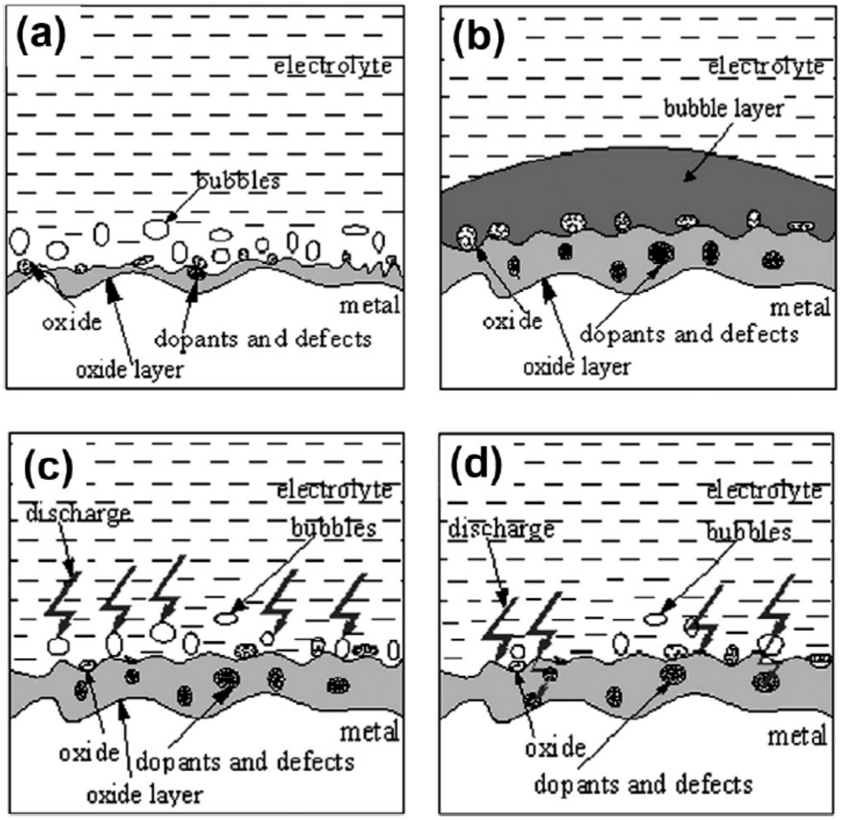


Figure 2.1. Schematic illustration of plasma discharge during different stages of MAO process (a) Conventional anodizing; (b) transition; (c) and (d) plasma discharge [25, 37]

Table 2.1. Chemical composition of AZ31 magnesium alloy

| Elements | Al | Zn | Mn | Si | Cu | Ni | Fe | Mg |
|---|---|---|---|---|---|---|---|---|
| Content (wt.%) | 2.5-3.5 | 0.7-1.3 | 0.2 (Min) | 0.05 | 0.01 | 0.005 (Max) | 0.005 (Max) | Remaining |

nology) and his students Yuanjun Guo and Wenming Xiong. The MAO process parameters of the two samples tested in this study are listed in Table 2.2.


Figure 2.2. The equipment to produce MAO-coated AZ31 magnesium alloys(credit: Prof. Chengyun Ning at South China University of Technology)

## 2.2 Characterizations of the MAO Coatings

### 2.2.1 Coating Morphology

The surface and cross-sectional views of the MAO coatings processed at various processing times were examined by using a scanning electron microscopy. The surface morphologies of the MAO coatings produced at 1-minute, 5-minute, 15-minute and 20-minute MAO processing times are shown in Figure 2.3 - 2.6. Typical porous microstructures were showed on all the coatings. The cracks and pores served as the micro-arc discharging channels during the MAO process. According to the surface morphologies, the surface microstructures of all MAO coated samples were not affected by the coating processing time. While the porosity of all samples cannot be

Table 2.2. MAO process parameters of the four MAO samples

| | Oxidation time (min) | Applied voltage (V) | Pulse frequency (Hz) | Electrolyte concentration (g/L) |
|---|---|---|---|---|
| 1-min MAO processing time | 1 | 350 | 500 | 30 |
| 5-min MAO processing time | 5 | 350 | 500 | 30 |
| 15-min MAO processing time | 15 | 350 | 500 | 30 |
| 20-min MAO processing time | 20 | 350 | 500 | 30 |

determined directly from the SEM images, the calculation of porosity is presented in Chapter 3.

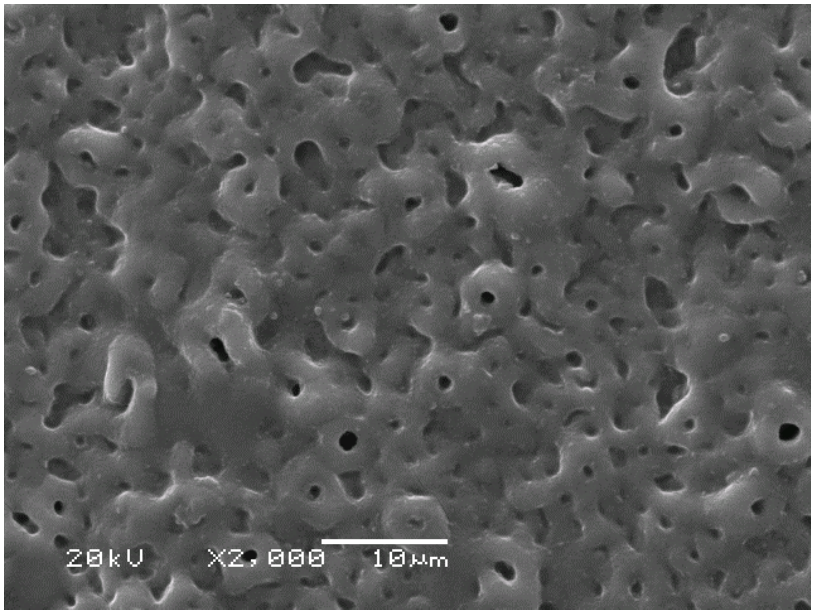


Figure 2.3. Surface morphology of MAO coatings produced at 1 minute

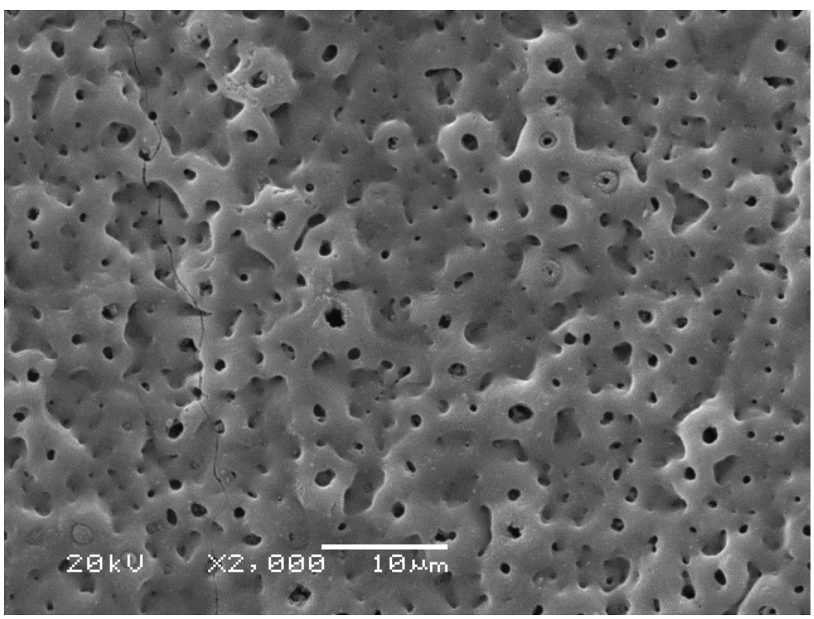


Figure 2.4. Surface morphology of MAO coatings produced at 5 minutes

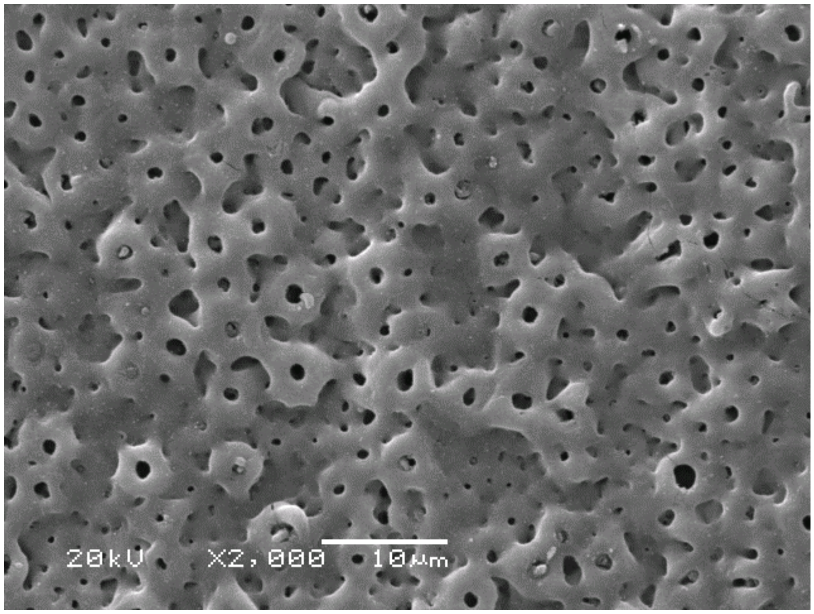


Figure 2.5. Surface morphology of MAO coatings produced at 15 minutes

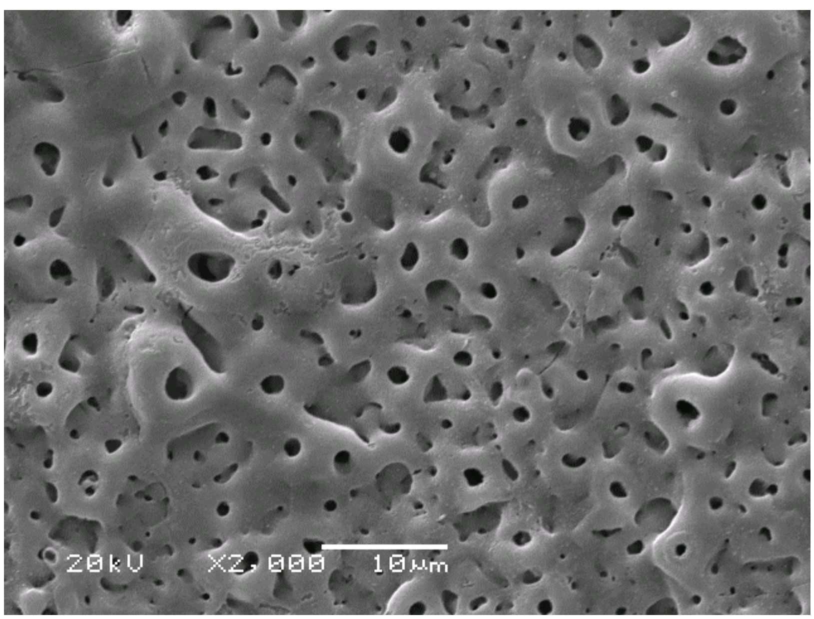


Figure 2.6. Surface morphology of MAO coatings produced at 20 minutes

The cross-sectional morphologies of the MAO coatings produced at different oxidation times are illustrated from Figure 2.7 to Figure 2.10. The thicknesses of all MAO coating layers are listed in Table 2.3. It was found that the thickness increases with increasing oxidation time. The 20-minute MAO coated sample has the thickest coating layer, and 1-minute one has the thinnest coating. Moreover, it shows that the deviation also increases with the MAO processing time, which means the less time MAO is processed, the better uniformity of thecoating.

Table 2.3. Thickness of MAO coating layer

| | 1-min MAO | 5-min MAO | 15-min MAO | 20-min MAO |
|---|---|---|---|---|
| Thickness ($\mu$m) | 3.11 ± 0.43 | 3.19 ± 0.61 | 3.93 ± 0.75 | 4.00 ± 0.99 |

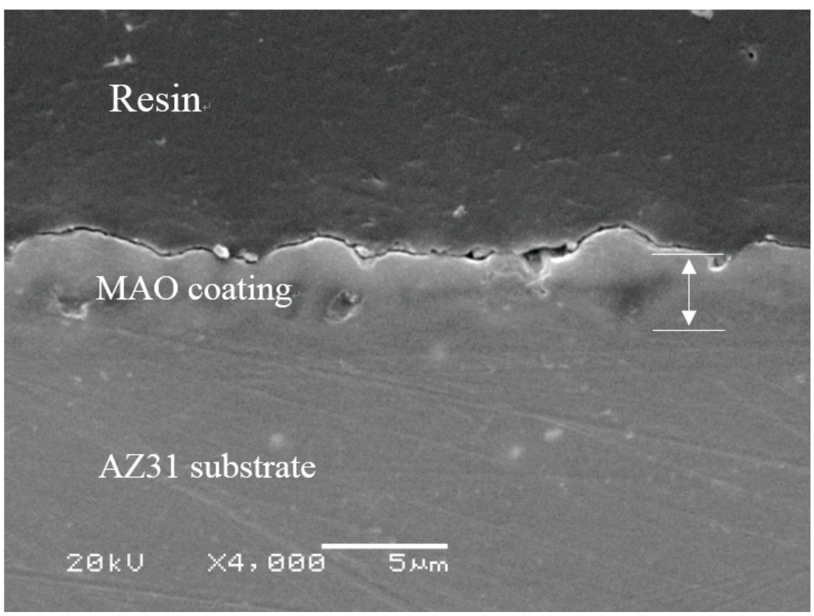


Figure 2.7. Cross-sectional morphology of MAO coatings produced at 1 minute

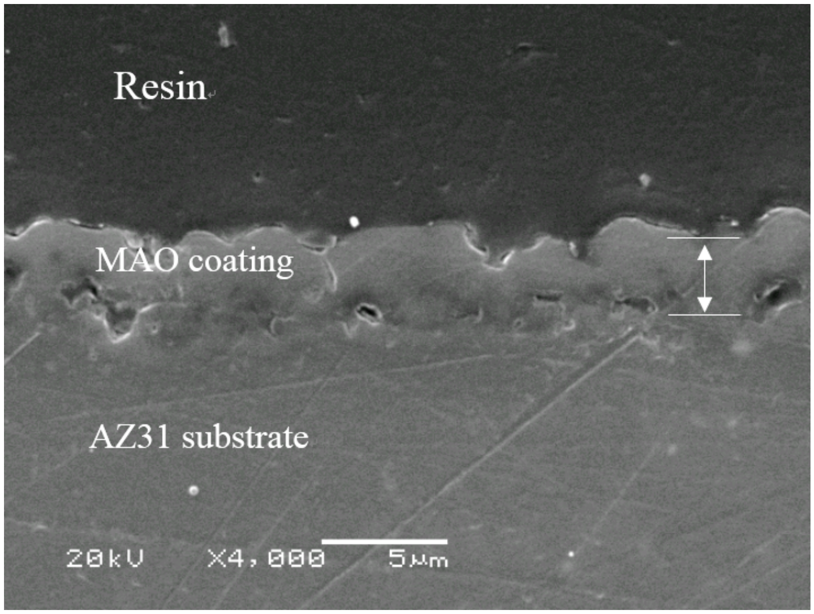


Figure 2.8. Cross-sectional morphology of MAO coatings produced at 5 minutes

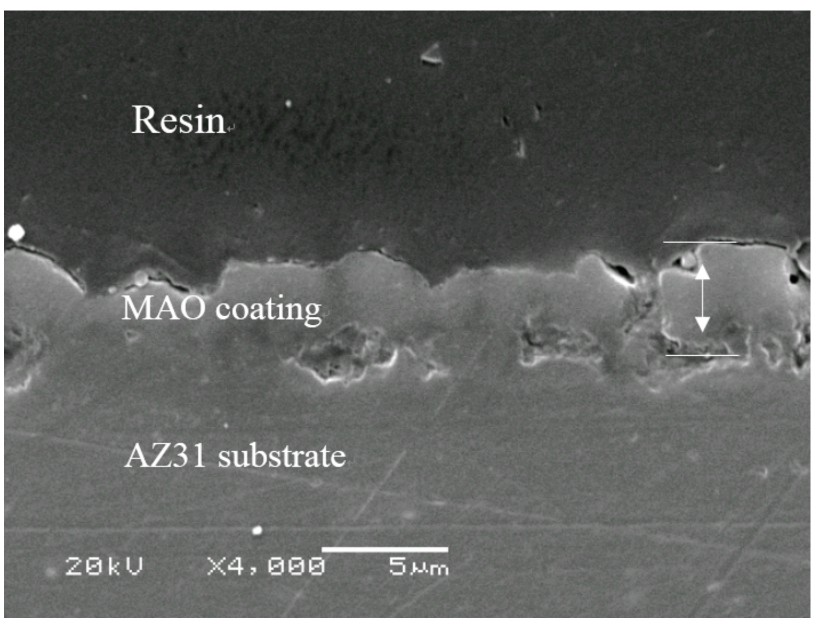


Figure 2.9. Cross-sectional morphology of MAO coatings produced at 15 minutes

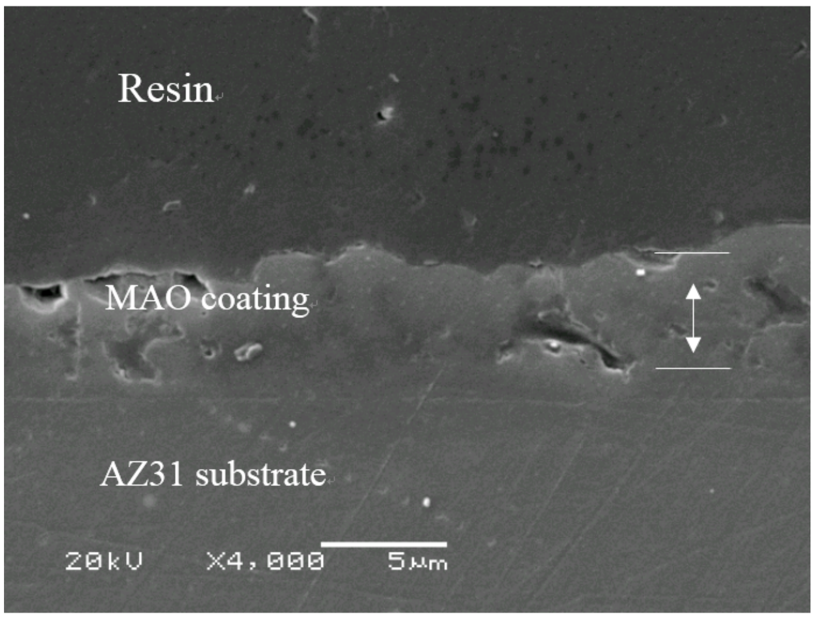


Figure 2.10. Cross-sectional morphology of MAO coatings produced at 20 minutes

### 2.2.2 Coating Composition Analysis

To determine the content in the coating, energy-dispersive X-ray spectroscopy (EDS) analysis was used to examine the surface of samples coated at different oxidation times. The results are listed in Table 2.4, and the EDS spectrum is presented from Figure 2.11 to Figure 2.14. According to the results, the concentrations do not change significantly with the MAO processing time.

Table 2.4. Elemental concentrations of MAO coating on surface (wt.%)

| Element | 1 min-MAO | 5 min-MAO | 15 min-MAO | 20 min-MAO |
|---|---|---|---|---|
| F | 11.23 | 17.64 | 10.25 | 18.86 |
| Na | 0.36 | 1.03 | 0.82 | 0.89 |
| Mg | 35.05 | 34.72 | 35.07 | 34.64 |
| Si | 13.70 | 10.34 | 14.26 | 10.52 |
| O | 33.00 | 35.67 | 39.61 | 35.09 |

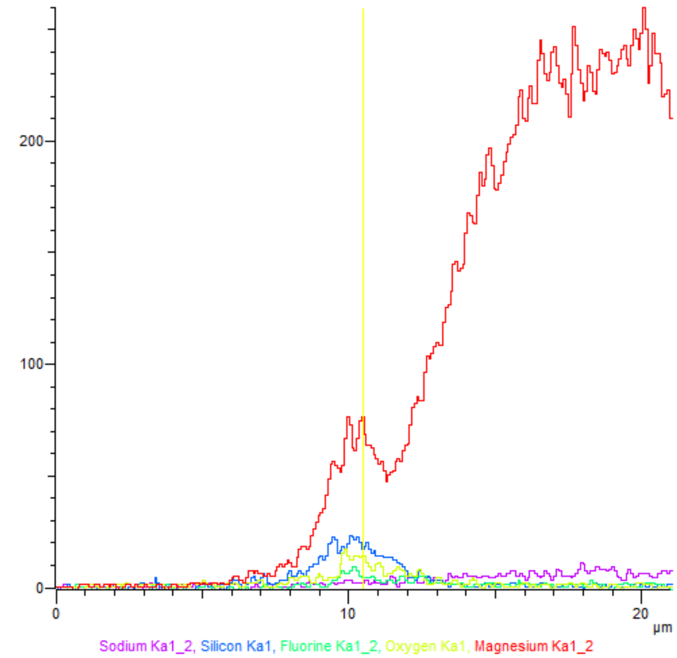


Figure 2.11. EDS spectrum of the MAO coating produced at 1 minute

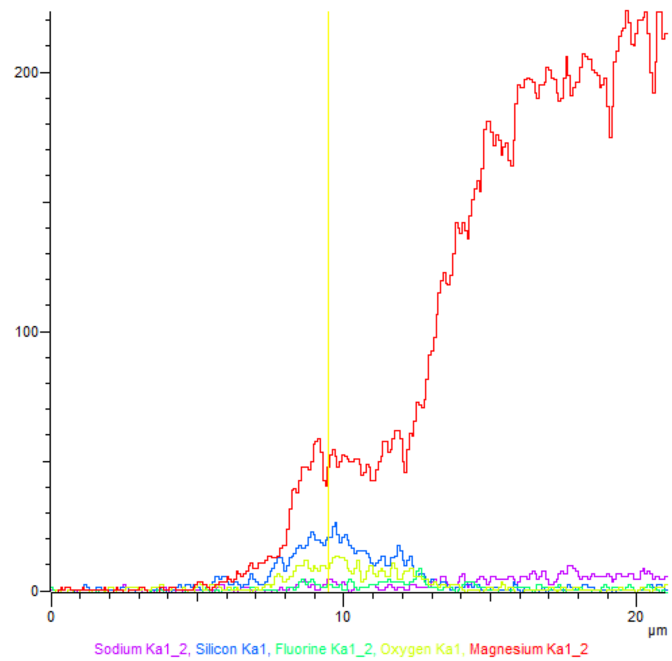


Figure 2.12. EDS spectrum of the MAO coating produced at 5 minutes

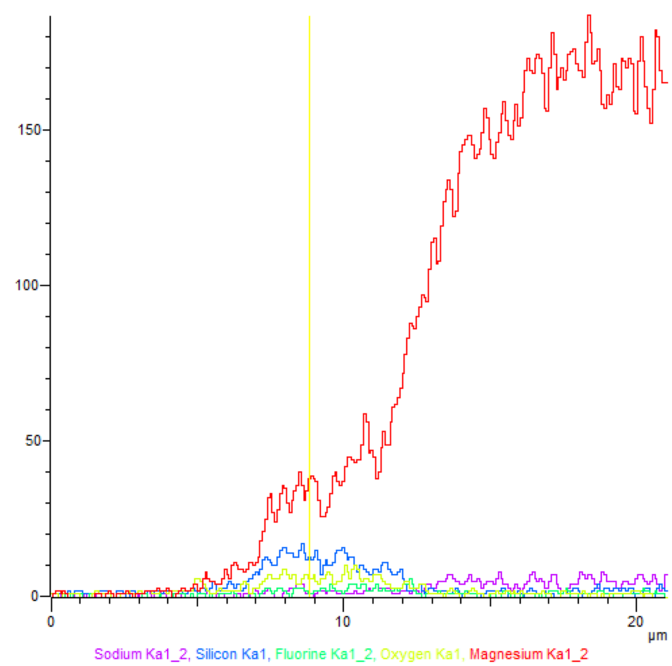


Figure 2.13. EDS spectrum of the MAO coating produced at 15 minutes

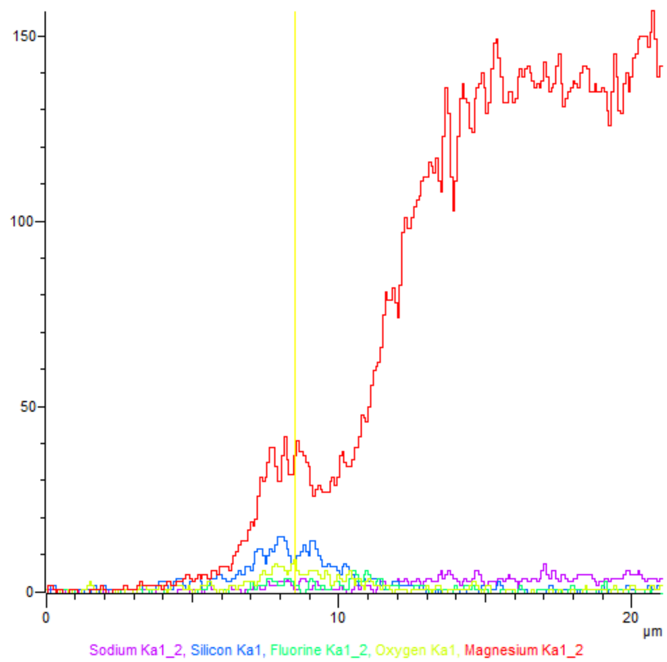


Figure 2.14. EDS spectrum of the MAO coating produced at 20 minutes

### 2.2.3 Coating Phase Analysis

The XRD spectura of all MAO coated samples with different processing times are shown in Figure 2.15. The phases of all MAO coated samples are similar. The results suggested that the MAO processing time does not have a large influence on the phase composition. XRD data show that the MAO coated samples mainly consist of Mg and MgO, regardless the MAO oxidation times.

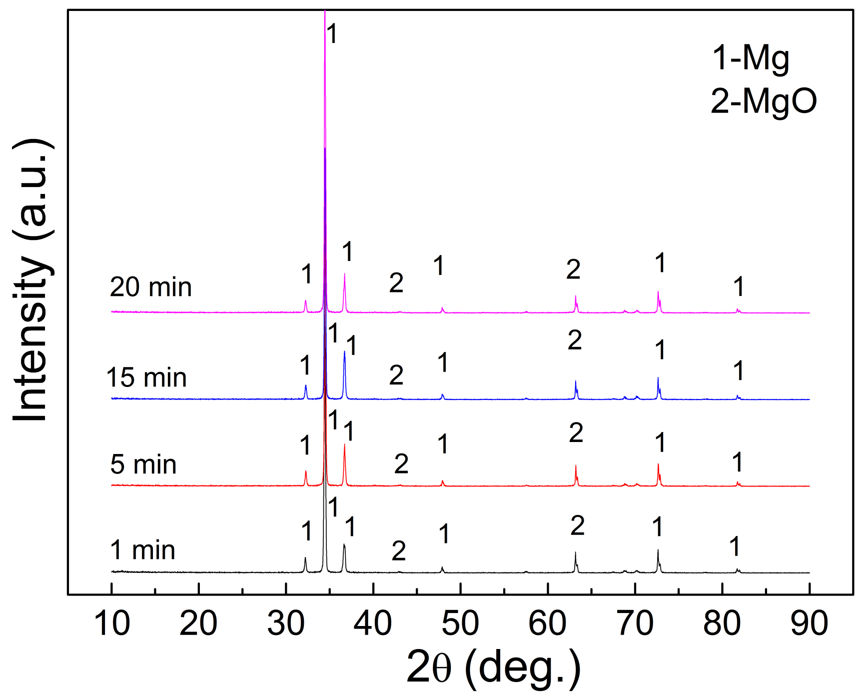


Figure 2.15. XRD spectra of MAO coatings produced at various oxidation times

# 3. ELECTROCHEMICAL BEHAVIORS OF UNCOATED AND MAO-COATED AZ31 MAGNESIUM ALLOY IN SIMULATED BODY FLUID

Potentiodynamic polarization is an effective method to obtain useful information on corrosion rate. Electrochemical impedance spectroscopy (EIS) is also used to demonstrate the electrochemical properties of interface between the conductive solution and a metal or alloy. The information determined from these two methods provides a way to understand the electrochemical corrosion behaviors.

## 3.1 Introduction of Electrochemical Experiments

In this study, the potentiodynamic polarization and electrochemical impedance spectroscopy tests were used to assess the electrochemical properties of both MAO coatings on Mg alloys and uncoated alloys in simulated body fluid.

### 3.1.1 Potentiodynamic Polarization

The potentiodynamic polarization technique can be used to illustrate the electrochemical corrosion system. When performing a potentiodynamic polarization experiment, an anodic or cathodic potentiodynamic scan is conducted. The corrosion rate is determined from a Tafel plot, in which the corrosion potential and current density can be measured. Polarization methods produce a function of potential and current through changing the potential value of the working electrode and recording the current.

### 3.1.2 Electrochemical Impedance Spectroscopy

Electrochemical impedance spectroscopy is an accurate technique to analyze corrosion properties. It measures the response of corroding electrodes to a small perturbative sine wave of the potential of current signals in widely different frequencies. EIS can determine several fundamental parameters related to electrochemical kinetics.

The time-dependent current response $I(t)$ of an electrode surface to a sinusoidal alternating potential signal $V(t)$ can be expressed as an angular frequency ($\omega$) dependent impedance Z($\omega$), as shown in following equation:

$$Z(\omega) = V(t)/I(t) \tag{3.1}$$

where

$V(t) = V_0 \sin \omega t$

$I(t) = I_0 \sin(\omega t + \theta)$

$t =$ time

$\theta =$ phase angle between $V(t)$ and $I(t)$

During the electrochemical behavior tests, the surface of the corroded sample absorbs electrical energy at detached frequencies, causing a time lag and a measurable phase angle, $\theta$, between the time-dependent excitation and response signals. The impedance $Z(\omega)$ can be presented in terms of a complex variable form: $Z\prime(\omega)$ as the real term and $Z\prime\prime(\omega)$ as the imaginary term.

$$Z(\omega) = Z'(\omega) + i \cdot Z''(\omega) \tag{3.2}$$

The EIS behavior of the working electrode is expressed as Nyquist plots of $Z\prime\prime(\omega)$ as a function of $Z\prime(\omega)$ or Bode plots of $log|Z|$ versus frequency $f$ in cycles per sec (Hertz), where

$$\omega = 2\pi f \tag{3.3}$$

### 3.1.3 Setup for Electrochemical Experiments

The electrochemical measurements were determined by using a conventional three-electrode procedure, which includes a silver/silver chloride reference electrode (Accumet electrode 13-620-216, Fisher Scientific) and a platinum foil (Fisher Scientific) as the counter electrode. All testing data were collected using an electrochemical tester (Solartron Electrochemical interface SI1287 and Impedance/Gain-phase analyzer SI1260). The area of the working electrode (AZ31 magnesium alloy sample) immersed in the solution was approximately 4 $cm^2$ . All tests were executed at a room temperature of 25 $\pm$ 1.0 $^oC$. All samples were wrapped with wax at the joint between the electrode clip and sample. The scanning rate of Tafel curves was 0.5 mV/s from -0.300 V to 0.300 V. The electrochemical impedance spectroscopy tests were surveyed in the range of 5 Hz to 150 kHz, and the voltage amplitude was 5 mV. The equivalent circuit model (ECM) was built and the EIS data were fitted by using Zsimpwin software.

The microscopic surface morphologies of the samples were observed using an Amscope optical microscope system, Nikon Measurescope 20, immediately upon removal from the simulated body fluid. Simultaneously, the macroscopic images of the surface were taken with a portable digital camera.

### 3.1.4 Preparation of MAO Samples

Sample substrates have the dimensions of 20 mm $\times$ 5 mm $\times$ 0.4 mm. The chemical composition of magnesium alloy AZ31 is as follows (in wt.%): 2.5-3.5 Al, 0.7-1.3 Zn, 0.2 Mn, 0.05 Si, 0.01 Cu, 0.005 Ni, 0.005 Fe, and Mg balance [38]. Before producing the MAO coating, all magnesium alloy samples were polished on various grade SiC papers up to 1200 grit. Then an ultrasonic metal agent was used to degrease the impurities on the surfaces of polished samples for 2 minutes. The samples were rinsed in deionized water for 1 minute and ethyl alcohol for 2 minutes. Finally, the samples were dried in flowing air. To simulate the body environment as closely as possible, a simulated body fluid (SBF, Table 3.1) was introduced in the current study to understand the corrosion behavior of coated samples [38–40]. The SBF was replenished every day.

Table 3.1. Reagents for SBF preparation (pH 7.25, 1L) [39]

| Reagent | Purity (%) | Amout |
|---|---|---|
| $NaCl$ | 99.5 | 7.996 g |
| $NaHCO_3$ | 99.5-100.5 | 0.350 g |
| $KCl$ | 99.0 | 0.224 g |
| $K_2HPO_4 \cdot 3H_2O$ | 99.0 | 0.228 g |
| $MgCl_2 \cdot 6H_2O$ | 99.0 | 0.305 g |
| 1 kmol/m$^3$ HCl | - | 40 ml |
| $CaCl_2$ | 96.0 | 0.278 g |
| $Na_2SO_4$ | 99.0 | 0.071 g |
| $(CH_2OH)_3CNH_2$ | 99.9 | 6.057 g |
| 1kmol/m$^3$ HCl | - | Adjusting pH |

## 3.2 Results of Electrochemical Behaviors in Simulated Body Fluid

### 3.2.1 Porosity Evaluation

The initial porosity of the MAO-coated magnesium alloys is a very important piece of information in estimating corrosion resistance. The pores can affect the interaction between the SBF solution and the magnesium substrate after the solution penetrates them. The porosity of the MAO-coated samples was evaluated according to the potentiodynamic polarization data after the samples were immersed in the SBF for a period of 1 hour. The porosity (F) is calculated as follows [41, 42]

$$F = (\frac{R_{pm}}{R_p}) \times 10^{-|\Delta E_{corr}/\beta_{uncoated}|} \tag{3.4}$$

where $R_p$ ($\Omega \times cm^2$)and $R_{pm}$ ($\Omega \times cm^2$) are the polarization resistance of the MAO-coated and uncoated samples, respectively. $\Delta E_{corr}$ (V) is the difference of corrosion potential between the uncoated and coated samples. $\beta_{uncoated}$ is the anodic Tafel constant of the uncoated sample of 501 mV/decade and $E_{corr}$ of uncoated samples of -1.457 V were used in the calculation [43] . The polarization resistance ($R_p$) is calculated by the Stern-Geary equation:

$$R_p = \frac{\beta_a \beta_c}{2.3 I_{corr}(\beta_a + \beta_c)} \tag{3.5}$$

where $I_{corr}$ is the corrosion current density, and $\beta_c$ and $\beta_a$ are the cathodic Tafel constants. Table 3.2 shows the data used in Eq. (3.4) and Eq. (3.5) and the calculation results of porosity of MAO coated samples produced at different oxidation times. The porosity of MAO-coated samples decreased with increasing MAO processing times. Therefore, the 20-minute MAO-coated sample has the highest density.

Table 3.2. Tafel data for MAO-coated AZ31 Mg alloys and porosity after immersion in the SBF for 1 hour

| Sample | $E_{corr}$ (V) | $I_{corr}$ (mA/cm$^2$) | $\beta_a$ (mV/decade) | $\beta_c$ (mV/decade) | $R_p$ ($\Omega \times$ cm$^2$) | Porosity (%) |
|---|---|---|---|---|---|---|
| Uncoated | -1.457 | 0.2256 | 0.501 | 0.41 | 434.5 | / |
| 1 min-MAO | -1.553 | 0.0021 | 0.1022 | 0.208 | 14188.1 | 2.0 |
| 5 min-MAO | -1.423 | 0.0031 | 0.0753 | 0.2453 | 8080.5 | 4.5 |
| 15 min-MAO | -1.534 | 0.0016 | 0.1238 | 0.2403 | 22202.7 | 1.3 |
| 20 min-MAO | -1.566 | 0.0008 | 0.1649 | 0.24 | 53121.0 | 1.0 |

The Tafel curves for the uncoated and MAO-coated AZ31 magnesium alloys after immersion in the SBF for 1 hour are illustrated in Figure 3.1

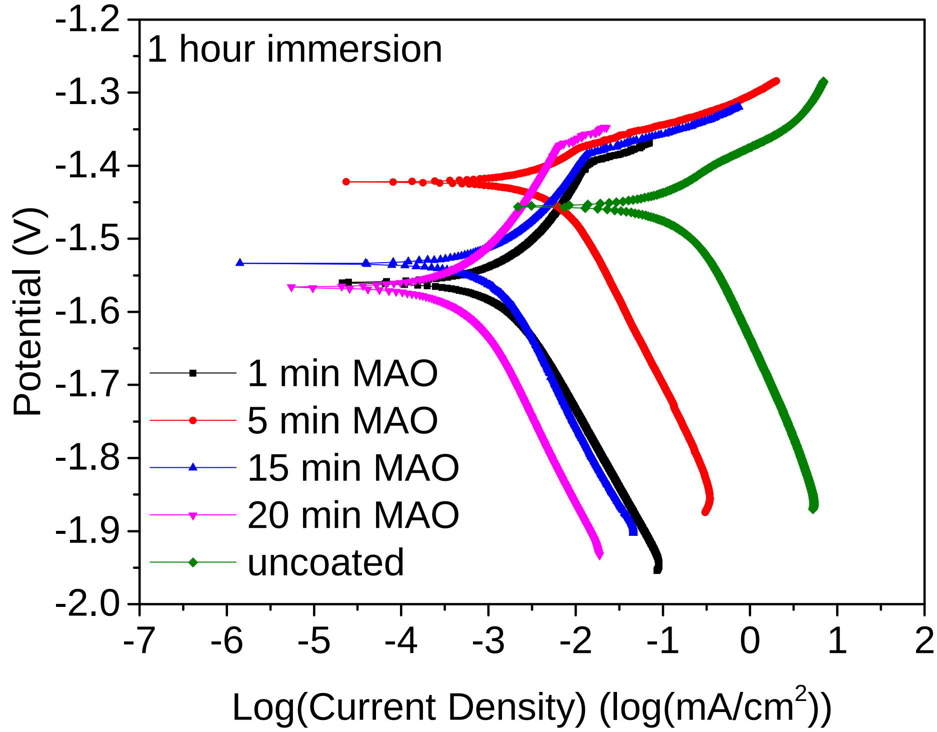


Figure 3.1. Tafel plots of the uncoated and MAO coated AZ31 Mg alloy after immersion in the SBF for 1 hour

### 3.2.2 Potentiodynamic Polarization

#### Uncoated Sample

The potentiodynamic polarization curves of the uncoated AZ31 alloy immersed in the simulated body fluid are shown in Figure 3.2. The corrosion potential ($E_{corr}$) and the corrosion current density ($I_{corr}$) were generated directly from the Tafel plots.

According to the Tafel curves, the anodic branches are the inflection points more positive than $E_{corr}$ at the potentials. The value of $E_{corr}$ from 1 hour to day 7 are shown in Table 3.3. The $E_{corr}$ value of the uncoated sample increased generally in 7 days of immersion.

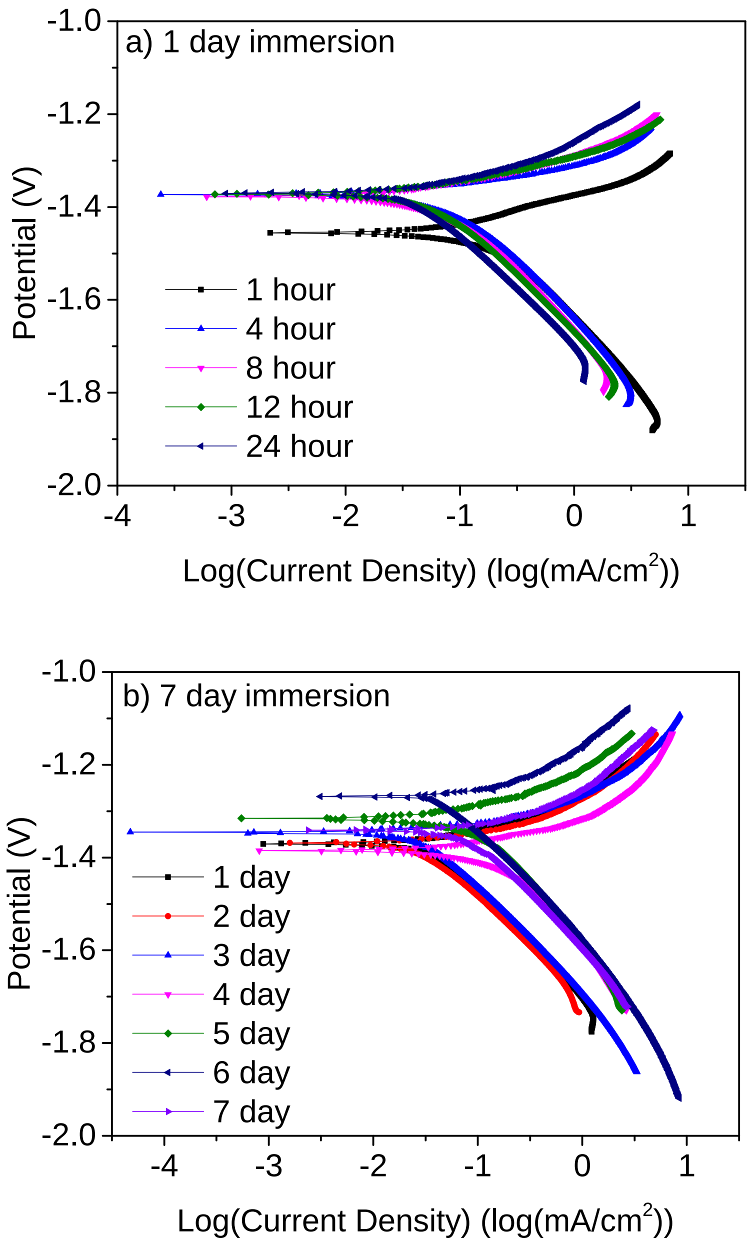


Figure 3.2. Tafel plots of the uncoated AZ31 alloys in simulated body fluid at: (a) 1-day immersion, and (b) 7-day immersion

The cathodic branch of potentialdynamic polarization plots showed a linear curve and is thought to represent cathodic hydrogen evolution through the reduction of the solution [44]. The corrosion current density $I_{corr}$ was deduced from the extrapolation

Table 3.3. Corrosion potential ($E_{corr}$) of uncoated sample

| Time | $E_{corr}$ (V) | Time | $E_{corr}$ (V) |
|---|---|---|---|
| 1 hour | -1.457 | 2 day | -1.369 |
| 2 hour | / | 3 day | -1.345 |
| 4 hour | -1.373 | 4 day | -1.372 |
| 8 hour | -1.378 | 5 day | -1.316 |
| 12 hour | -1.370 | 6 day | -1.269 |
| 24 hour | -1.370 | 7 day | -1.342 |

of the cathodic branch of Tafel curves to the corrosion potential. Table 3.4 shows the results of corrosion current density $I_{corr}$.

Table 3.4. Corrosion current density ($I_{corr}$) of the uncoated sample

| Time | $I_{corr}$ (mA/cm$^2$) | Time | $I_{corr}$ (mA/cm$^2$) |
|---|---|---|---|
| 1 hour | 0.2256 | 2 day | 0.1020 |
| 2 hour | / | 3 day | 0.1037 |
| 4 hour | 0.1059 | 4 day | 0.1879 |
| 8 hour | 0.1047 | 5 day | 0.2052 |
| 12 hour | 0.1035 | 6 day | 0.1920 |
| 24 hour | 0.1015 | 7 day | 0.1823 |

According to the corrosion current density results, the $I_{corr}$ values increased with the accumulation of immersion time after one day. That means the corrosion rate accelerated as the time increased. The increase of corrosion current density occurs because the pores and cracks appeared on the surface of the sample as shown in section 3.3.

### 1-minute MAO-coated Sample

The potentiodynamic polarization curves of the 1-minute MAO coated AZ31 alloy immersed in the simulated body fluid are shown in Figure 3.3.

The $E_{corr}$ values from 1 hour to 7 day are shown in Table 3.5. The $E_{corr}$ of the 1-minute MAO-coated sample increased in the first immersion day and maintained a stable value afterwards. While after 1 day immersion, the $E_{corr}$ slightly decreased from day 1 to day 7. The results suggest that the 1-minute MAO coated samples became inactive in the first day with increase of immersion time [45]. The $E_{corr}$ showed a more negative value after 1 day immersion. That means the 1-minute MAO coated sample became more active. The results may be caused by the dissolution of surface film.

Table 3.5. Corrosion potential ($E_{corr}$) of the 1-minute MAO-coated sample

| Time | $E_{corr}$ (V) | Time | $E_{corr}$ (V) |
|---|---|---|---|
| 1 hour | -1.553 | 2 day | -1.310 |
| 2 hour | -1.502 | 3 day | -1.313 |
| 4 hour | -1.381 | 4 day | -1.316 |
| 8 hour | -1.360 | 5 day | -1.351 |
| 12 hour | -1.324 | 6 day | -1.368 |
| 24 hour | -1.307 | 7 day | -1.344 |

Table 3.6 shows the results of corrosion current density $I_{corr}$. The $I_{corr}$ values increased with the accumulation of immersion time after day 1 to day 6. That means the corrosion rate accelerated as the time increased. The increase of corrosion current density occurred because the pores and cracks appeared in the surface of the sample. The corrosiveness of these ions to magnesium alloys increased from their tendency to cause surface film breakdown by the dissolution of the deposited corrosion product. The $I_{corr}$ decreased in day 7. This is due to the decrease of the sample surface area.

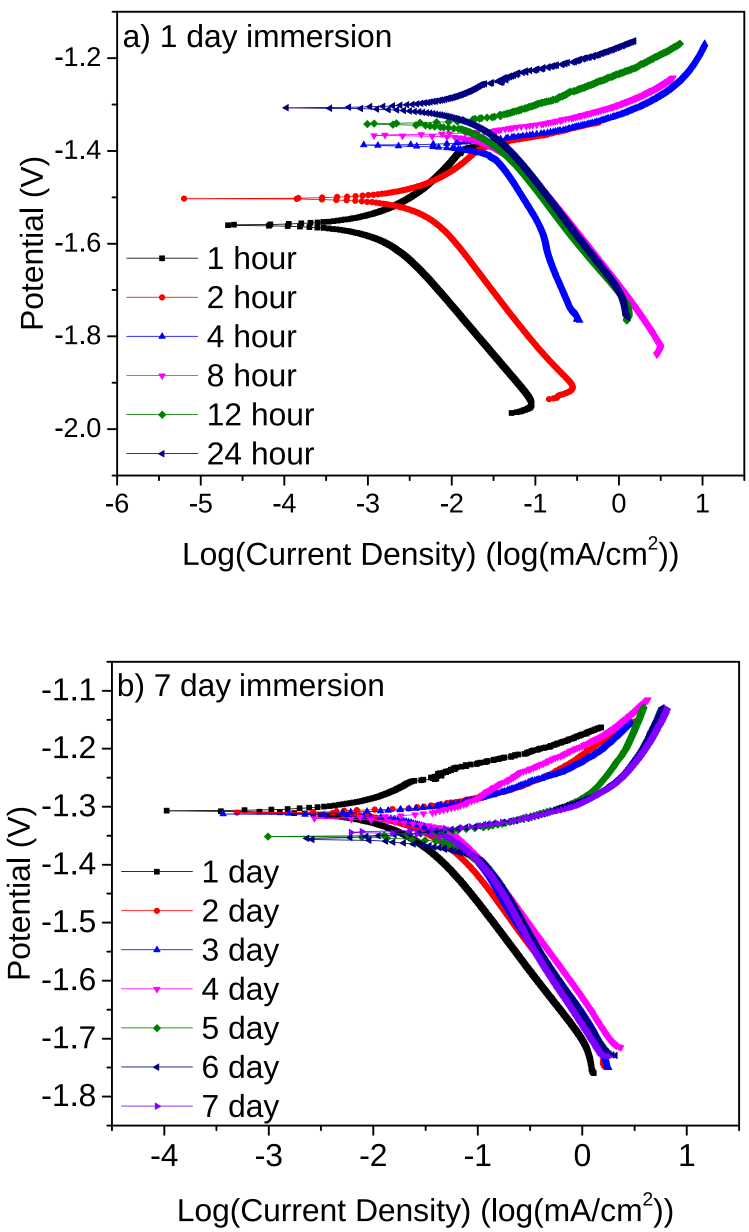


Figure 3.3. Tafel plots of the 1-minute MAO-coated AZ31 alloys in simulated body fluid at: (a) 1-day immersion, and (b) 7-day immersion

**5-minute MAO-coated Sample**

The potentiodynamic polarization curves of the 5-minute MAO coated AZ31 alloy immersed in the simulated body fluid are shown in Figure 3.4.

Table 3.6. Corrosion current density ($I_{corr}$) of the 1-minute MAO-coated sample

| Time | $I_{corr}$ (mA/cm$^2$) | Time | $I_{corr}$ (mA/cm$^2$) |
|---|---|---|---|
| 1 hour | 0.0021 | 2 day | 0.0428 |
| 2 hour | 0.0053 | 3 day | 0.0471 |
| 4 hour | 0.0452 | 4 day | 0.0612 |
| 8 hour | 0.0558 | 5 day | 0.0841 |
| 12 hour | 0.0360 | 6 day | 0.0958 |
| 24 hour | 0.0208 | 7 day | 0.0863 |

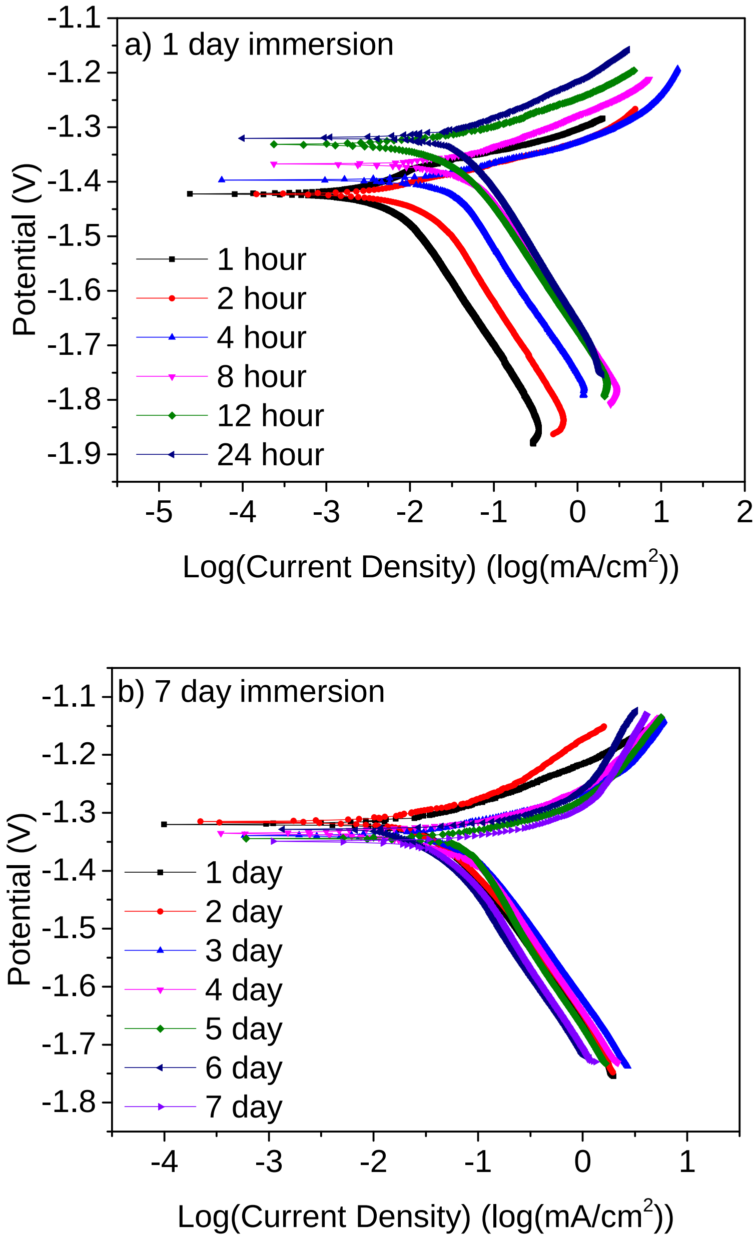


Figure 3.4. Tafel plots of the 15-minute MAO-coated AZ31 alloys in simulated body fluid at: (a) 1-day immersion, and (b) 7-day immersion

The values of $E_{corr}$ from 1 hour to day 7 are shown in Table 3.7. The Tafel curves show that the $E_{corr}$ of the 5-minute MAO-coated sample increased in the first immersion day. While after 1 day immersion, the $E_{corr}$ floated around -1.330 V from day 1 to day 7 . This result suggests that the 5-minute MAO-coated samples became inactive in the first day with increase of immersion time. However, the curves showed a more negative corrosion potential after 1 day immersion. That means the 5-minute MAO coated sample was more active than it was in the first day.

Table 3.7. Corrosion potential ($E_{corr}$) of the 5-minute MAO-coated sample

| Time | $E_{corr}$ (V) | Time | $E_{corr}$ (V) |
|---|---|---|---|
| 1 hour | -1.423 | 2 day | -1.312 |
| 2 hour | -1.429 | 3 day | -1.339 |
| 4 hour | -1.391 | 4 day | -1.342 |
| 8 hour | -1.360 | 5 day | -1.345 |
| 12 hour | -1.372 | 6 day | -1.338 |
| 24 hour | -1.320 | 7 day | -1.349 |

Table 3.8. Corrosion current density ($I_{corr}$) of the 5-minute MAO-coated sample

| Time | $I_{corr}$ (mA/cm$^2$) | Time | $I_{corr}$ (mA/cm$^2$) |
|---|---|---|---|
| 1 hour | 0.0031 | 2 day | 0.0451 |
| 2 hour | 0.0142 | 3 day | 0.0594 |
| 4 hour | 0.0355 | 4 day | 0.0612 |
| 8 hour | 0.0528 | 5 day | 0.1024 |
| 12 hour | 0.0445 | 6 day | 0.1212 |
| 24 hour | 0.0501 | 7 day | 0.1005 |

Table 3.8 shows the results of corrosion current density ($I_{corr}$) of 5-minute MAO-coated sample. The $I_{corr}$ values increased with the accumulation of immersion time after day 1 to day 6. The $I_{corr}$ decreased in day 7. This is due to the reduction of the sample surface area.

### 15-minute MAO-coated Sample

The potentiodynamic polarization curves of the 15-minute MAO-coated AZ31 alloy immersed in the simulated body fluid are shown in Figure 3.5. The values of $E_{corr}$ from 1 hour to day 6 are shown in Table 3.9. The $E_{corr}$ of the 15-minute MAO-coated sample increased in the first immersion day. While after 1 day immersion, the $E_{corr}$ values decreased from day 1 to day 6 generally and almost maintained a stable value.

Table 3.9. Corrosion potential ($E_{corr}$) of the 15-minute MAO-coated sample

| Time | $E_{corr}$ (V) | Time | $E_{corr}$ (V) |
|---|---|---|---|
| 1 hour | -1.534 | 2 day | -1.324 |
| 2 hour | -1.449 | 3 day | -1.333 |
| 4 hour | -1.363 | 4 day | -1.356 |
| 8 hour | -1.340 | 5 day | -1.346 |
| 12 hour | -1.342 | 6 day | -1.351 |
| 24 hour | -1.323 | 7 day | / |

Table 3.10 shows the results of corrosion current density ($I_{corr}$). The $I_{corr}$ values increased with the accumulation of immersion time from day 1 to day 6. That means the corrosion rate of 15-minute MAO-coated sample accelerated as the time increased.

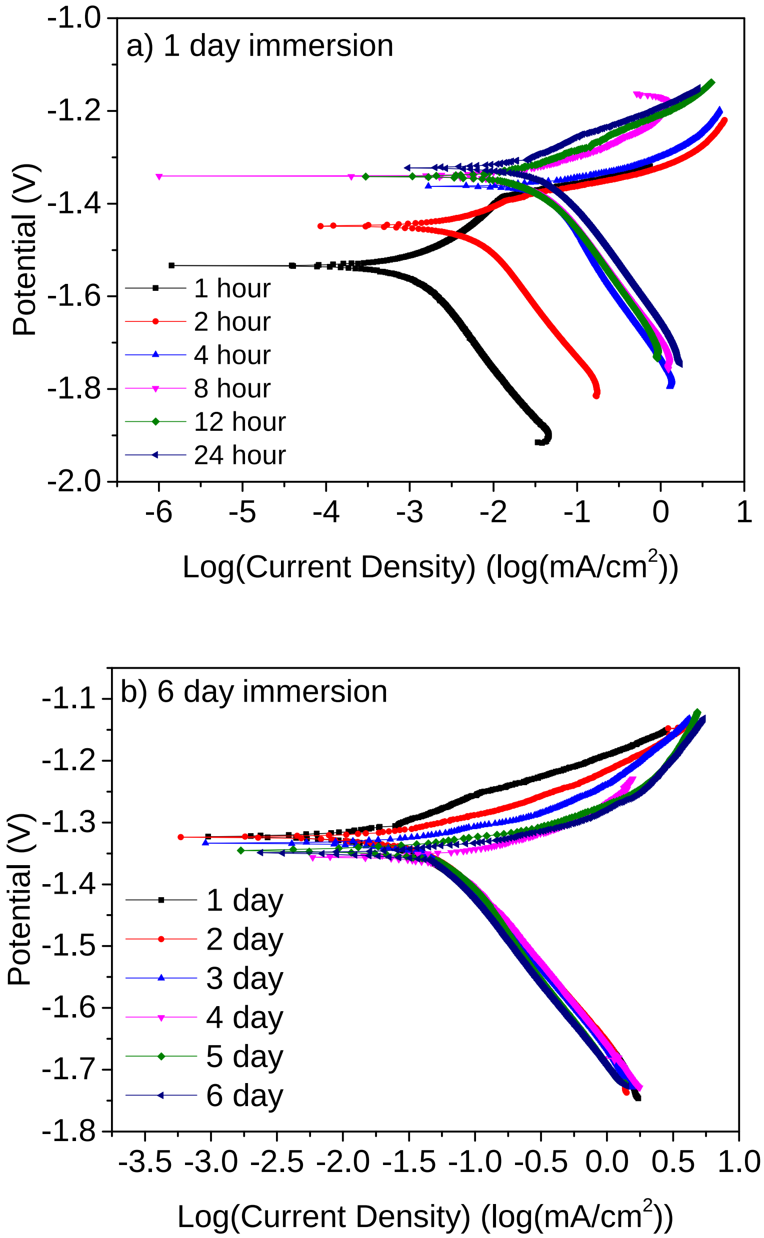


Figure 3.5. Tafel plots of the 15-minute MAO-coated AZ31 alloys in simulated body fluid at: (a) 1-day immersion, and (b) 7-day immersion

Table 3.10. Corrosion current density ($I_{corr}$) of the 15-minute MAO-coated sample

| Time | $I_{corr}$ (mA/cm$^2$) | Time | $I_{corr}$ (mA/cm$^2$) |
|---|---|---|---|
| 1 hour | 0.0016 | 2 day | 0.0474 |
| 2 hour | 0.0053 | 3 day | 0.0458 |
| 4 hour | 0.0332 | 4 day | 0.0481 |
| 8 hour | 0.0392 | 5 day | 0.0507 |
| 12 hour | 0.0415 | 6 day | 0.0532 |
| 24 hour | 0.0456 | 7 day | / |

**20-minute MAO-coated Sample**

The potentiodynamic polarization curves of the 20-minute MAO-coated AZ31 alloy immersed in the simulated body fluid are shown in Figure 3.6.

The values of $E_{corr}$ of 20-minute MAO-coated sample from 1 hour to day 7 are shown in Table 3.11. Similarly with other MAO-coated samples, the $E_{corr}$ of the 20-minute MAO-coated sample increased in the first immersion day with the increase of immersion time. And the $E_{corr}$ decreased from day 1 to day 7, keeping at a stable value.

Table 3.11. Corrosion potential ($E_{corr}$) of the 20-minute MAO-coated sample

| Time | $E_{corr}$ (V) | Time | $E_{corr}$ (V) |
|---|---|---|---|
| 1 hour | -1.566 | 2 day | -1.330 |
| 2 hour | -1.527 | 3 day | -1.328 |
| 4 hour | -1.386 | 4 day | -1.359 |
| 8 hour | -1.325 | 5 day | -1.342 |
| 12 hour | -1.311 | 6 day | -1.338 |
| 24 hour | -1.321 | 7 day | -1.349 |

Table 3.12 shows the results of corrosion current density ($I_{corr}$). The $I_{corr}$ values increased with the accumulation of immersion time after day 1 to day 7 generally. That means the corrosion rate accelerated as the time increased.

Figure 3.7 shows the comparison of the corrosion potentials of all MAO-coated samples from 1 day to 7 day. According to the results, at the beginning of immersion, the uncoated sample has the lowest corrosion potential. After 7 day immersion, all the MAO-coated samples, except the 15-minute MAO-coated one, have lower corrosion potential than the uncoated one. Furthermore, the 20-minute MAO-coated sample has the lowest corrosion potential.

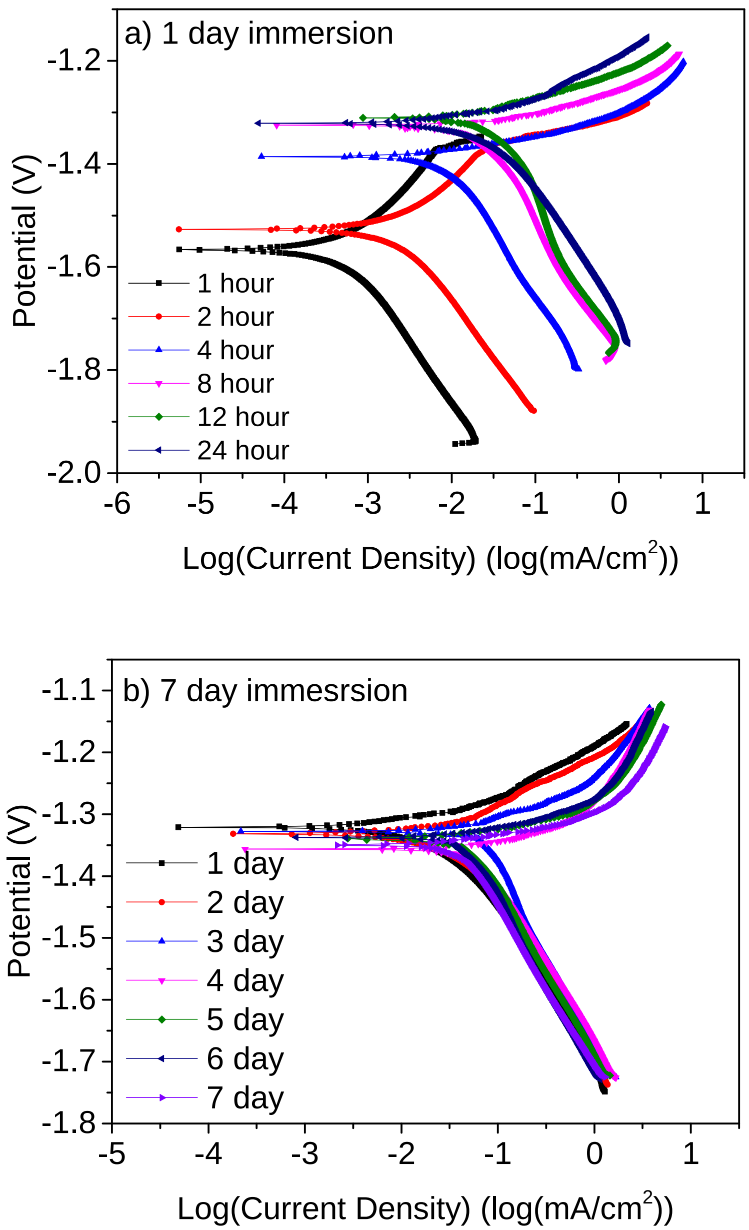


Figure 3.6. Tafel plots of the 20-minute MAO-coated AZ31 alloys in simulated body fluid at: (a) 1-day immersion, and (b) 7-day immersion

The corrosion rate ($CR$,mm/year) is calculated using the following equation [44]:

$$CR(mm/year) = 0.00327 \times \frac{EW \times I_{corr}}{d} \tag{3.6}$$

Table 3.12. Corrosion current density ($I_{corr}$) of the 20-minute MAO-coated sample

| Time | $I_{corr}$ (mA/cm$^2$) | Time | $I_{corr}$ (mA/cm$^2$) |
|---|---|---|---|
| 1 hour | 0.0008 | 2 day | 0.0451 |
| 2 hour | 0.0031 | 3 day | 0.0462 |
| 4 hour | 0.0011 | 4 day | 0.0425 |
| 8 hour | 0.0298 | 5 day | 0.0468 |
| 12 hour | 0.0438 | 6 day | 0.0479 |
| 24 hour | 0.0281 | 7 day | 0.0475 |

where $EW$ is the equivalent weight, $I_{corr}$ is the corrosion current density (A/cm$^2$), and $d$ is the sample density (g/cm$^3$). The EW is a weighted average of a/n for the major alloying elements in the sample. The recommended procedure for calculating the equivalent weight, is:

$$EW = \sum \frac{f_i a_i}{n_i} \tag{3.7}$$

where $f_i$, $n_i$ and $a_i$ are mass fraction, electrons exchanged, and atomic weight (g/mol), respectively, of the ith major alloying element in the sample. Table 3.13 shows the mass fraction, electrons exchanged, and atomic weight of the MAO coatings and uncoated AZ31 alloy. Table 3.14 shows the equivalent weight of all the samples.

Figure 3.8 shows the corrosion rate evolution of MAO-coated and uncoated samples. It can be found that MAO-coated samples have lower corrosion rates than the uncoated one. The corrosion rates of all the MAO-coated and uncoated samples increase with immersion time. Furthermore, the 20-minute MAO-coated sample demonstrates the lowest corrosion rate in simulated body fluid, which means the 20-minute MAO-coated sample has the best corrosion resistance.

Table 3.13. Mass fraction, electrons exchanged, and atomic weight of MAO coatings and uncoated AZ31 alloy

| Major alloying elements | Mg | Al | Zn | Na |
|---|---|---|---|---|
| $f_i$ (%) AZ31 alloy | 95.44 | 3.00 | 1.00 | 0 |
| $f_i$ (%) 1-min MAO coated | 35.05 | 0 | 0 | 0.36 |
| $f_i$ (%) 5-min MAO coated | 34.72 | 0 | 0 | 1.03 |
| $f_i$ (%) 15-min MAO coated | 35.07 | 0 | 0 | 0.82 |
| $f_i$ (%) 20-min MAO coated | 34.64 | 0 | 0 | 0.89 |
| $a_i$ (g/mol) | 24.31 | 26.98 | 65.38 | 22.99 |
| $n_i$ | 2 | 3 | 2 | 1 |

Table 3.14. The equivalent weight of the MAO-coated and uncoated AZ31 Mg alloy

| Sample | 1-min MAO | 5-min MAO | 15-min MAO | 20-min MAO | uncoated |
|---|---|---|---|---|---|
| EW (g/mol) | 4.34 | 4.46 | 4.45 | 4.41 | 12.20 |

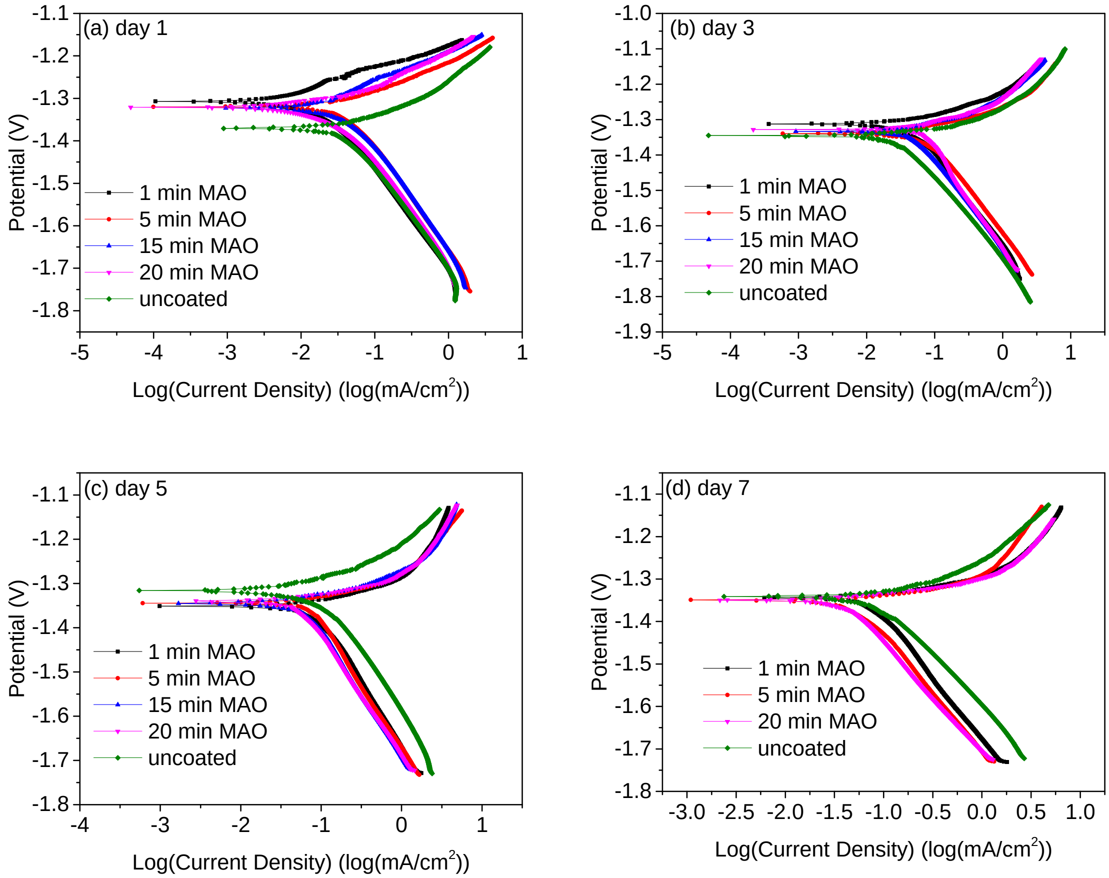


Figure 3.7. Tafel plots of all samples in the simulated body fluid at(a) day 1; (b) day 3; (c) day 5; (d) day 7

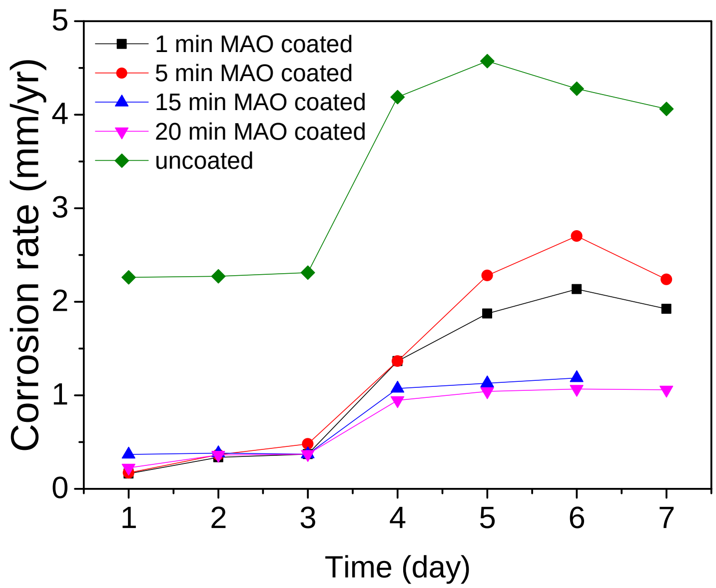


Figure 3.8. Corrosion rate evolution of the uncoated and MAO-coated samples in the simulated body fluid during 7-day immersion.

### 3.2.3 Electrochemical Impedance Spectroscopy

#### Uncoated Sample

The EIS data of uncoated and MAO-coated AZ31 alloys can be represented using an equivalent circuit, as shown in Figure 3.9. Using a Nyquist curve, two equivalent circuit models are built, to simulate the electrochemical behaviors [46–48]. Figure 3.9 (a) is used to fit the Nyquist curves from the first day to the third day on the MAO-coated samples. After immersing in the SBF for 3 days, the MAO coating dissolved into the solution, and the substrate layers were exposed in the solution. As part of the major coating dissolved away from the substrate, the coated samples behaved similar to the uncoated sample. Figure 3.9 (b) shows the equivalent circuits of uncoated samples, and MAO-coated samples after 4 day when the coating layers were almost completely dissolved.

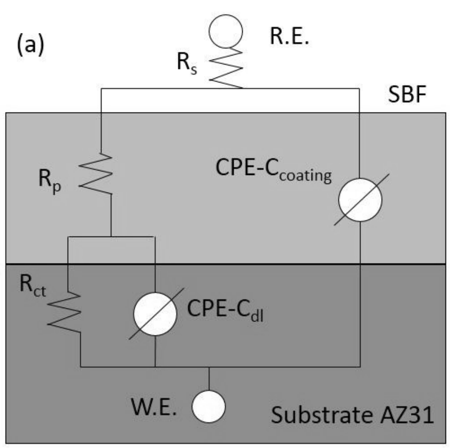


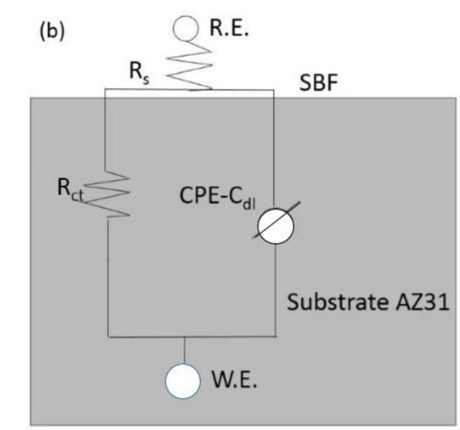


Figure 3.9. Equivalent circuits for fitting the electrochemical behaviors: (a) MAO-coated samples from day 1 to day 3, and (b) uncoated and MAO-coated samples from day 4 to day 7.

In the equivalent circuit, $R_s$ represents the solution resistance between the reference electrode and working electrode. $C_{dl}$, which is in parallel with $R_{ct}$, is the CPE of the double layer. $R_p$ is the resistance of the MAO coating from the porous regions, parallel to the CPE-$C_{coating}$. The charge transfer resistance, $R_{ct}$, is the parameter characterizing the corrosion behavior of coated samples. The $R_{ct}$ value reflects how difficult the electrochemical corrosion reaction can be. The results of equivalent circuit for uncoated AZ31 magnesium alloys are summarized in Table 3.15. The larger the $R_{ct}$ is, the lower corrosion rate of the sample [50]. The Nyquist plots for the corrosion of uncoated AZ31 alloy in simulated body fluid are shown in Figure 3.10.

Table 3.15. EIS data for uncoated AZ31 magnesium alloys after immersion in the SBF for various durations

| Time | $R_s$ ($\Omega \times cm^2$) | CPE-$C_{dl}$ (F) | $R_{ct}$ ($\Omega \times cm^2$) |
|---|---|---|---|
| 1 hour | 40.65 | 2.16E-05 | 369.8 |
| 2 hour | 40.45 | 2.42E-05 | 357 |
| 4 hour | 41.22 | 2.26E-05 | 423.9 |
| 8 hour | 41.05 | 2.36E-05 | 503.4 |
| 12 hour | 39.42 | 2.37E-05 | 513.4 |
| 24 hour | 42.39 | 2.48E-05 | 584.1 |
| 2 day | 41.15 | 5.16E-05 | 386.1 |
| 3 day | 40.55 | 3.72E-05 | 404.4 |
| 4 day | 41.06 | 4.98E-05 | 340.6 |
| 5 day | 40.72 | 5.53E-05 | 330.5 |
| 6 day | 37.29 | 6.49E-05 | 313.4 |
| 7 day | 29.32 | 8.19E-05 | 307.7 |

According to Table 3.15 and Figure 3.10, it is obvious that the AZ31 magnesium alloy exhibited a capacity loop. The variation of $R_{ct}$ values is related to the dynamic process of the crack or stripping of the corrosion layer. It could be pointed out that a vivid corrosion reaction was generated between the magnesium alloy and simulated body fluid. The diameter of the capacitive loop in the high frequency range represents the charge transfer resistance $R_{ct}$. The $R_s$ value remained around 40 $\Omega \times cm^2$. That is because the same recipe for simulated body fluid in this corrosion test. The resistance

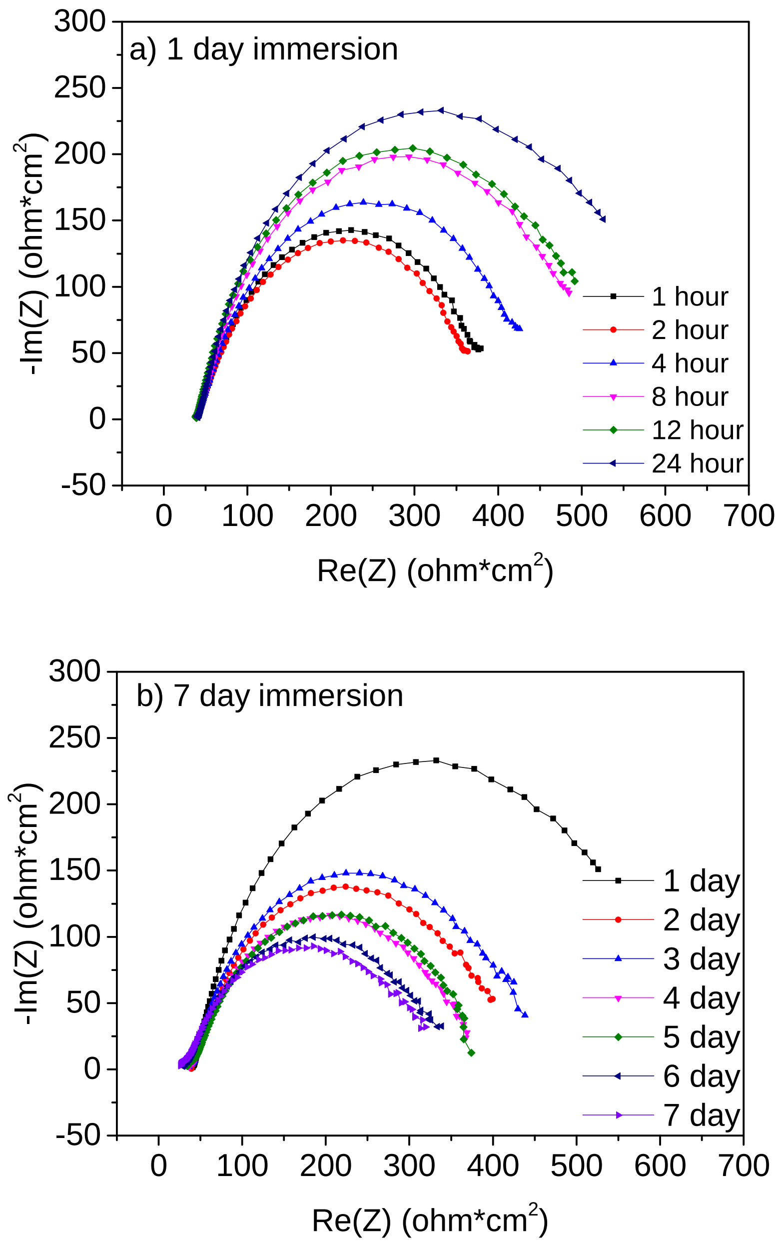


Figure 3.10. Nyquist plots of uncoated AZ31 alloy in SBF (a) 1-day immersion, and (b) 7-day immersion

of charge transfer $R_s$ increased in the first day with the time increase because of the rapid formation of a corrosion product layer. However, on the second day, the value of $R_{ct}$ decreased quickly due to increased stripping. Then, from the second day to the seventh day, the values decreased generally. The CPE-$C_{dl}$ also increased with the time. These results demonstrate that the surface of the uncoated sample became rougher with increasing immersion time. The number of pits on the uncoated alloy also increased over time.

### 1-minute MAO-coated Sample

The Nyquist plots for the corrosion of the 1-minute MAO-coated AZ31 alloy in simulated body fluid are shown in Figure 3.11.

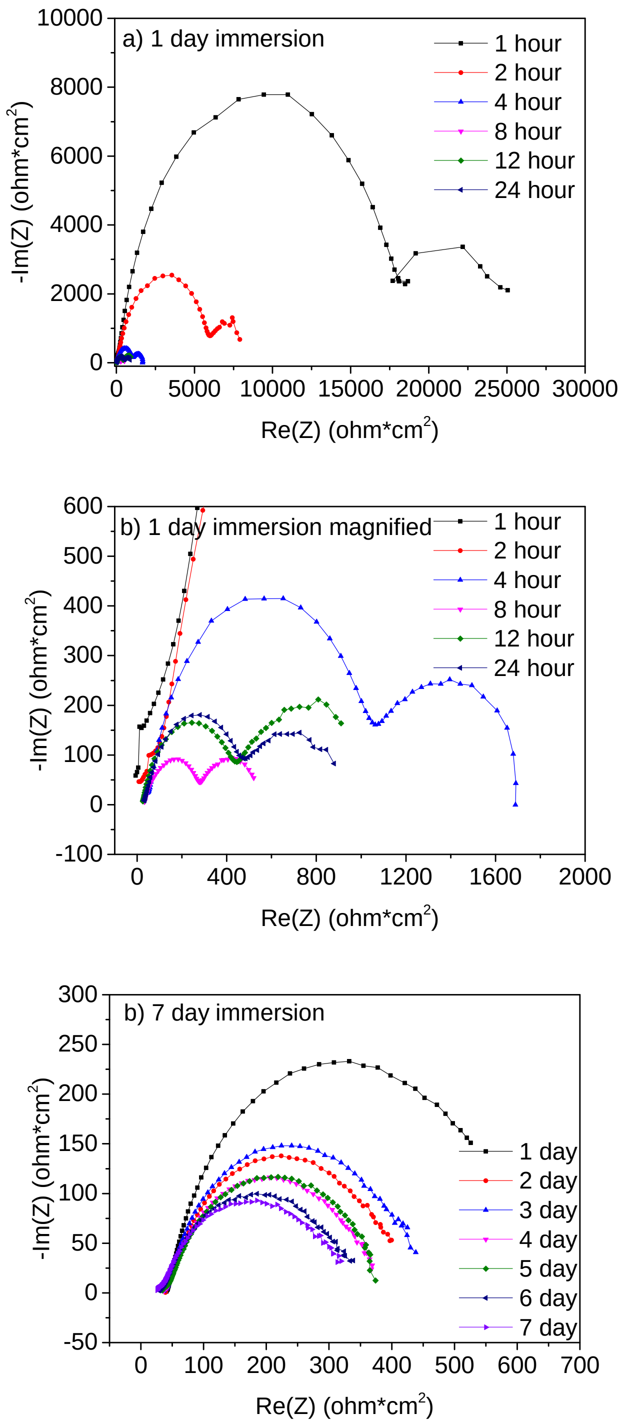


Figure 3.11. Nyquist plots of the 1-minute MAO-coated AZ31 alloy in SBF (a) 1-day immersion, (b) 1-day immersion, magnified Nyquist Re(Z) from -100 to 2000 (ohm*cm$^2$), and (c) 7-day immersion

Table 3.16. EIS data for the 1-minute MAO-coated AZ31 magnesium alloys after immersion in the SBF for various durations

| Time | $R_s$ ($\Omega\times$cm$^2$) | CPE-$C_{coating}$ (F) | $R_p$ ($\Omega\times$cm$^2$) | CPE-$C_{dl}$ (F) | $R_{ct}$ ($\Omega\times$cm$^2$) |
|---|---|---|---|---|---|
| 1 hour | 35.1 | 4.7280E-05 | 6274 | 3.1650E-07 | 19210 |
| 2 hour | 29.8 | 2.2590E-04 | 2499 | 1.1490E-06 | 6314 |
| 4 hour | 42.5 | 8.6760E-04 | 755.9 | 7.3840E-06 | 1080 |
| 8 hour | 30.58 | 3.1570E-03 | 237.8 | 4.8440E-05 | 272.7 |
| 12 hour | 24.02 | 1.9580E-03 | 558.1 | 2.5400E-05 | 448.4 |
| 24 hour | 30.87 | 2.3050E-03 | 331.1 | 3.9120E-05 | 506.2 |
| 2 day | 26.42 | 2.8780E-03 | 307.1 | 3.4480E-05 | 315.2 |
| 3 day | 29.59 | 2.7120E-03 | 212.5 | 5.3870E-05 | 288 |
| 4 day | 29.27 | / | / | 9.1490E-05 | 243.3 |
| 5 day | 35.81 | / | / | 7.6040E-05 | 251.3 |
| 6 day | 36.36 | / | / | 8.3960E-05 | 250 |
| 7 day | 37.71 | / | / | 8.5780E-05 | 308.6 |

According to Table 3.16 and Figure 3.11, it is obvious that the 1-minute MAO-coated sample exhibited two capacity loops in the first 3 days. It shows that a vivid corrosion reaction generated between the MAO coating and simulated body fluid, and between the substrate layer and SBF. The diameter of the capacitive loop in the high frequency range represents the charge transfer resistance ($R_{ct}$). The low frequency range represents the $R_p$, the resistance between the coating and simulated body fluid. The Rs value is around 30 $\Omega\times$cm$^2$. The resistance of charge transfer ($R_{ct}$) decreased in the first 8 hours with the time increasing. The similar trend is observed for the $R_p$. These are due to the fact that the corrosion happened on the film and more pits were created on the surface. From 8 hours to 24 hours, the $R_{ct}$ increased with the time increase. The passive layer occurred on the surface of substrate increased corrosion resistance. However, on the second day, the value of $R_{ct}$ decreased fast since the cracks and the stripping increased. Then, during the second day to the seventh day, the values decreased slowly and kept at a stable value since the corrosion passive layer produced on the substrate surface after the coating layer dissolved in the SBF. The CPE-$C_{dl}$ increased with the time and maintained a stable range after 3 days immersion. This result demonstrates that the surface of uncoated sample became rougher with increasing immersion time and more pits occuerred on the substrate magnesium alloys.

### 5-minute MAO-coated Sample

The Nyquist plots for the corrosion of the 5-minute MAO-coated AZ31 alloy in simulated body fluid are shown in Figure 3.12.

Table 3.17. EIS data for the 5-minute MAO-coated AZ31 magnesium alloys after immersion in the SBF for various durations

| Time | $R_s$ ($\Omega\times$cm$^2$) | CPE-$C_{coating}$ (F) | $R_p$ ($\Omega\times$cm$^2$) | CPE-$C_{dl}$ (F) | $R_{ct}$ ($\Omega\times$cm$^2$) |
|---|---|---|---|---|---|
| 1 hour | 30.18 | 5.0770E-04 | 1275 | 2.9310E-06 | 2181 |
| 2 hour | 38.29 | 8.8710E-04 | 717.2 | 8.8220E-06 | 1220 |
| 4 hour | 29.39 | 1.6050E-03 | 583.3 | 2.4710E-05 | 532.2 |
| 8 hour | 19.48 | 3.9560E-03 | 238.5 | 5.6220E-05 | 257.3 |
| 12 hour | 23.36 | 2.7330E-03 | 355.4 | 3.9940E-05 | 371 |
| 24 hour | 23.36 | 2.7330E-03 | 72.98 | 4.5570E-05 | 315.5 |
| 2 day | 30.36 | 3.8150E-03 | 153.5 | 5.0650E-05 | 318.1 |
| 3 day | 33.79 | 4.0360E-03 | 58.66 | 8.0940E-05 | 281.6 |
| 4 day | 31.43 | / | / | 8.6440E-05 | 336.6 |
| 5 day | 29.77 | / | / | 6.6130E-05 | 383.5 |
| 6 day | 33.08 | / | / | 5.4960E-05 | 542.8 |
| 7 day | 31.22 | / | / | 7.6160E-05 | 449.2 |

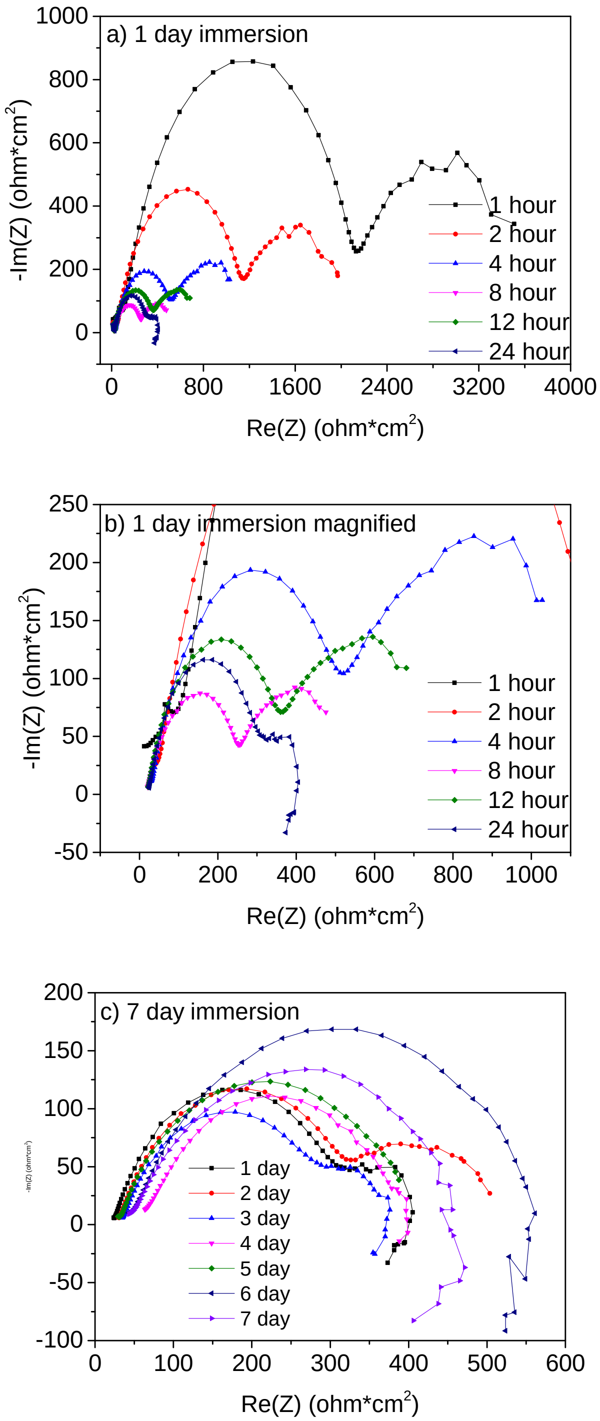


Figure 3.12. Nyquist plots of the 5-minute MAO-coated AZ31 alloy in SBF (a) 1-day immersion, (b) 1-day immersion, magnified Nyquist Re(Z) from -100 to 1100 (ohm*cm$^2$), and (c) 7-day immersion

Figure 3.12 shows that the 5-minute MAO-coated sample also has two capacity loops in the first 3 day immersion. The $R_s$ values stand around 30 $\Omega\times cm^2$. The resistance of charge transfer ($R_{ct}$) dropped in the first 8 hours, the $R_p$ has the similar result when the corrosion happened on the film and more pits were created on the surface. After one day immersion, the values of $R_{ct}$ floated around 300 $\Omega\times cm^2$. This result means the coating layer dissolved from the substrate, and in the meanwhile, the passive layer was created on the surface by chemical reaction. From 4 day to 7 day immersion, the values of $R_{ct}$ increased generally. Table 3.17 shows the EIS data for the 5-minute MAO-coated sample after immersion in the SBF for 7 days.

**15-minute MAO-coated Sample**

The Nyquist plots for the corrosion of the 15-minute MAO-coated AZ31 alloy in simulated body fluid are shown in Figure 3.13.

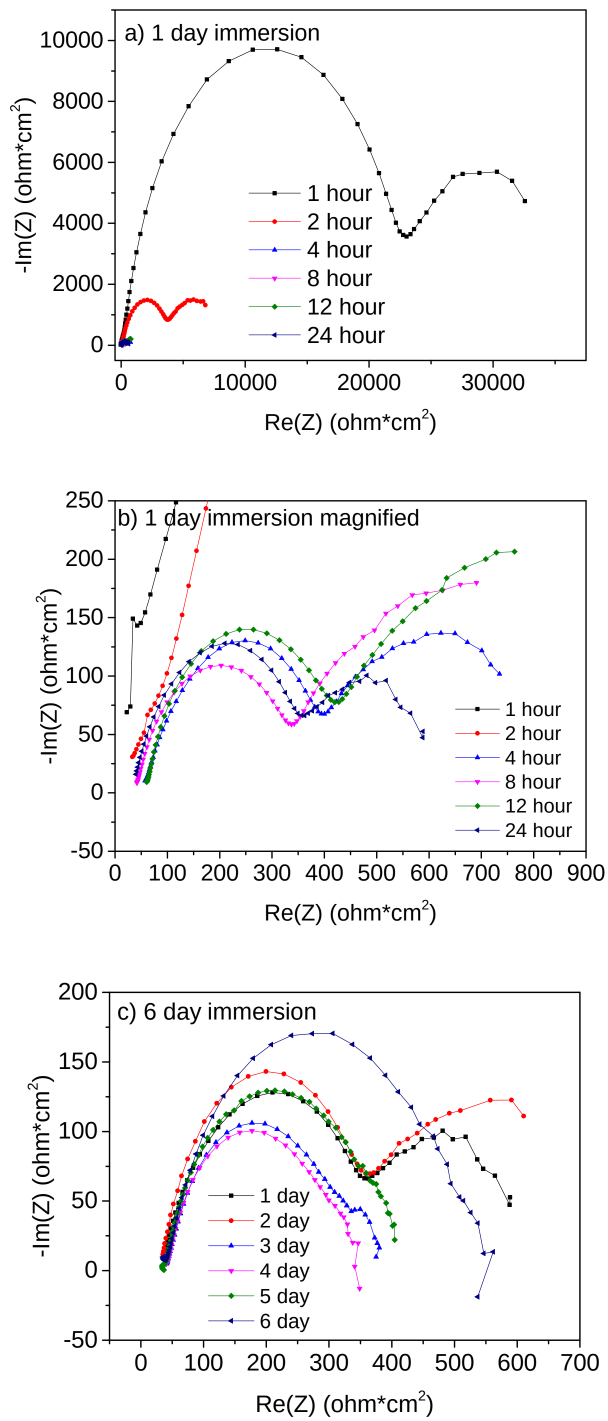


Figure 3.13. Nyquist plots of the 15-minute MAO-coated AZ31 alloy in SBF (a) 1-day immersion, (b) 1-day immersion, magnified Nyquist Re(Z) from 0 to 900 (ohm*cm2), and (c) 6-day immersion

Table 3.18. EIS data for the 15-minute MAO-coated AZ31 magnesium alloys after immersion in the SBF for various durations

| Time | $R_s$ ($\Omega\times$cm$^2$) | CPE-$C_{coating}$ (F) | $R_p$ ($\Omega\times$cm$^2$) | CPE-$C_{dl}$ (F) | $R_{ct}$ ($\Omega\times$cm$^2$) |
|---|---|---|---|---|---|
| 1 hour | 40.1 | 3.6850E-05 | 1.59E+04 | 1.7380E-07 | 2.23E+04 |
| 2 hour | 49.8 | 2.2420E-04 | 3503 | 3.8700E-06 | 4155 |
| 4 hour | 56.72 | 2.3230E-03 | 392.1 | 3.3170E-05 | 367.2 |
| 8 hour | 39.31 | 2.7170E-03 | 553.2 | 3.0700E-05 | 309.7 |
| 12 hour | 59.48 | 2.3500E-03 | 616.5 | 2.1200E-05 | 358.3 |
| 24 hour | 32.74 | 3.1790E-03 | 208.4 | 4.9760E-05 | 359.4 |
| 2 day | 30.93 | 2.5040E-03 | 323.4 | 2.9430E-05 | 353.4 |
| 3 day | 41.78 | 2.6630E-03 | 50.67 | 5.3150E-05 | 286.8 |
| 4 day | 39.98 | / | / | 6.8330E-05 | 298.8 |
| 5 day | 36.75 | / | / | 5.1850E-05 | 375.8 |
| 6 day | 39.97 | / | / | 4.4200E-05 | 494.7 |

Two capacity loops exhibited in the first 3 day immersion for 15-minute MAO-coated sample. The $R_s$ values of 15-minute MAO-coated sample are around 40 $\Omega\times cm^2$. The resistance of charge transfer ($R_{ct}$) decreased until 3 day immersion. That is due to the coating layer dissolved in the electrolyte. From 4 day to 7 day immersion, the $R_{ct}$ values increased since the passive layer was produced on the substrate.

**20-minute MAO-coated Sample**

The Nyquist plots for the corrosion of the 20-minute MAO-coated AZ31 alloy in simulated body fluid are shown in Figure 3.14.

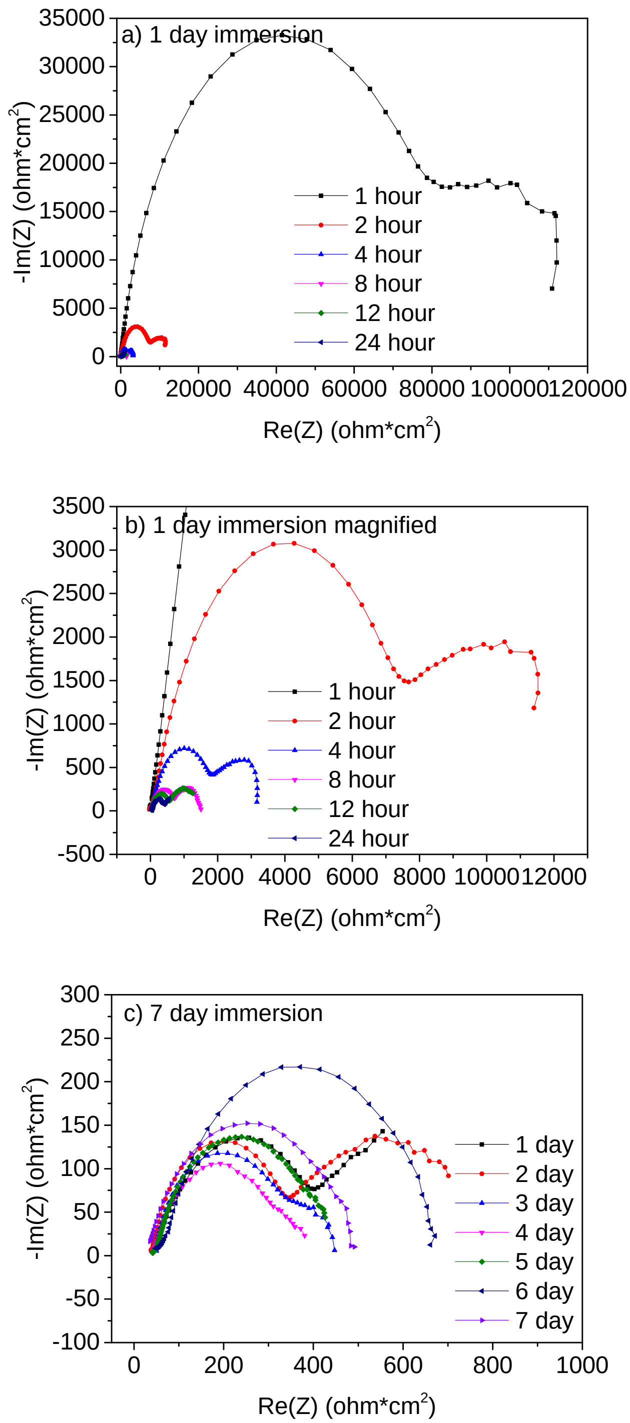


Figure 3.14. Nyquist plots of the 20-minute MAO-coated AZ31 alloy in SBF (a) 1-day immersion, (b) 1-day immersion, magnified Nyquist Re(Z) from -1000 to 13000 (ohm*cm$^2$), and (c) 7-day immersion

Table 3.19. EIS data for the 20-minute MAO-coated AZ31 magnesium alloys after immersion in the SBF for various durations

| Time | $R_s$ ($\Omega\times$cm$^2$) | CPE-$C_{coating}$ (F) | $R_p$ ($\Omega\times$cm$^2$) | CPE-$C_{dl}$ (F) | $R_{ct}$ ($\Omega\times$cm$^2$) |
|---|---|---|---|---|---|
| 1 hour | 43.5 | 2.6690E-05 | 2.31E+04 | 3.3020E-07 | 9.37E+04 |
| 2 hour | 34.23 | 1.7810E-04 | 3514 | 2.3550E-06 | 8652 |
| 4 hour | 49.58 | 5.6370E-04 | 1281 | 1.0250E-05 | 1978 |
| 8 hour | 33.98 | 1.0780E-03 | 658.7 | 2.5020E-05 | 761.9 |
| 12 hour | 37.17 | 1.3030E-03 | 837.5 | 1.8780E-05 | 544.9 |
| 24 hour | 44.89 | 3.4920E-03 | 466.5 | 5.6360E-05 | 394.7 |
| 2 day | 39.56 | 2.7030E-03 | 393.1 | 2.7950E-05 | 317.7 |
| 3 day | 45.1 | 1.7460E-03 | 80.79 | 3.9970E-05 | 317.1 |
| 4 day | 43.18 | / | / | 6.8060E-05 | 321.4 |
| 5 day | 46.05 | / | / | 5.1890E-05 | 401.4 |
| 6 day | 54.42 | / | / | 4.7140E-05 | 653.7 |
| 7 day | 27.22 | / | / | 4.6300E-05 | 471.5 |

According to Table 3.19, it can be found that the $R_{ct}$ was decreased from the first hour to the third day, reaching 317.1 $\Omega\times$cm$^2$. However, after 6 day immersion, the $R_{ct}$ reached 653.7 $\Omega\times$cm$^2$, which is the highest charge transfer resistance from day 2 to day 7. The high corrosion resistance was caused by the passive layer produced on substarte. The $R_s$ values were around 40 $\Omega\times$cm$^2$. The CPE-$C_{dl}$ increased at the beginning of immersion. After 2 day immersion, the CPE-$C_{dl}$ stopped dropping and kept at a stable range at the rest days.

Comparing all the values of uncoated and MAO-coated magensium alloys AZ31, it can be found that the charge transfer resistance ($R_{ct}$) of the 20-minute MAO-coated sample has the highest value at the beginning corrosion since the coating is the thickest. While after 1 day corrosion, the uncoated has the highst $R_{ct}$. The result is due to the coating layer protected the substrate. The passive layer can only be produced on the uncoated substrate. However, with the increase of time, the coating layer provented the simulated body fluid corroding the substarte. However, the uncoated one has been completely exposed in the solution. After dissolving in the solution, the substrate of MAO-coated samples can be protected by creating the passive layers, which increased the corrosion resistance. After 7 day immersion, the 20-minute MAO-coated sample has the highest $R_{ct}$, which means the 20-minute MAO-coated sample can provide the best corrosion resistance. Figure 3.15 and Figure 3.16 show the Nyquist plots and Bode plots of uncoated and MAO-coated samples of 1 day, 3 day, 5 day and 7 day immersion.

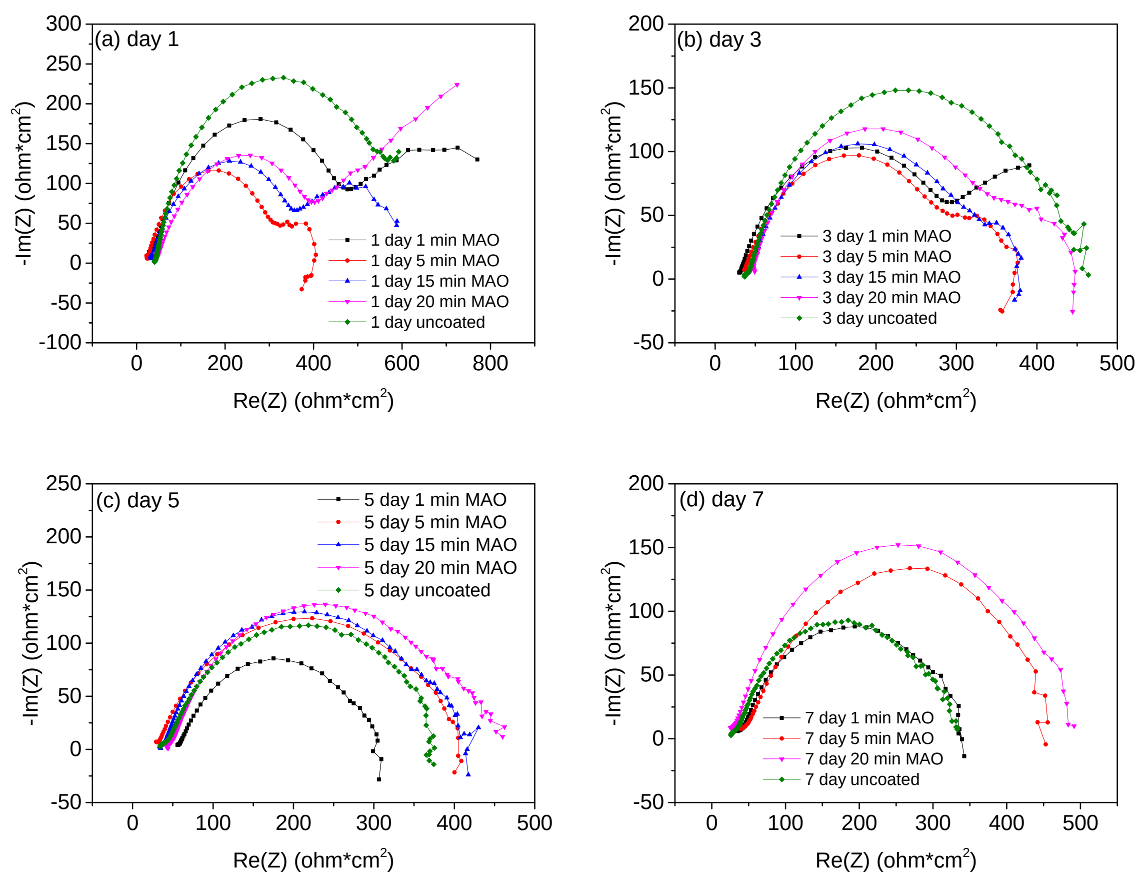


Figure 3.15. Nyquist plots of all samples in the simulated body fluid at(a) day 1, (b) day 3, (c) day 5, and (d) day 7

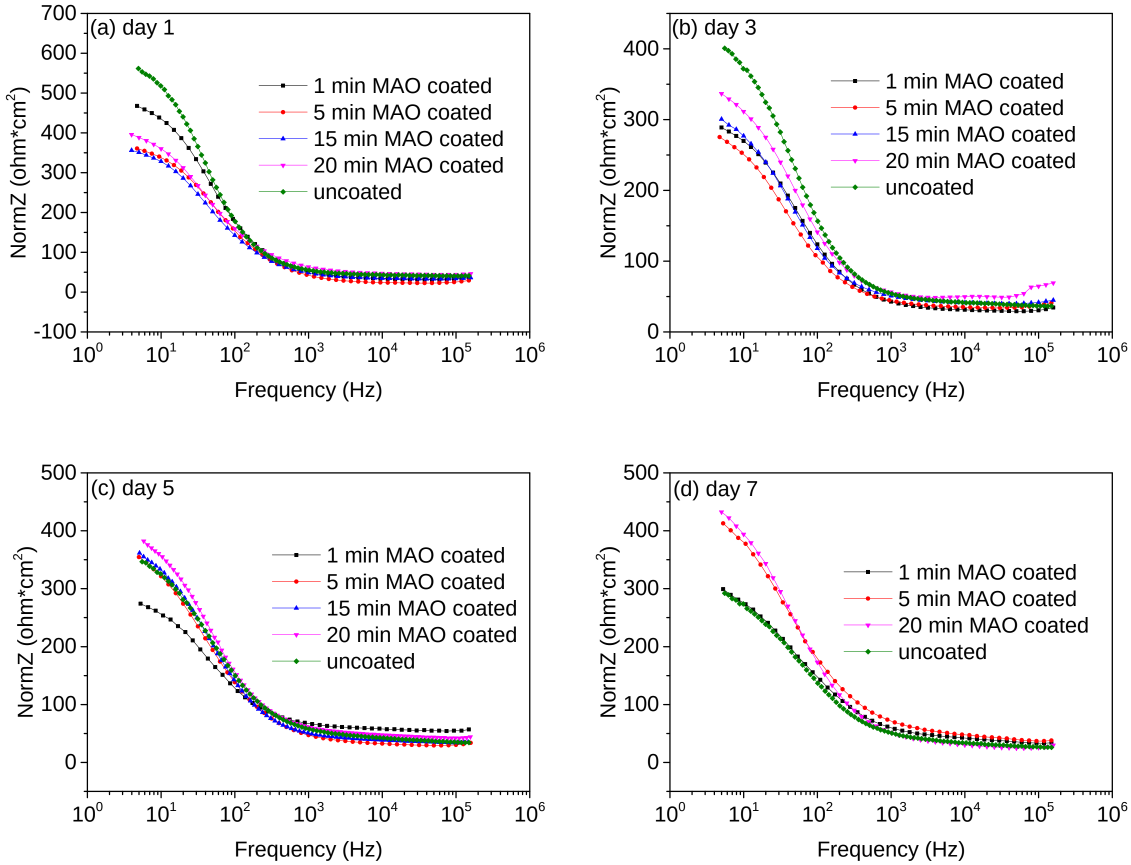


Figure 3.16. Bode plots of all samples in the simulated body fluid at(a) day 1; (b) day 3; (c) day 5, and (d) day 7

## 3.3 Macroscopic and Microscopic Appearances

### 3.3.1 Macroscopic Appearances

Figures 3.17-3.21 demonstrate the changes on the macroscopic surfaces of the uncoated sample and MAO-coated samples after immersing in the SBF from day 1 to day 7. It is apparent that the uncoated and MAO-coated AZ31 magnesium alloys immersed in simulated body fluid dissolved with time. It is also clear that there were pits on the surface. It can be clearly seen that the extent of corrosion damage is significantly increased on the surface of all samples and much alloy dissolved in the SBF. So the area gradually dissolved and the corrosion areas increased as the time increased. For the uncorroded of area, it is easy to find all of the coating samples had a larger area than the uncoated one. Also, the 20-minute MAO-coated samples had the largest remaining area, which means the 20-minute MAO coating is the most effective in protecting the AZ31 magnesium alloy from dissolving in the simulated body fluid.

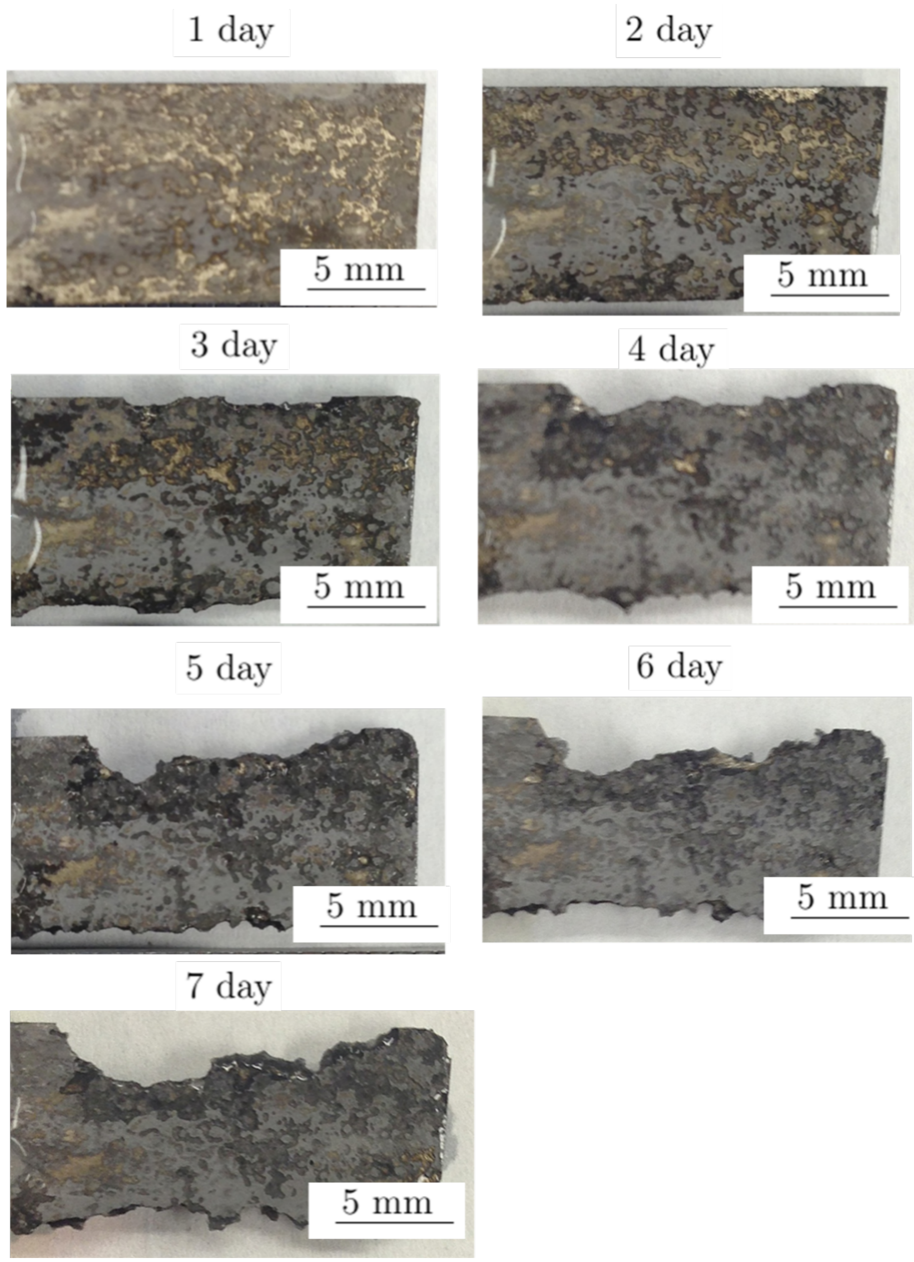


Figure 3.17. Macroscopic appearances of the uncoated AZ31 alloy after immersion in the SBF

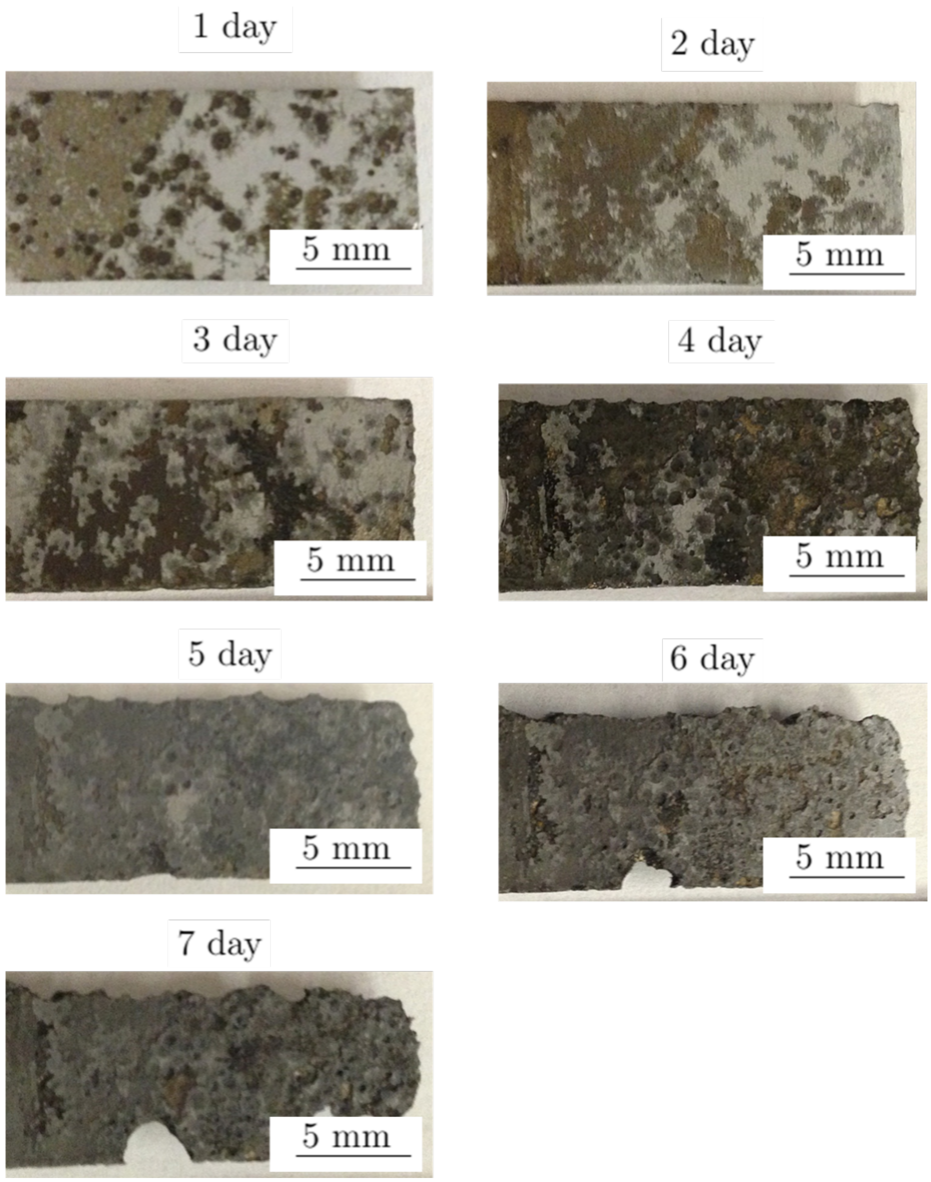


Figure 3.18. Macroscopic appearances of the 1-minute MAO-coated AZ31 alloy after immersion in the SBF

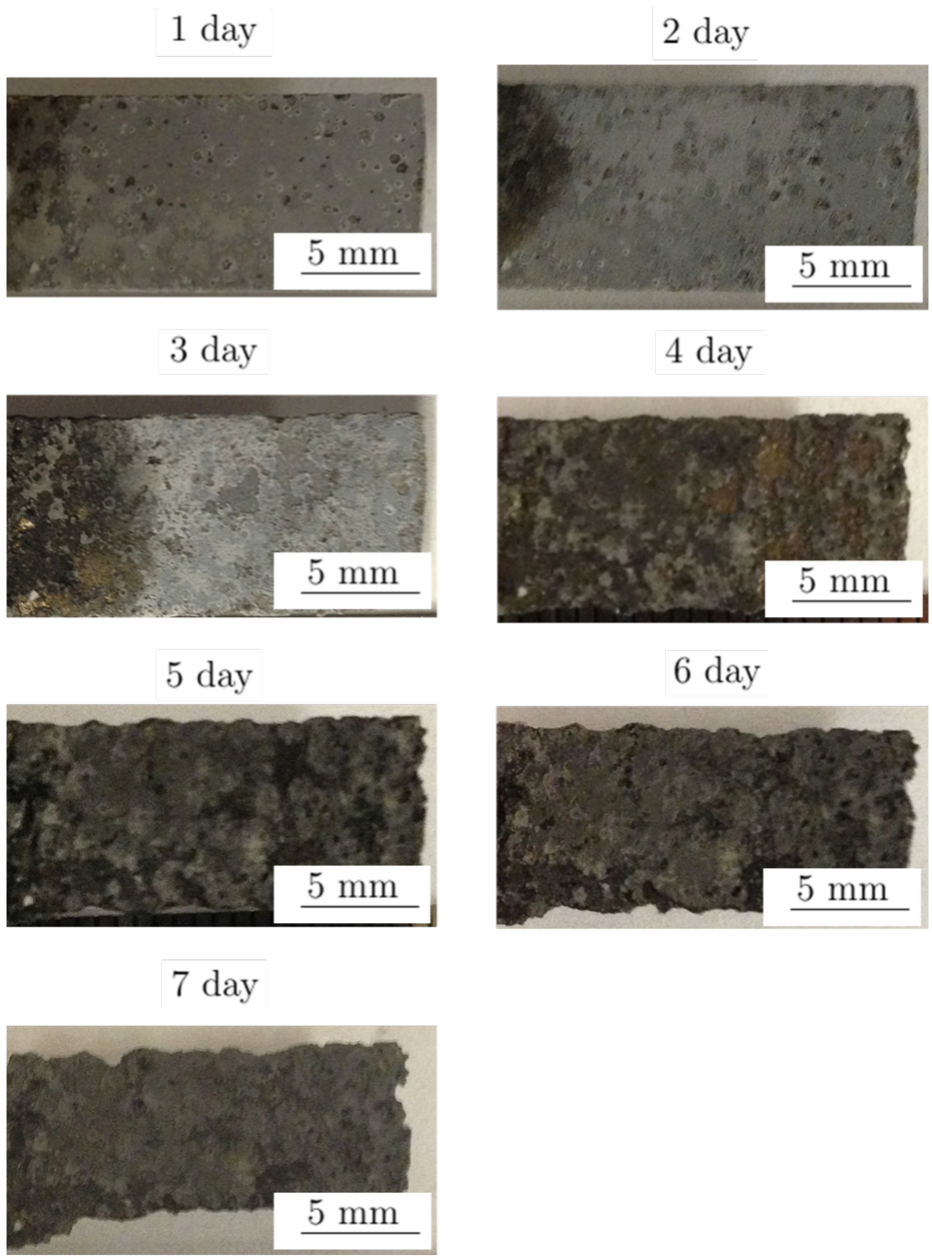


Figure 3.19. Macroscopic appearances of the 5-minute MAO-coated AZ31 alloy after immersion in the SBF

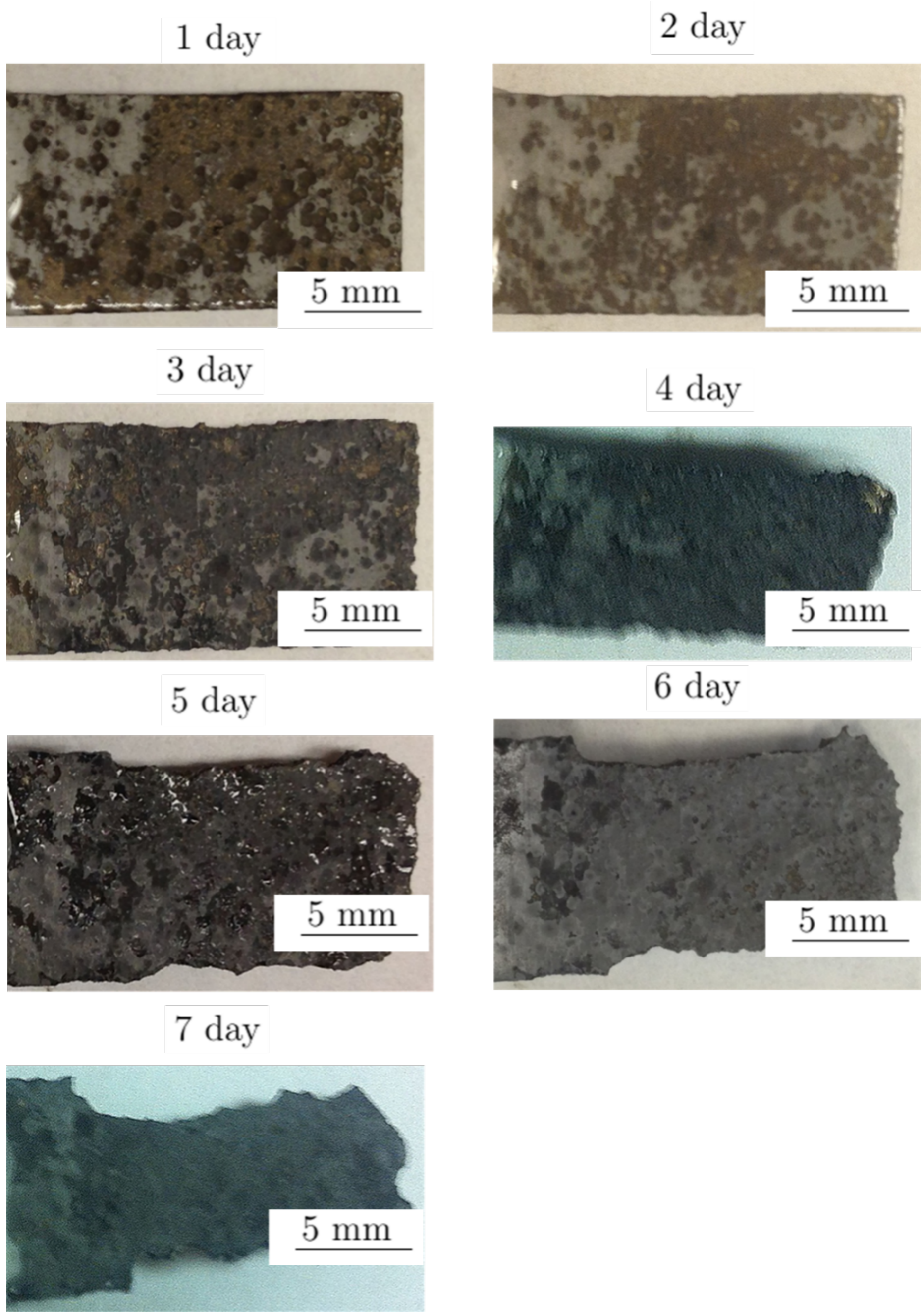


Figure 3.20. Macroscopic appearances of the 15-minute MAO-coated AZ31 alloy after immersion in the SBF

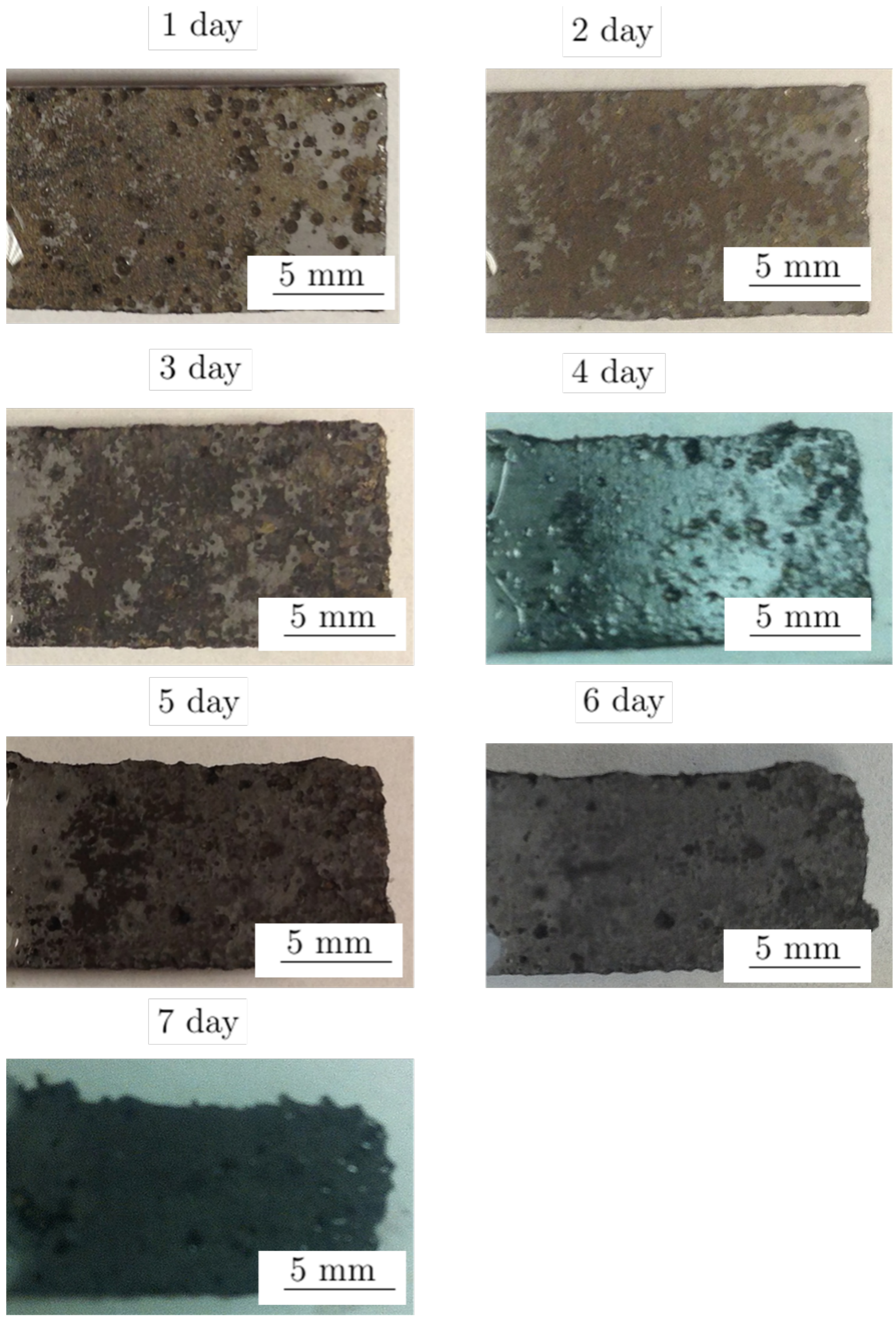


Figure 3.21. Macroscopic appearances of the 20-minute MAO-coated AZ31 alloy after immersion in the SBF

### 3.3.2 Microscopic Appearances

Using the microscopic images in Figures 3.22-3.26, the evaluations of the corrosion damage were observed. It shows that the surfaces of MAO-coated samples were protected by a dense coating layer in the beginning days of immersion, while the dark areas increased with the increasing time. At the end of seven days of immersion, the coatings were totally dissolved in the solution. The formation and promotion of pits were caused by prior large cathodic polarization [49].

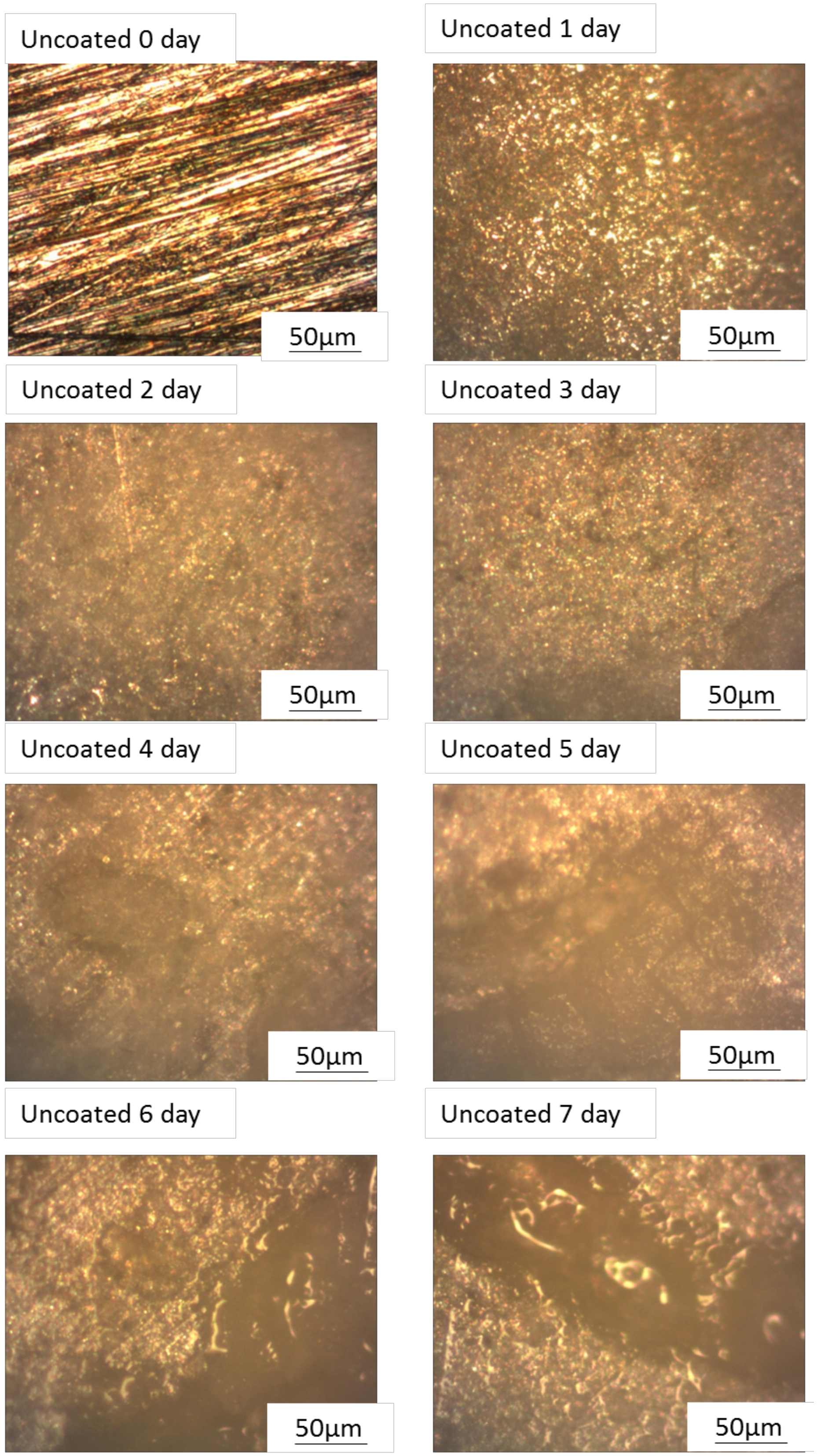


Figure 3.22. Surface microscopic images of the uncoated AZ31 magnesium alloy after immersion in the SBF for various durations

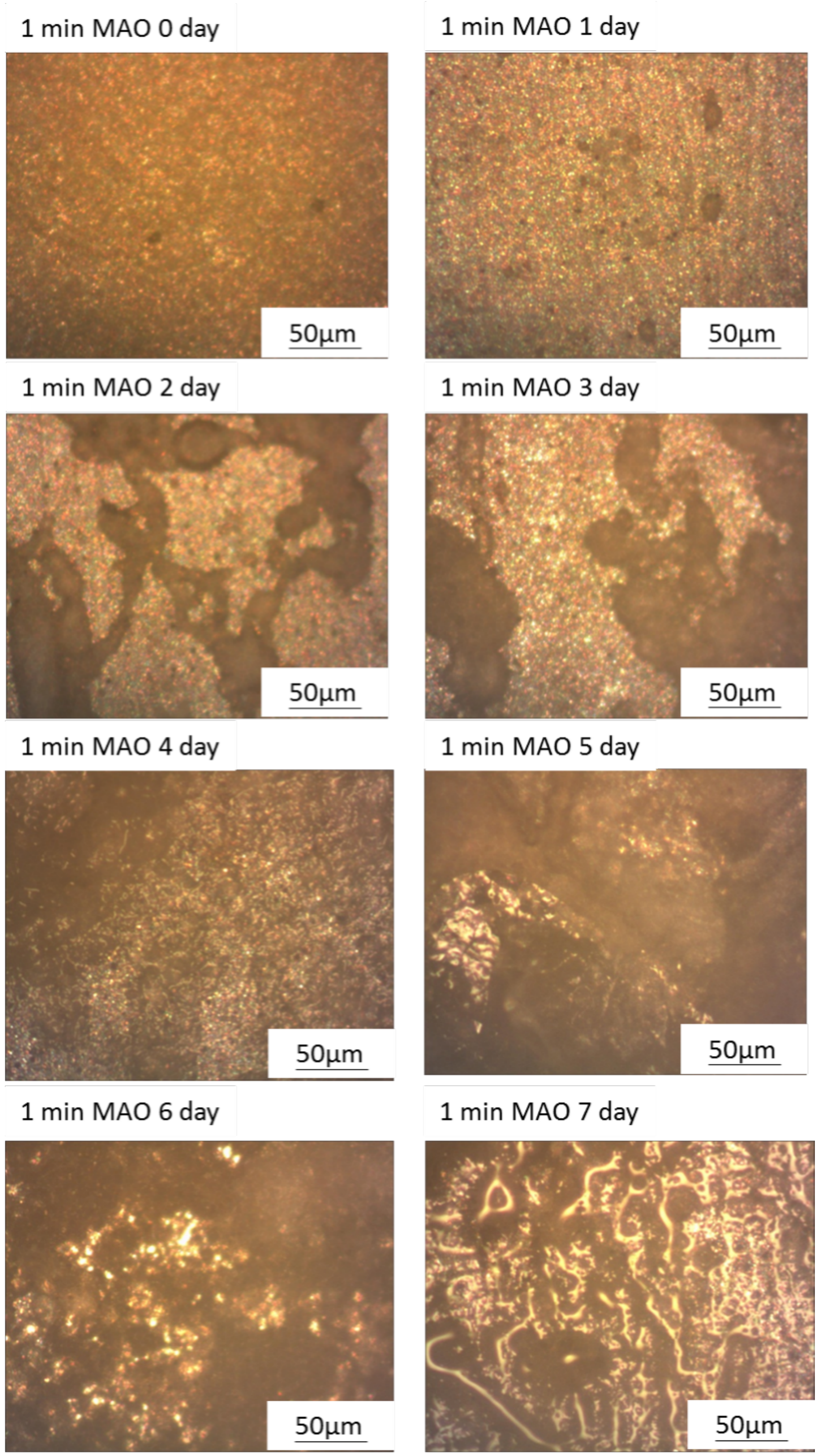


Figure 3.23. Surface microscopic images of the 1-minute MAO-coated AZ31 magnesium alloy after immersion in the SBF for various durations

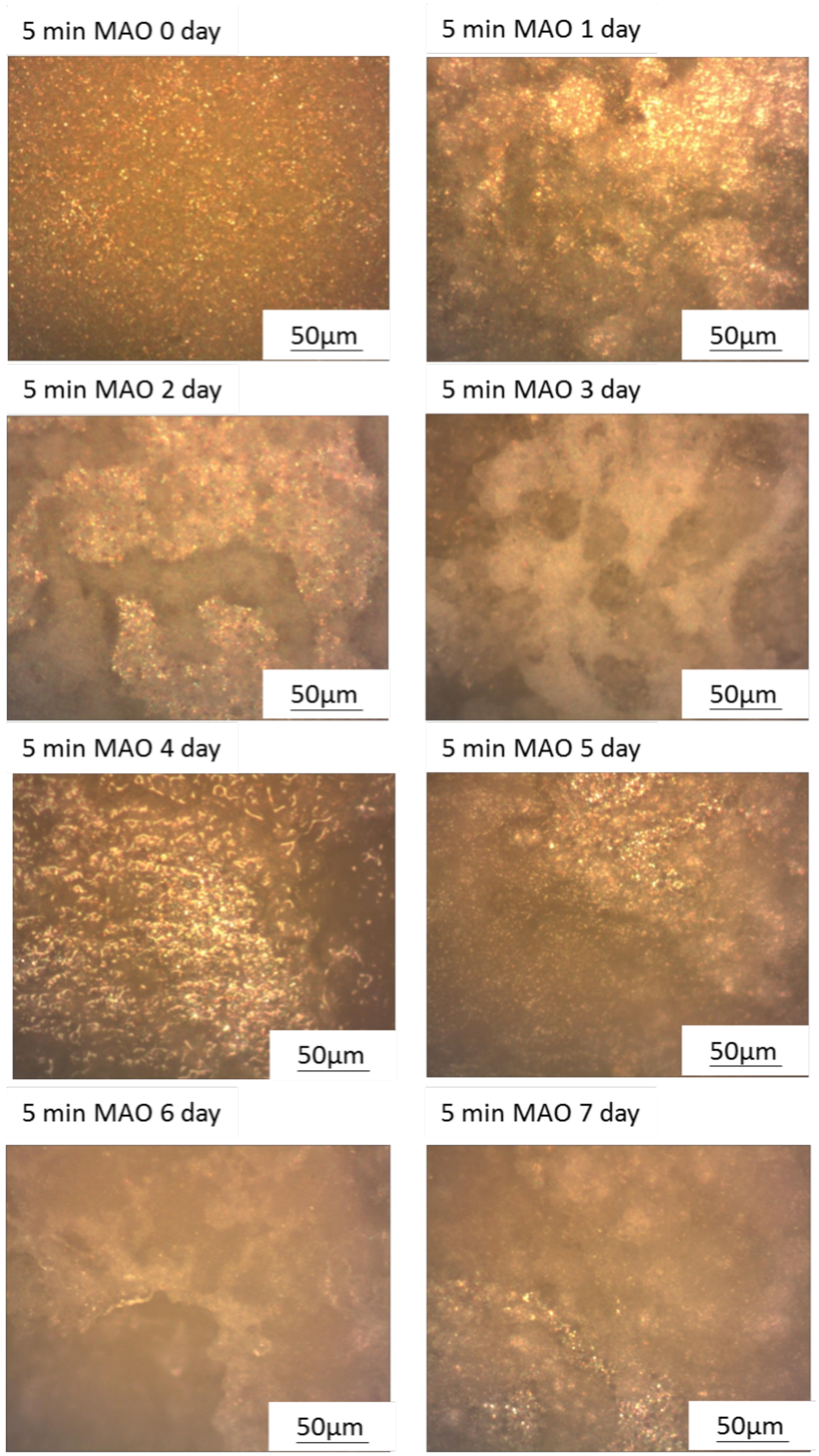


Figure 3.24. Surface microscopic images of the 5-minute MAO-coated AZ31 magnesium alloy after immersion in the SBF for various durations

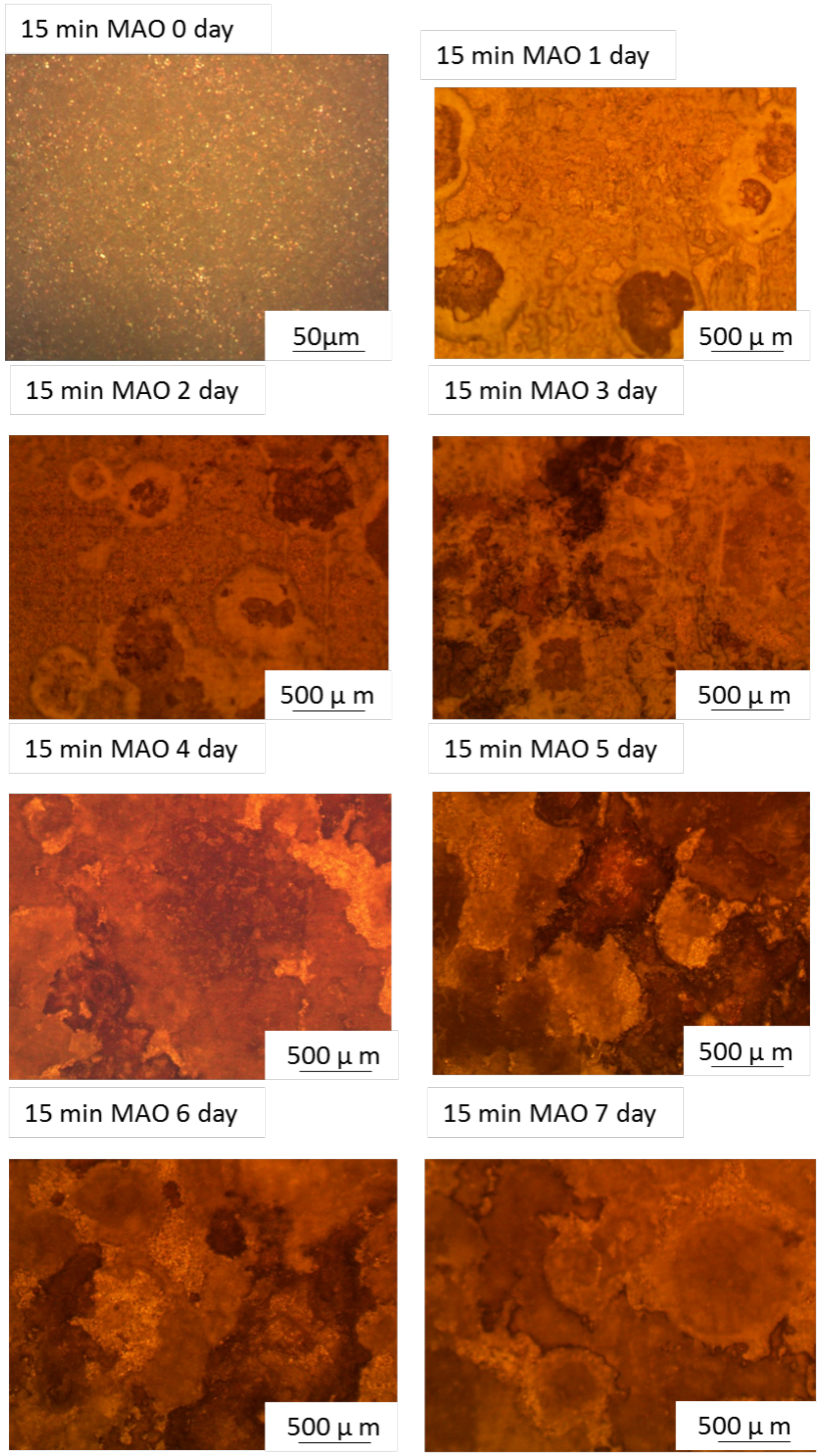


Figure 3.25. Surface microscopic images of the 15-minute MAO-coated AZ31 magnesium alloy after immersion in the SBF for various durations

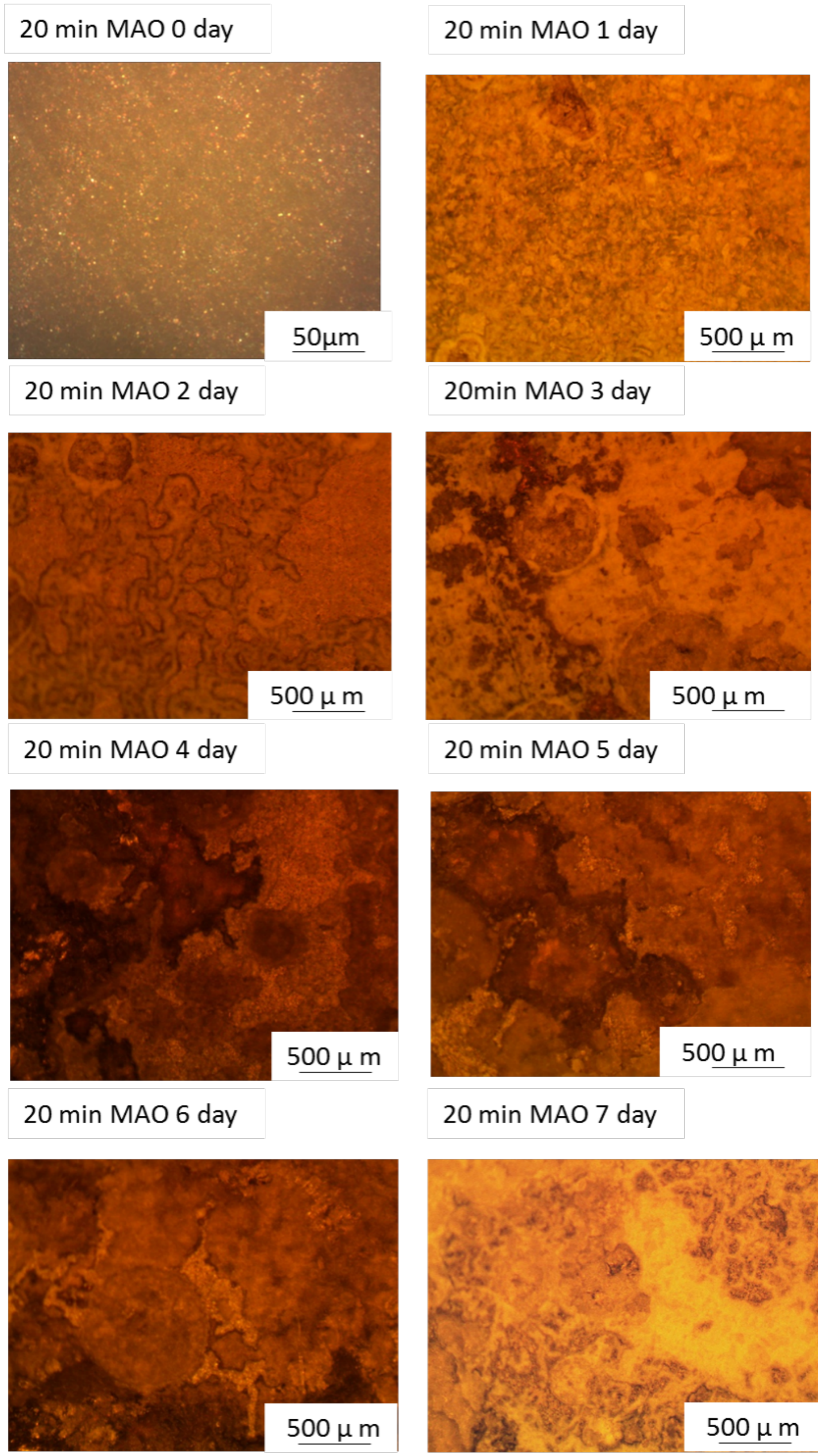


Figure 3.26. Surface microscopic images of the 20-minute MAO-coated AZ31 magnesium alloy after immersion in the SBF for various durations

Figure 3.27 shows the schematical corrosion process of the MAO-coated and uncoated samples. The bubbles represent hydrogen gas. The passive layer occurred when the MAO coating dissolved into the electrolyte. The chemical reactions are listed: In the anode regions:

$$Mg + H_2O \rightarrow Mg^{2+} + OH^- + \frac{1}{2}H_2 + e^- \tag{3.8}$$

In the cathode regions:

$$H_2O + e^- \rightarrow OH^- + 1/2H_2 \tag{3.9}$$

The total reaction:

$$Mg + H_2O \rightarrow Mg(OH)_2 + H_2 \tag{3.10}$$

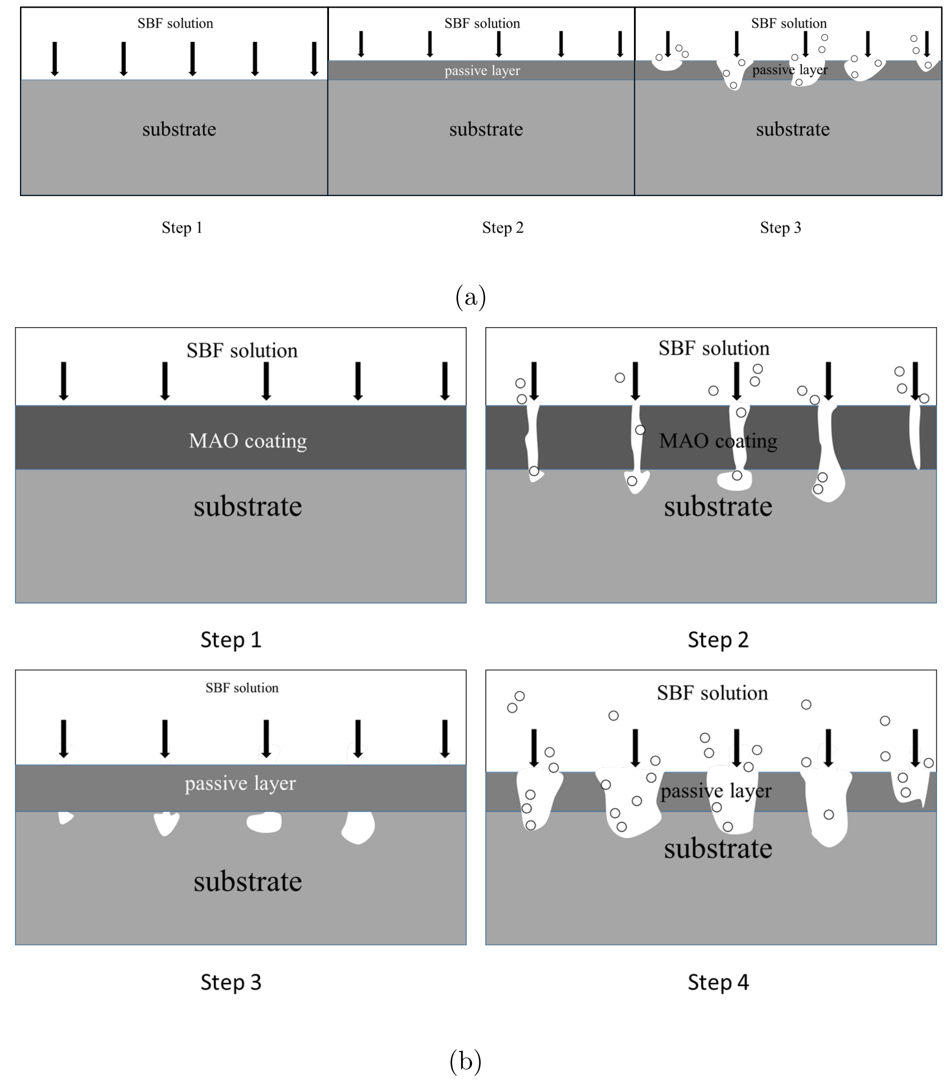


Figure 3.27. Schematic diagram of the corrosion process and mechanism in the SBF (a) uncoated sample; (b) the MAO-coated samples

# 4. ELECTROCHEMICAL BEHAVIORS OF UNCOATED AND MAO-COATED AZ31 MAGNESIUM ALLOY IN CELL CULTURE MEDIUM

The use of magnesium and its alloys for biomedical applications is limited by some obstacles, including their kinetic biodegradation in human physiological fluids, which are considered highly complex media due to the presence of many components, such as amino acids, salts, glucose or vitamins [13, 50–52]. One issue that must be taken into account is that corrosion tests are strongly influenced by the composition of the physiological solution used as an electrolyte when evaluating the biodegradation of magnesium and its alloys [53]. In this chapter, the electrolyte solution used for testing is the cell culture medium, which is much closer to vivo biological fluid than simulated body fluid but with fewer ions. The same tests, potentiodynamic polarization and electrochemical impedance spectroscopy (EIS), were also conducted.

## 4.1 Electrochemical Corrosion Experiments

In this research, the potentiodynamic polarization and electrochemical impedance spectroscopy tests were used to assess the electrochemical properties of both MAO-coated and uncoated magnesium alloys AZ31 samples in a cell culture medium.

### 4.1.1 Experimental Setup and Preparation of Cell Culture Medium

The experimental approaches for culture medium tests on uncoated and MAO-coated samples were the same as the approaches for simulated body fluid ones, including potentiodynamic polarization and electrochemical impedance spectroscopy. All the tested samples had been treated in the same way as the samples in the SBF tests. The cell culture medium contains all the ingredients needed to maintain cells in a culture (amino acids, vitamins, salts, glucose, buffers, phenol red, etc ) [58]. The reagents of cell culture medium are shown in the Table 4.1.

Table 4.1. Reagents for preparation of the cell culture medium (pH 7.4, 1L)

| Reagent | Vender | Amount |
|---|---|---|
| $\alpha$-Minimal Essential Medium | Sigma | 10mg |
| 10% fetal bovine serum | GeneTex | 100ml |
| Antibiotic | Sigma | 10ml |
| $NaHCO_3$ | Sigma | 2.2g |

## 4.2 Results of Electrochemical Behaviors in Immersed in Cell Culture Medium

### 4.2.1 Potentiodynamic Polarization

**Uncoated Sample**

The behaviors of potentiodynamic polarization in the cell culture medium are presented in this section. The potentiodynamic polarization curves of uncoated AZ31 alloy immersed in the culture medium are shown in Figure 4.1.The corrosion potential ($E_{corr}$) and the corrosion current density ($I_{corr}$), were generated directly from the Tafel plots.

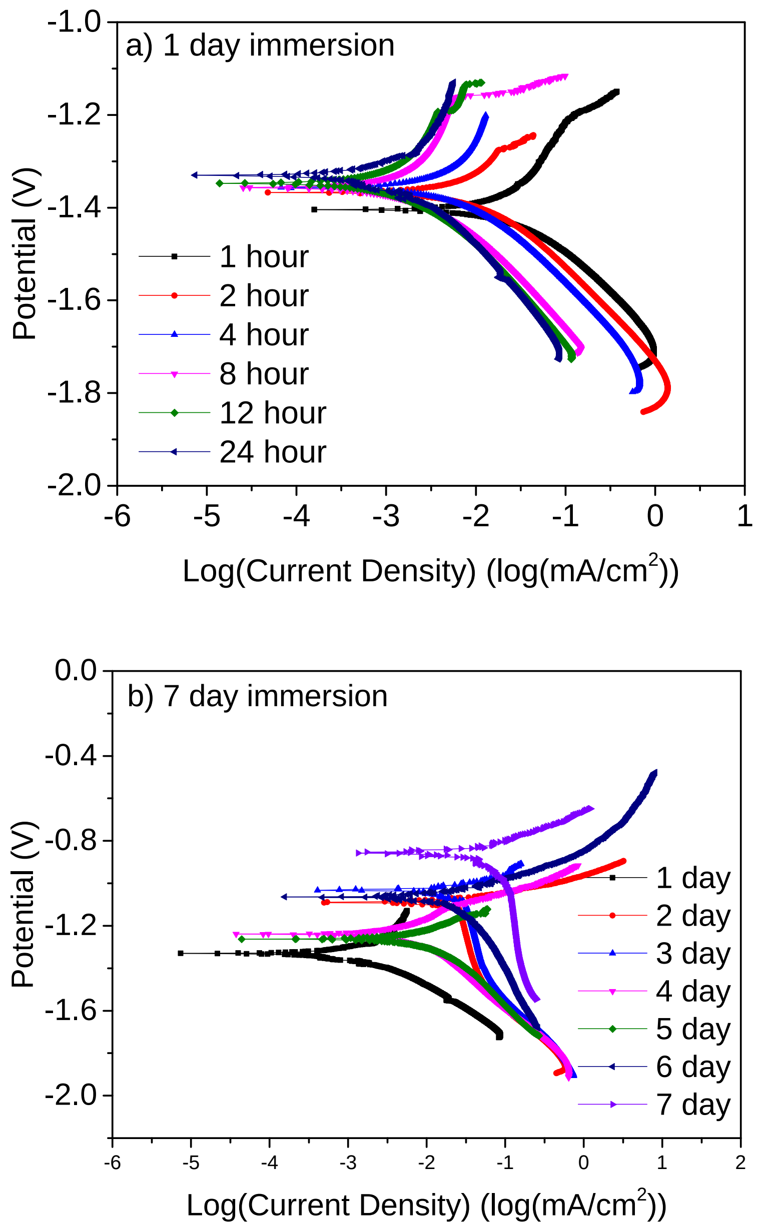


Figure 4.1. Tafel plots of the uncoated AZ31 alloys in the cell culture medium at: (a) 1-day immersion, and (b) 7-day immersion

According to Table 4.2, the $E_{corr}$ values of the uncoated sample increased generally after 7 days of immersion. Furthermore, the breakdown voltage can be observed on the Tafel curves, which means the AZ31 magnesium alloy became electrically conductive when the voltage increased beyond the potential on the turning point. The values of $E_{corr}$ from the 1st hour to day 7 are shown in Table 4.2.

Table 4.2. Corrosion potential ($E_{corr}$) of the uncoated sample in the cell culture medium

| Time | $E_{corr}$ (V) | Time | $E_{corr}$ (V) |
|---|---|---|---|
| 1 hour | -1.406 | 2 day | -1.091 |
| 2 hour | -1.368 | 3 day | -1.029 |
| 4 hour | -1.356 | 4 day | -1.240 |
| 8 hour | -1.357 | 5 day | -1.262 |
| 12 hour | -1.346 | 6 day | -1.062 |
| 24 hour | -1.330 | 7 day | -0.851 |

The corrosion current density ($I_{corr}$) was deduced from the extrapolation of the cathodic branch of the Tafel curves to the corrosion potential. Table 4.3 shows the results of corrosion current density ($I_{corr}$).

The $I_{corr}$ values decreased with the accumulation of immersion time in the first day. That means the corrosion rate dropped in the first day. The passive layer was created by phosphate ions and carbonate ions, and these precipitated with the magnesium alloy on the surface of sample [54]. The corrosion current density reached a stable value since the inhibitory reaction and corrosion reaction worked on the sample surface in the same time. On the last day, a great increase in the corrosion current density was caused by the impetus of some corrosion pits, which can be found in microscopic images.

Table 4.3. Corrosion potential ($I_{corr}$) of the uncoated sample in the cell culture medium

| Time | $I_{corr}$ (mA/cm$^2$) | Time | $I_{corr}$ (mA/cm$^2$) |
|---|---|---|---|
| 1 hour | 0.0359 | 2 day | 0.0255 |
| 2 hour | 0.0137 | 3 day | 0.0292 |
| 4 hour | 0.0071 | 4 day | 0.0101 |
| 8 hour | 0.0031 | 5 day | 0.0105 |
| 12 hour | 0.0022 | 6 day | 0.0297 |
| 24 hour | 0.0015 | 7 day | 0.0930 |

**1-minute MAO-coated Sample**

The potentiodynamic polarization curves of the 1-minute MAO-coated AZ31 alloy immersed in the culture medium are shown in Figure 4.2.

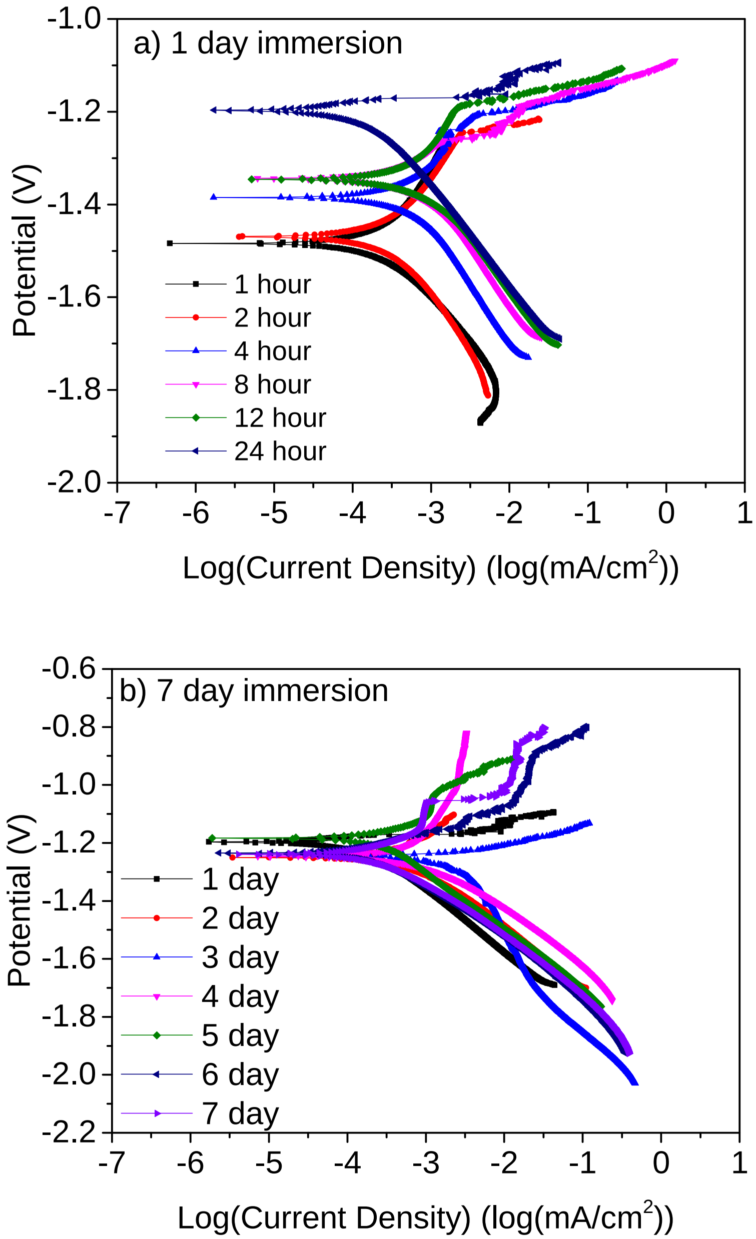


Figure 4.2. Tafel plots of 1-minute MAO-coated AZ31 alloys in the cell culture medium at: (a) 1-day immersion, and (b) 7-day immersion

The $E_{corr}$ values of the 1-minute MAO-coated sample are shown in Table 4.4. It is demonstrated that the $E_{corr}$ increased generally in the 7-day immersion. The breakdown voltage can also be found on the Tafel curves, around -1.2 V, which is lower than the uncoated sample.

Table 4.4. Corrosion potential ($E_{corr}$) of the 1-minute MAO-coated sample in the cell culture medium

| Time | $E_{corr}$ (V) | Time | $E_{corr}$ (V) |
|---|---|---|---|
| 1 hour | -1.484 | 2 day | -1.251 |
| 2 hour | -1.471 | 3 day | -1.245 |
| 4 hour | -1.385 | 4 day | -1.253 |
| 8 hour | -1.342 | 5 day | -1.181 |
| 12 hour | -1.341 | 6 day | -1.234 |
| 24 hour | -1.199 | 7 day | -1.236 |

Table 4.5. Corrosion potential ($I_{corr}$) of the 1-minute MAO-coated sample in the cell culture medium

| Time | $I_{corr}$ (mA/cm$^2$) | Time | $I_{corr}$ (mA/cm$^2$) |
|---|---|---|---|
| 1 hour | 2.332E-04 | 2 day | 7.274E-04 |
| 2 hour | 3.325E-04 | 3 day | 1.239E-03 |
| 4 hour | 6.194E-04 | 4 day | 8.351E-04 |
| 8 hour | 7.821E-04 | 5 day | 1.651E-04 |
| 12 hour | 9.412E-04 | 6 day | 2.281E-04 |
| 24 hour | 1.621E-04 | 7 day | 4.252E-04 |

The corrosion current density ($I_{corr}$) of the 1-minute MAO-coated sample is shown in Table 4.5. The average value of $I_{corr}$ is much lower than that of the uncoated sample in cell culture medium. The $I_{corr}$ increased with the accumulation of immersion time in the first 12 hours. It is caused by chloride ions effect, which can shuttle into the coating pores and induce the pitting corrosion on the substrate surface [52]. While after 24 hours, the tunnels in the coating were blocked by some large molecules which contained in the culture medium solution and stopped the chloride ion touching the surface of substrate. After one day immersion, the corrosion current density kept at a stable range because the corrosion bahaviors and inhibitory actions provided by protected layer reached the balance after one day immersion.

**5-minute MAO-coated Sample**

The potentiodynamic polarization curves of the 5-minute MAO-coated AZ31 alloy immersed in the culture medium are shown in Figure 4.3.

The value of $E_{corr}$ from 1 hour to day 7 are shown in Table 4.6. The $E_{corr}$ values of the 5-minute MAO-coated sample increased generally in 7 day immersion. Similarly, the breakdown potential points occurred on the Tafel curves, which made the 5-minute MAO coated sample become electrically conductive in the cell culture medium as the voltage beyond the potential around -1.0 V.

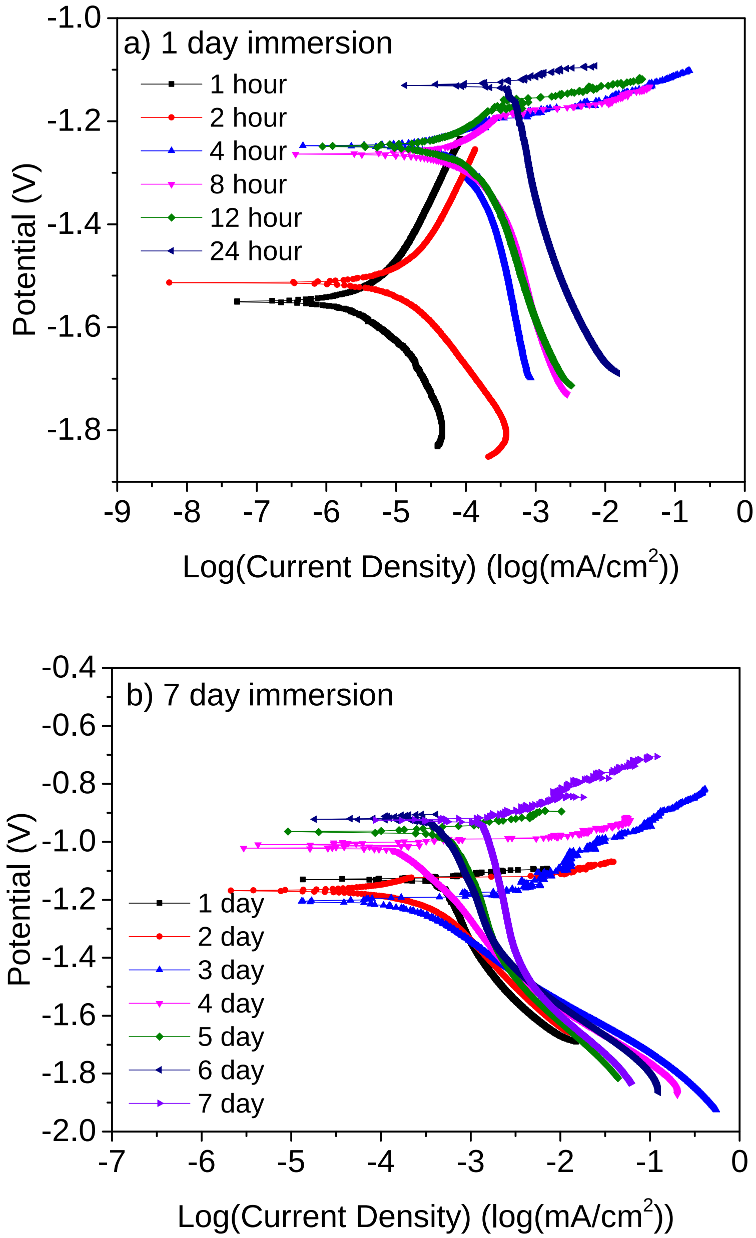


Figure 4.3. Tafel plots of the 5-minute MAO-coated AZ31 alloys in the cell culture medium at: (a) 1-day immersion, and (b) 7-day immersion

Table 4.6. Corrosion potential ($E_{corr}$) of the 5-minute MAO-coated sample in the cell culture medium

| Time | $E_{corr}$ (V) | Time | $E_{corr}$ (V) |
|---|---|---|---|
| 1 hour | -1.549 | 2 day | -1.167 |
| 2 hour | -1.514 | 3 day | -1.204 |
| 4 hour | -1.247 | 4 day | -1.022 |
| 8 hour | -1.265 | 5 day | -0.964 |
| 12 hour | -1.250 | 6 day | -0.924 |
| 24 hour | -1.132 | 7 day | -0.929 |

Table 4.7. Corrosion potential ($I_{corr}$) of the 5-minute MAO-coated sample in the cell culture medium

| Time | $I_{corr}$ (mA/cm$^2$) | Time | $I_{corr}$ (mA/cm$^2$) |
|---|---|---|---|
| 1 hour | 7.332E-06 | 2 day | 3.536E-04 |
| 2 hour | 1.244E-05 | 3 day | 1.746E-04 |
| 4 hour | 1.506E-04 | 4 day | 1.798E-04 |
| 8 hour | 1.988E-04 | 5 day | 6.716E-04 |
| 12 hour | 1.622E-04 | 6 day | 5.379E-04 |
| 24 hour | 4.961E-04 | 7 day | 1.482E-03 |

Table 4.7 shows the results of corrosion current density ($I_{corr}$). The $I_{corr}$ values rose with the accumulation of immersion time in the first day. After one day immersion, the corrosion current density kept at a stable range. The varied trend of $I_{corr}$ values of 5-minute MAO-coated sample is similar to the one of the 1-minute MAO-coated sample.

**15-minute MAO-coated Sample**

The potentiodynamic polarization curves of the 15-minute MAO-coated AZ31 alloy immersed in the culture medium are shown in Figure 4.4.

The values of $E_{corr}$ from 1 hour to day 7 are shown in Table 4.8. Similar to the 5-minute MAO-coated sample, the $E_{corr}$ values of the 15-minute MAO-coated sample increased in 7-day immersion. Also some breakdown points occurred on the Tafel curves which means the AZ31 magnesium alloy with the 15-minute MAO coating became electrically conductive when the voltage beyond the potential on the turning point.

Table 4.8. Corrosion potential ($E_{corr}$) of the 15-minute MAO-coated sample in the cell culture medium

| Time | $E_{corr}$ (V) | Time | $E_{corr}$ (V) |
|---|---|---|---|
| 1 hour | -1.419 | 2 day | -1.297 |
| 2 hour | -1.453 | 3 day | -1.290 |
| 4 hour | -1.236 | 4 day | -1.184 |
| 8 hour | -1.345 | 5 day | -1.196 |
| 12 hour | -1.335 | 6 day | -1.080 |
| 24 hour | -1.286 | 7 day | -1.218 |

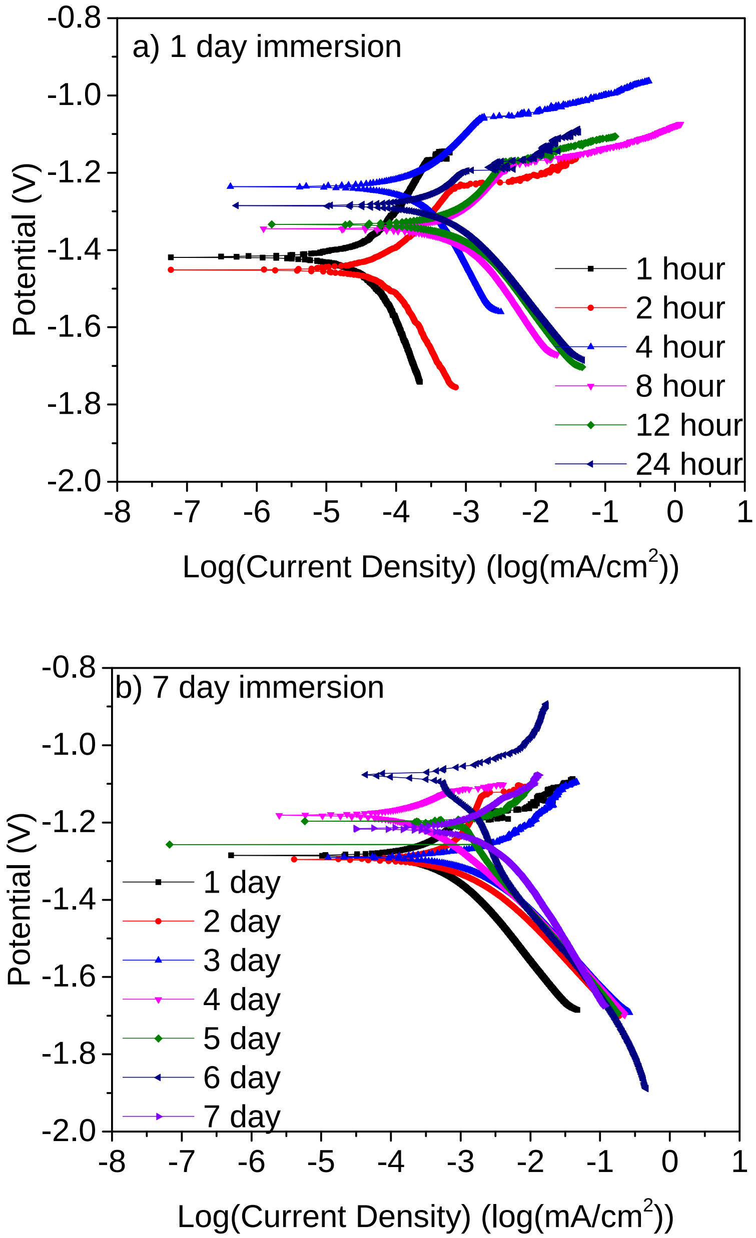


Figure 4.4. Tafel plots of the 15-minute MAO-coated AZ31 alloys in the cell culture medium at: (a) 1-day immersion, and (b) 7-day immersion

Table 4.9. Corrosion potential ($I_{corr}$) of the 15-minute MAO-coated sample in the cell culture medium

| Time | $I_{corr}$ (mA/cm$^2$) | Time | $I_{corr}$ (mA/cm$^2$) |
|---|---|---|---|
| 1 hour | 4.538E-05 | 2 day | 4.041E-03 |
| 2 hour | 7.534E-05 | 3 day | 1.589E-03 |
| 4 hour | 2.597E-04 | 4 day | 2.811E-04 |
| 8 hour | 9.945E-04 | 5 day | 1.153E-03 |
| 12 hour | 1.077E-03 | 6 day | 1.203E-03 |
| 24 hour | 3.716E-04 | 7 day | 3.203E-03 |

Table 4.9 shows the results of corrosion current density ($I_{corr}$). The $I_{corr}$ values of the 15-minute MAO-coated sample increased from 1 hour to 7 day immersion. The average value of the $I_{corr}$ is a little bit higher than the 1-minute and 5-minute MAO coated samples.

**20-minute MAO-coated Sample**

The potentiodynamic polarization curves of the 20-minute MAO-coated AZ31 alloy immersed in the culture medium are shown in Figure 4.5.

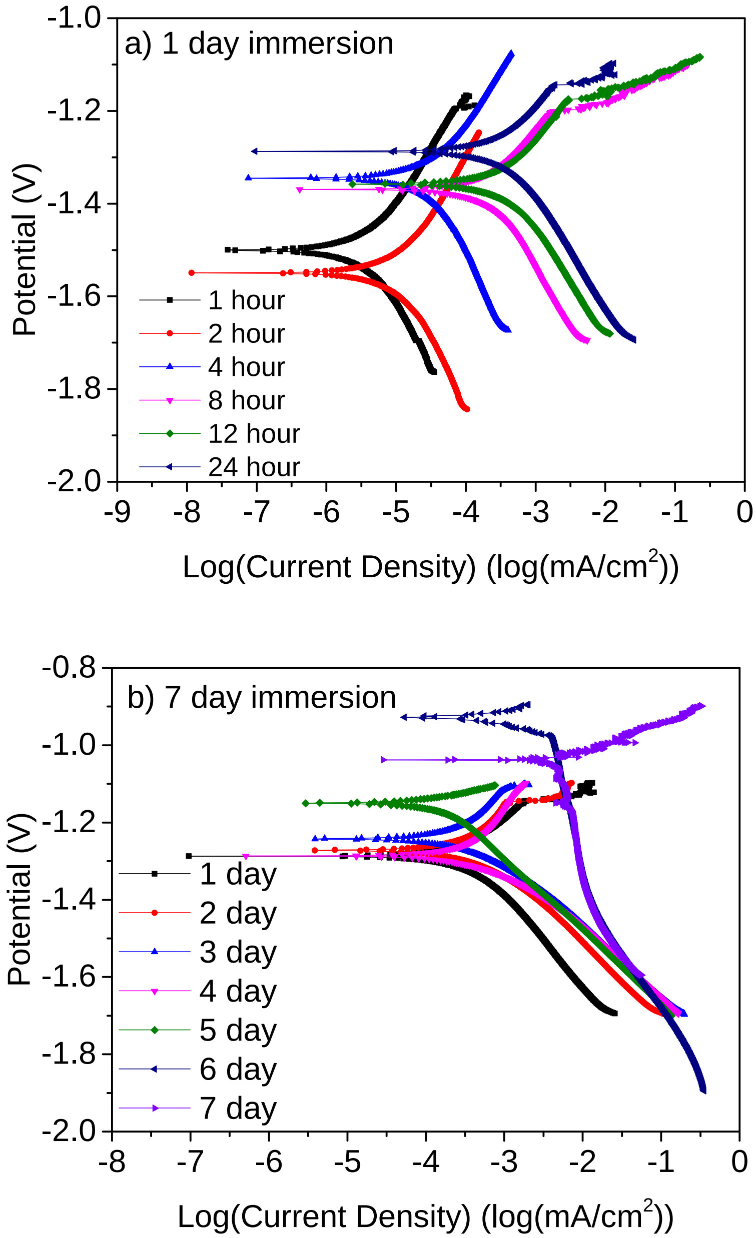


Figure 4.5. Tafel plots of the 20-minute MAO-coated AZ31 alloys in the cell culture medium at: (a) 1-day immersion, and (b) 7-day immersion

The values of $E_{corr}$ from 1 hour to day 7 are shown in Table 4.10. The shape of the Tafel curves of 20-minuite MAO-coated sample is similar to the other MAO-coated samples, with the breakdown points on the Tafel curves. The $E_{corr}$ values of the 20-minute MAO-coated sample increased generally in 7 days immersion.

Table 4.10. Corrosion potential ($E_{corr}$) of the 20-minute MAO-coated sample in the cell culture medium

| Time | $E_{corr}$ (V) | Time | $E_{corr}$ (V) |
|---|---|---|---|
| 1 hour | -1.499 | 2 day | -1.272 |
| 2 hour | -1.550 | 3 day | -1.243 |
| 4 hour | -1.347 | 4 day | -1.286 |
| 8 hour | -1.371 | 5 day | -1.150 |
| 12 hour | -1.358 | 6 day | -0.925 |
| 24 hour | -1.287 | 7 day | -1.037 |

Table 4.11. Corrosion potential ($I_{corr}$) of the 20-minute MAO-coated sample in the cell culture medium

| Time | $I_{corr}$ (mA/cm$^2$) | Time | $I_{corr}$ (mA/cm$^2$) |
|---|---|---|---|
| 1 hour | 3.776E-06 | 2 day | 7.208E-04 |
| 2 hour | 1.190E-05 | 3 day | 4.660E-04 |
| 4 hour | 3.545E-05 | 4 day | 6.502E-04 |
| 8 hour | 2.616E-04 | 5 day | 2.049E-04 |
| 12 hour | 4.753E-04 | 6 day | 3.670E-03 |
| 24 hour | 5.129E-04 | 7 day | 5.317E-03 |

According to the corrosion current density results in Table 4.11, the $I_{corr}$ values increased generally with the accumulation of immersion time in the whole process of the immersion test. Although the $I_{corr}$ values of 20-minute MAO-coated sample increased and reached the highest value after 7 day immersion, it is close to the $I_{corr}$ values of other MAO-coated samples. Also, the $I_{corr}$ of 20-minute MAO-coated sample in the cell culture medium is much lower than the value in the simulated body fluid.

Figure 4.6 shows the comparison of all MAO-coated samples from day 1 to day 7. According to those results, it is clear to see that at the beginning of immersion, the uncoated sample showed the lowest corrosion potential, while all the MAO-coated samples had lower corrosion current densities. This means all the coated samples have lower corrosion rates. After the 7-day immersion, all the MAO-coated samples had lower corrosion potential than the uncoated one.

Figure 4.7 shows the corrosion rate evolution of the MAO-coated and uncoated samples in the cell culture medium. It can be found that the corrosion rates of MAO-coated samples in the cell culture medium are similar. They are much lower than the uncoated one. Also, the corrosion rates in the cell culture medium are much lower than those in the simulate body fluid.

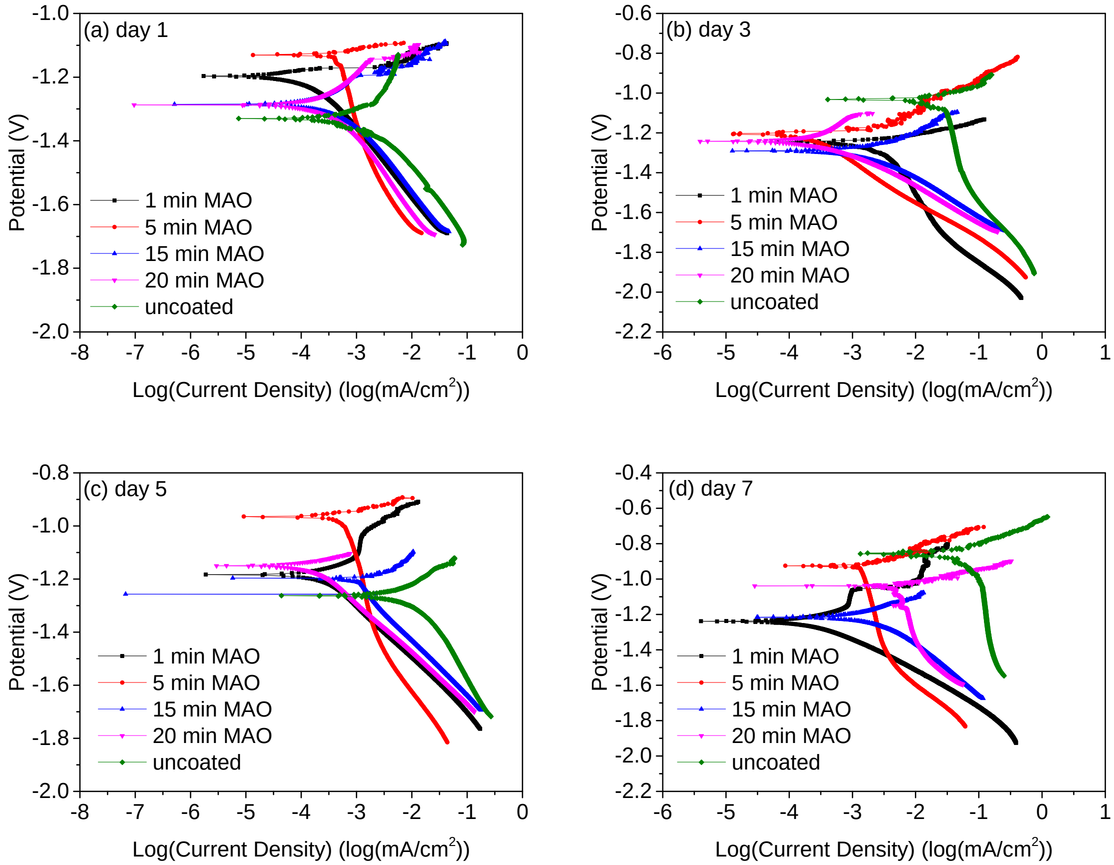


Figure 4.6. Tafel plots of all samples in the cell culture medium at(a) day 1; (b) day 3; (c) day 5; (d) day 7

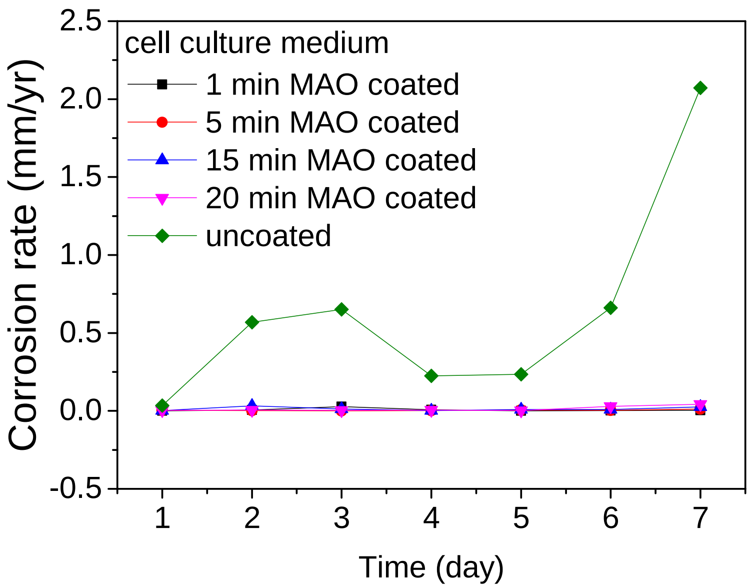


Figure 4.7. Corrosion rate comparison of the uncoated and MAO-coated samples in the cell culture medium during 7 day immersion

### 4.2.2 Electrochemical Impedance Spectroscopy

#### Uncoated Sample

The equivalent circuit in Figure 3.9 (b) is used to fit the EIS plots for all the samples immersed in the cell culture medium. The Nyquist plots for the corrosion of uncoated AZ31 alloy in the cell culture medium are shown in Figure 4.8.

Table 4.12. EIS data for the uncoated magnesium AZ31 alloy alloys after immersion in the culture medium for various durations

| Time | $R_s$ ($\Omega\times$cm$^2$) | CPE-$C_{dl}$ (F) | $R_{ct}$ ($\Omega\times$cm$^2$) |
|---|---|---|---|
| 1 hour | 53.81 | 8.00E-05 | 1428 |
| 2 hour | 44.79 | 4.40E-05 | 1562 |
| 4 hour | 48.56 | 3.40E-05 | 2451 |
| 8 hour | 78.66 | 2.17E-05 | 1.14E+04 |
| 12 hour | 65.21 | 1.86E-05 | 1.36E+04 |
| 24 hour | 67.1 | 1.58E-05 | 1.26E+04 |
| 2 day | 112.8 | 4.36E-05 | 2346 |
| 3 day | 121.1 | 5.66E-05 | 1452 |
| 4 day | 118.1 | 3.48E-05 | 2544 |
| 5 day | 116.4 | 3.68E-05 | 1688 |
| 6 day | 124 | 6.63E-05 | 779.8 |
| 7 day | 119.1 | 8.03E-05 | 532.9 |

The results of the equivalent circuit for the uncoated MAO-coated AZ31 magnesium alloys are summarized in Table 4.12. According to Figure 4.7, it has one capacity loop. The variation of $R_{ct}$ values was related to the dynamic process of crack or stripping of the corrosion layer. The diameter of the capacitive loop in the high frequency range represented the charge transfer resistance ($R_{ct}$). The $R_s$ values are around from 50 to 120 $\Omega\times$cm$^2$. The resistance of charge transfer ($R_{ct}$) increased

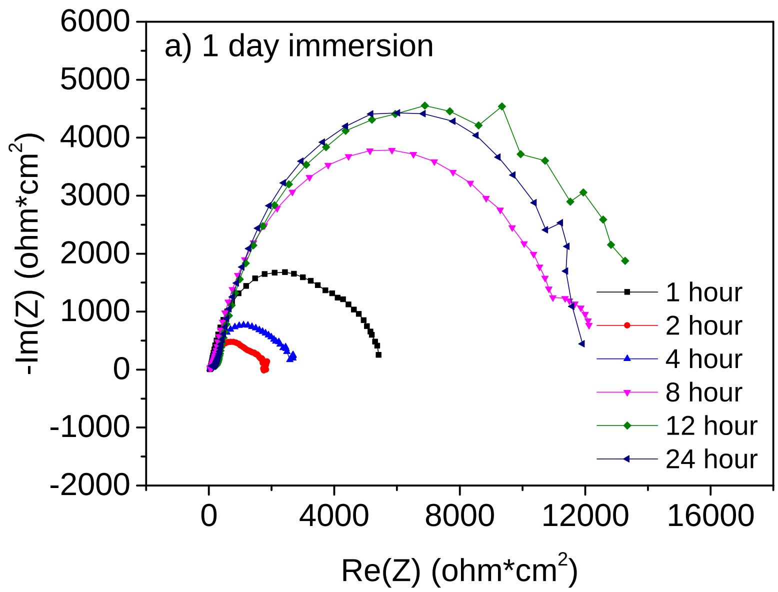


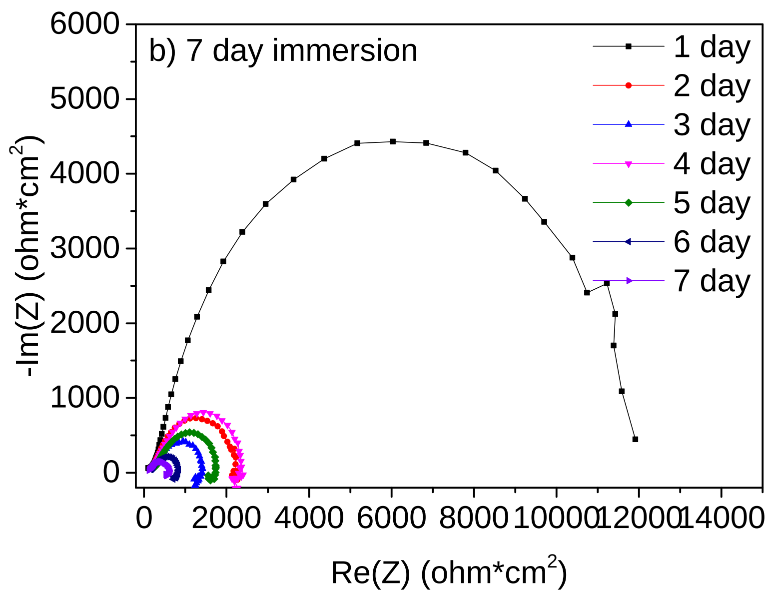


Figure 4.8. Nyquist plots of the uncoated magnesium AZ31 alloy in culture medium (a) 1-day immersion, and (b) 7-day immersion

in the first 24 hours with the time increase because the rapid formation of a corrosion product layer. However, the value of $R_{ct}$ decreased after 2 day immersion. During 2 day to 7 day immersion, the values decreased generally. The CPE-$C_{dl}$ increased during the whole immersion test. This result demonstrates that the surface of uncoated sample became rougher with increasing immersion time and more pits occuerred on the uncoated magnesium alloys.

### 1-minute MAO-coated Sample

The Nyquist plots for the corrosion of the 1-minute MAO-coated magnesium AZ31 alloy in the cell culture medium are shown in Figure 4.9.

Table 4.13. EIS data for the 1-minute MAO-coated magnesium AZ31 alloy after immersion in the culture medium for various durations

| Time | $R_s$ ($\Omega\times$cm$^2$) | CPE-$C_{dl}$ (F) | $R_{ct}$ ($\Omega\times$cm$^2$) |
|---|---|---|---|
| 1 hour | 127.2 | 4.44E-07 | 2.14E+05 |
| 2 hour | 135.8 | 7.04E-07 | 1.35E+05 |
| 4 hour | 153.1 | 2.91E-06 | 5.32E+04 |
| 8 hour | 129.5 | 3.89E-06 | 4.85E+04 |
| 12 hour | 150.2 | 4.23E-06 | 3.52E+04 |
| 24 hour | 135.2 | 5.32E-06 | 3.68E+04 |
| 2 day | 101.2 | 1.17E-05 | 8366 |
| 3 day | 93.87 | 1.71E-05 | 3582 |
| 4 day | 154 | 1.09E-05 | 1.51E+04 |
| 5 day | 135.2 | 1.53E-05 | 1.26E+04 |
| 6 day | 157.6 | 1.38E-05 | 1.73E+04 |
| 7 day | 147.4 | 1.40E-05 | 1.46E+04 |

The results of equivalent circuit for the 1-minute MAO-coated AZ31 magnesium alloys are illustrated in Table 4.13. The $R_s$ values are from 90 to 150 $\Omega\times$cm$^2$. Only one capacity loop is presented on all of the Nyquist plots in Figure 4.8. The $R_{ct}$ decreased with the time increase in the first day immersion. A great reduction of the

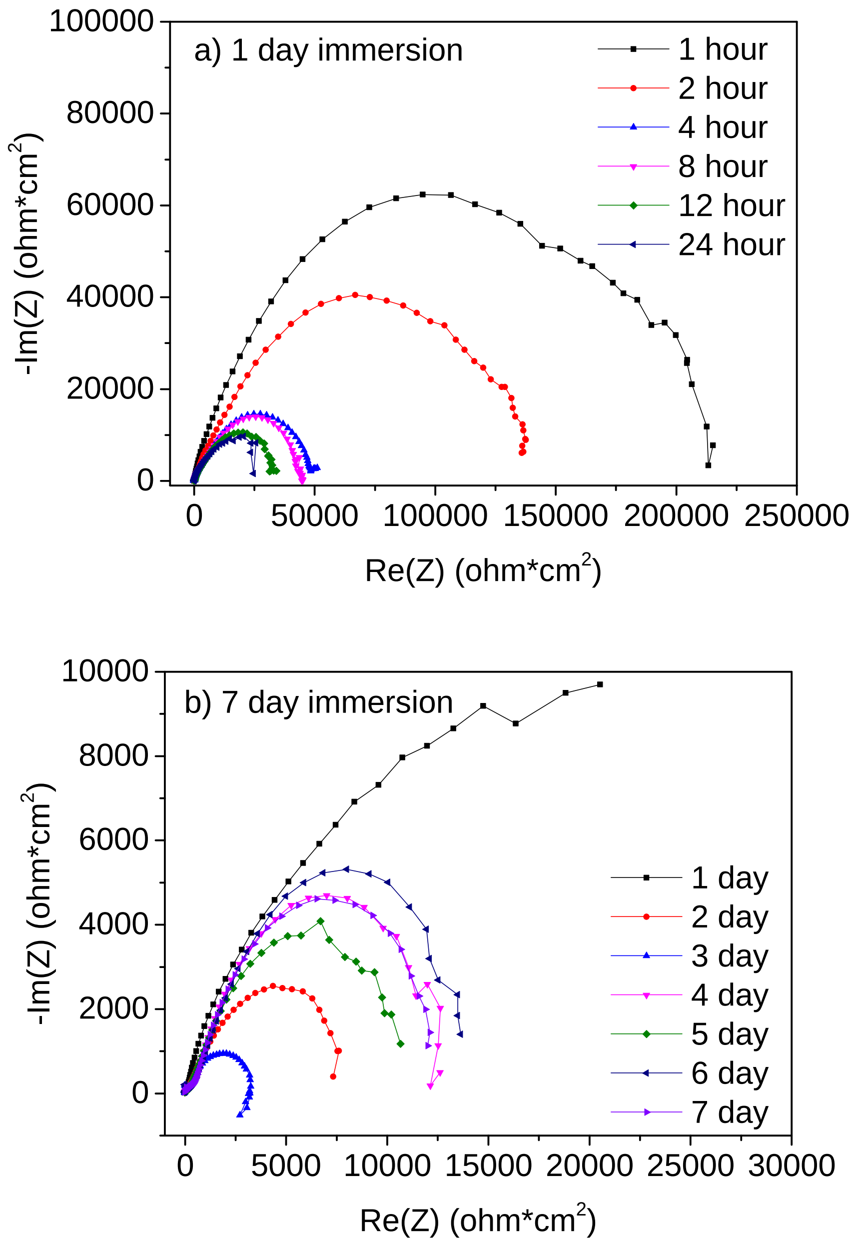


Figure 4.9. Nyquist plots of the 1-minute MAO-coated magnesium AZ31 alloy in the cell culture medium (a) 1-day immersion, and (b) 7-day immersion

$R_{ct}$ value occurred on the second day and reached to the lowest value on the third day. The values of $R_{ct}$ kept in stable range from 4 day to 7 day immersion. The passive layer on the substrate surface provided the corrosion resistance of sample.

### 5-minute MAO-coated Sample

The Nyquist plots for the corrosion of the 5-minute MAO-coated magnesium AZ31 alloy in the cell culture medium are shown in Figure 4.10.

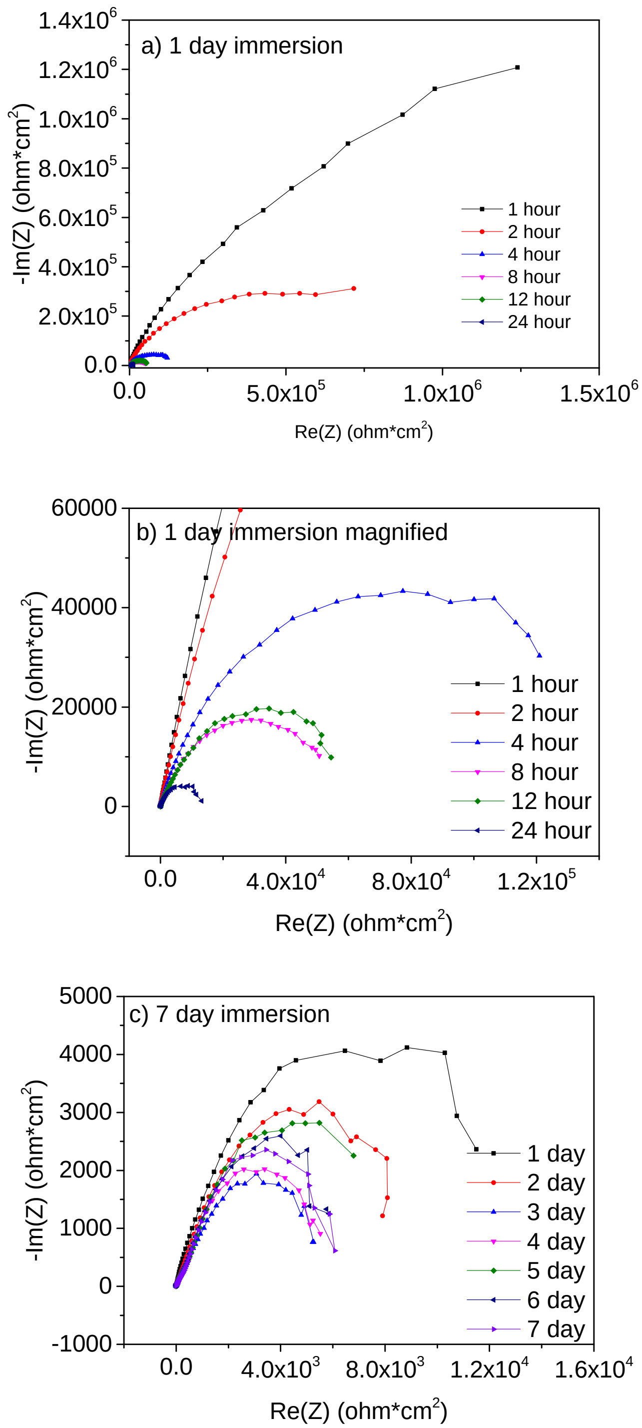


Figure 4.10. Nyquist plots of the 5-minute MAO-coated magnesium AZ31 alloy in the cell culture medium (a) 1-day immersion, (b) 1-day immersion magnified Nyquist Re(Z) from -10000 to 140000 ($\Omega \times cm^2$), and (c) 7-day immersion

Table 4.14. EIS data for the 5-minute MAO-coated magnesium AZ31 alloy after immersion in the cell culture medium for various durations

| Time | $R_s$ ($\Omega\times$cm$^2$) | CPE-$C_{dl}$ (F) | $R_{ct}$ ($\Omega\times$cm$^2$) |
|---|---|---|---|
| 1 hour | 124.3 | 3.56E-07 | 3.65E+06 |
| 2 hour | 168.7 | 4.36E-07 | 7.85E+05 |
| 4 hour | 153.3 | 1.58E-06 | 1.36E+05 |
| 8 hour | 119.4 | 3.46E-06 | 5.52E+04 |
| 12 hour | 140.2 | 4.63E-06 | 6.51E+04 |
| 24 hour | 123.3 | 9.89E-06 | 1.53E+04 |
| 2 day | 120.6 | 2.07E-05 | 1.12E+04 |
| 3 day | 113.4 | 2.84E-05 | 7199 |
| 4 day | 148.04 | 3.47E-05 | 7.38E+03 |
| 5 day | 143.57 | 3.02E-05 | 1.02E+04 |
| 6 day | 114.53 | 3.30E-05 | 8.19E+03 |
| 7 day | 128.4 | 3.31E-05 | 7.95E+03 |

Table 4.14 and Figure 4.10 provide the EIS information of the 5-minute MAO-coated sample. One capacity loop is shown on the Nyquist plots. The $R_s$ values are from 110 to 150 $\Omega\times$cm$^2$. The resistance of charge transfer ($R_{ct}$) decreased generally from 1 hour to 3 day immersion because the aggressive ions attacked the sample surface. The value of $R_{ct}$ increased after 4 day immersion and kept at a stable range. The CPE-$C_{dl}$ decreased the whole duration of immersion.

**15-minute MAO-coated Sample**

The Nyquist plots for the corrosion of the 15-minute MAO-coated magnesium AZ31 alloy in the cell culture medium are shown in Figure 4.11.

The $R_s$ values are from 90 to 150 $\Omega \times cm^2$. The resistance of charge transfer ($R_{ct}$) decreased in the first 3 days with the time increase. Then, the values of $R_{ct}$ increased quickly on the fourth day and maintain around $5.50 \times 10^3$ $\Omega \times cm^2$ in the last 4 days immersion. The CPE-$C_{dl}$ has the similar value as the 1-minute and 5 minute MAO-coated samples. The EIS data of 15-minute MAO-coated sample are shown in Table 4.15.

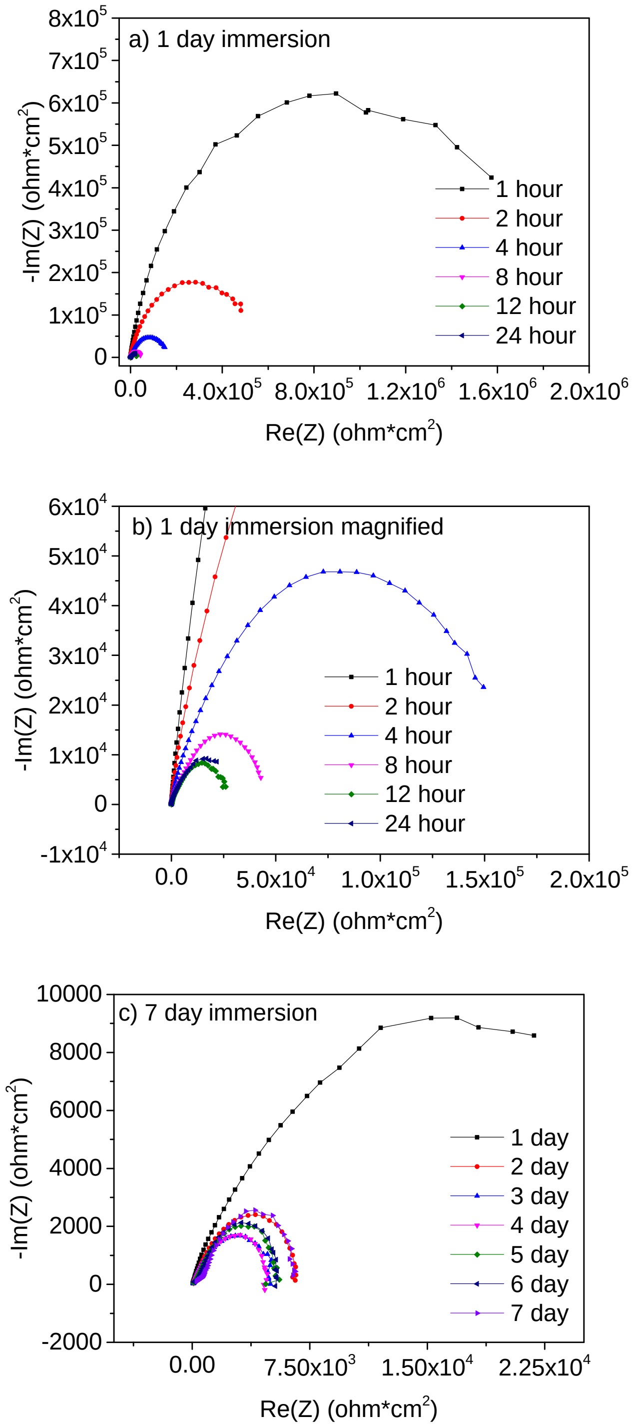


Figure 4.11. Nyquist plots of the 15-minute MAO-coated magnesium AZ31 alloy in the cell culture medium (a) 1-day immersion, (b) 1-day immersion magnified Nyquist Re(Z) from -25000 to 200000 ($\Omega \times cm^2$), and (c) 7-day immersion

Table 4.15. EIS data for the 15-minute MAO-coated magnesium AZ31 alloy after immersion in the culture medium for various durations

| Time | $R_s$ ($\Omega\times$cm$^2$) | CPE-$C_{dl}$ (F) | $R_{ct}$ ($\Omega\times$cm$^2$) |
|---|---|---|---|
| 1 hour | 113.5 | 1.03E-07 | 1.79E+06 |
| 2 hour | 128.3 | 2.89E-07 | 6.08E+05 |
| 4 hour | 133.6 | 3.60E-07 | 1.40E+05 |
| 8 hour | 129.7 | 3.14E-06 | 5.02E+04 |
| 12 hour | 158.19 | 3.92E-06 | 2.81E+04 |
| 24 hour | 114.3 | 4.09E-06 | 2.87E+04 |
| 2 day | 114 | 1.08E-05 | 6.78E+03 |
| 3 day | 133.4 | 1.50E-05 | 5140 |
| 4 day | 109.4 | 1.45E-05 | 5.28E+03 |
| 5 day | 158 | 1.23E-05 | 5.57E+03 |
| 6 day | 112.5 | 1.10E-05 | 5.46E+03 |
| 7 day | 120.3 | 1.12E-05 | 6.45E+03 |

**20-minute MAO-coated Sample**

The Nyquist plots for the corrosion of the 20-minute MAO-coated magnesium AZ31 alloy in culture medium are shown in Figure 4.12.

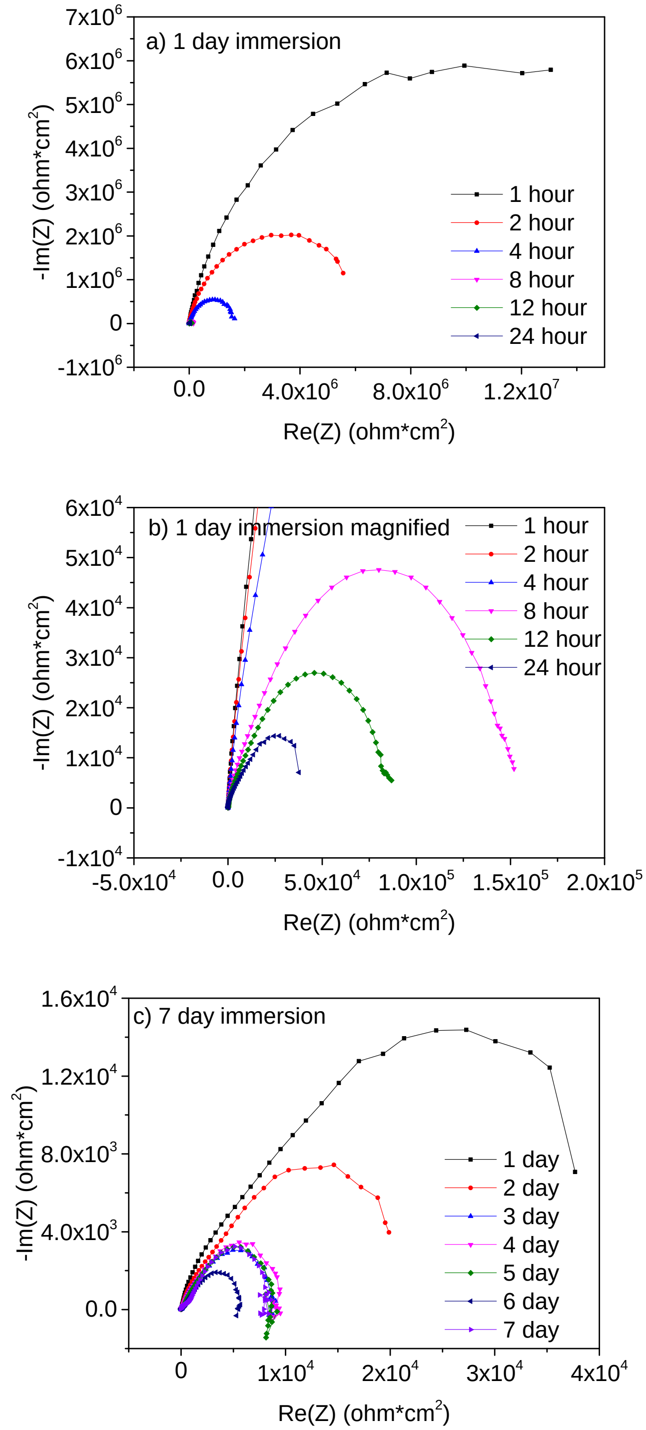


Figure 4.12. Nyquist plots of the 20-minute MAO-coated magnesium AZ31 alloy in the cell culture medium (a) 1-day immersion, (b) 1-day immersion magnified Nyquist Re(Z) from -50000 to 200000 ($\Omega\times cm^2$), and (c) 7-day immersion

Table 4.16. EIS data for the 20-minute MAO-coated magnesium AZ31 alloy after immersion in the cell culture medium for various durations

| Time | $R_s$ ($\Omega\times$cm$^2$) | CPE-$C_{dl}$ (F) | $R_{ct}$ ($\Omega\times$cm$^2$) |
|---|---|---|---|
| 1 hour | 119.5 | 7.91E-08 | 1.50E+07 |
| 2 hour | 107.6 | 1.07E-07 | 5.89E+06 |
| 4 hour | 120.85 | 1.33E-07 | 1.44E+06 |
| 8 hour | 137.4 | 7.45E-07 | 1.50E+05 |
| 12 hour | 121.9 | 1.55E-06 | 8.81E+04 |
| 24 hour | 121.7 | 2.69E-06 | 4.68E+04 |
| 2 day | 156.3 | 9.47E-06 | 2.46E+04 |
| 3 day | 154.6 | 1.30E-05 | 9762 |
| 4 day | 138.02 | 1.45E-05 | 1.05E+04 |
| 5 day | 117.81 | 1.74E-05 | 1.10E+04 |
| 6 day | 125.5 | 2.31E-05 | 6.68E+03 |
| 7 day | 122.7 | 1.41E-05 | 9.10E+03 |

According to Table 4.16 and Figure 4.12, it can be found that the 20-minute MAO-coated sample has one capacity loop. The $R_s$ values are from 100 to 150 $\Omega\times$cm$^2$. The resistance of charge transfer ($R_{ct}$) has the same trend as the other MAO-coated samples. The CPE-$C_{dl}$ decreased from 1 day to 7 day immersion.

Comparing all the values of the uncoated and MAO-coated magensium alloys AZ31, it can be found that the charge transfer resistance of the 20-minute MAO-coated sample has the highest value at the beginning corrosion since the coating thickness is the largest. All of the corrosion resistances of coated samples are much higher than the uncoated one. While after 5-day immersion, the 1-minute MAO-coated sample has the highst $R_{ct}$. This result is due to the coating layer protected the substrate and aggressive ions, such as chloride ions, cannot touch the substrate by being blocked by the large organic molecules. With the increase of time, after the pores are filled by the molecules, the 1-minute MAO-coated sample maintained a balance. The corrosion resistance kept at a stable range. However, the other MAO-coated samples can not create a closed environment for the substrate due to the larger pore size, so that the chloride ions can enter into the coatings pores and cause the decrease of corrosion resistance. Figure 4.13 and Figure 4.14 show the Nyquist plots and Bode plots of the uncoated and MAO-coated samples of 1-day, 3-day, 5-day and 7-day immersions.

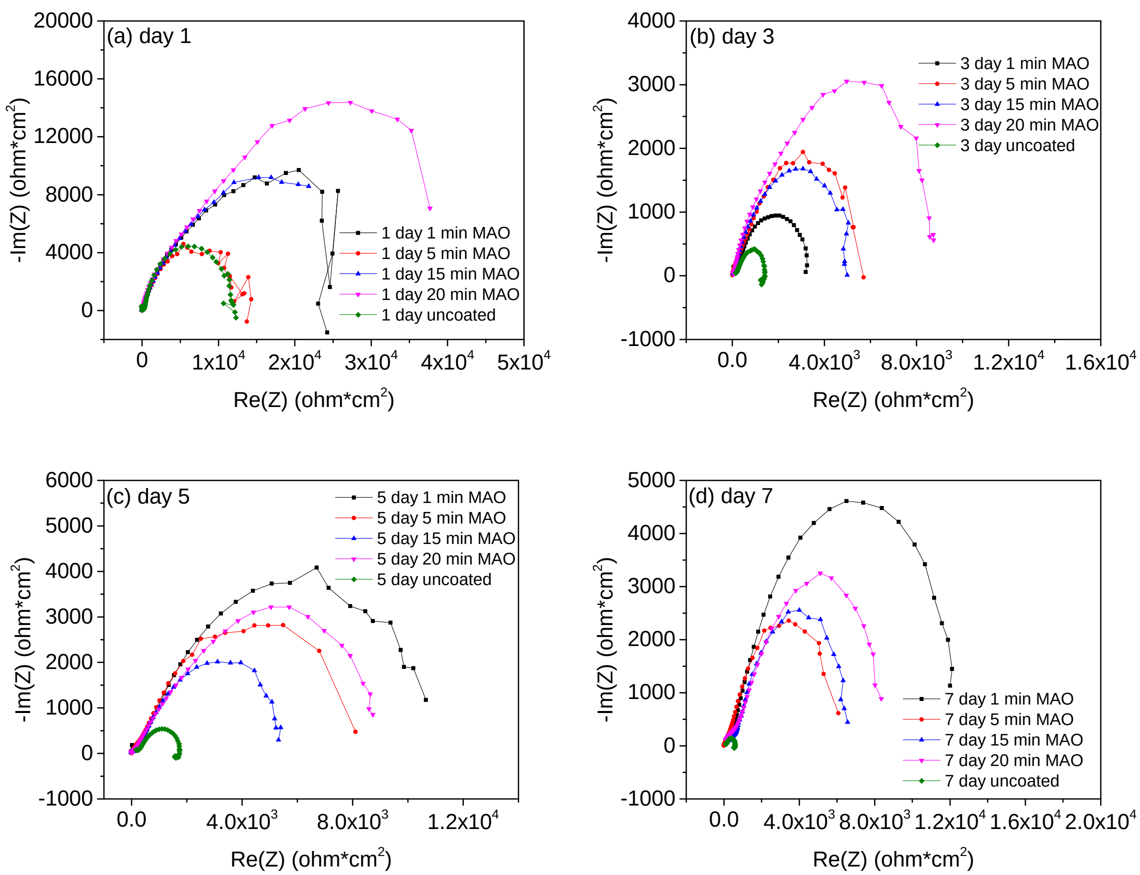


Figure 4.13. Nyquist curves of all samples in the cell culture medium at(a) day 1, (b) day 3, (c) day 5, and (d) day 7

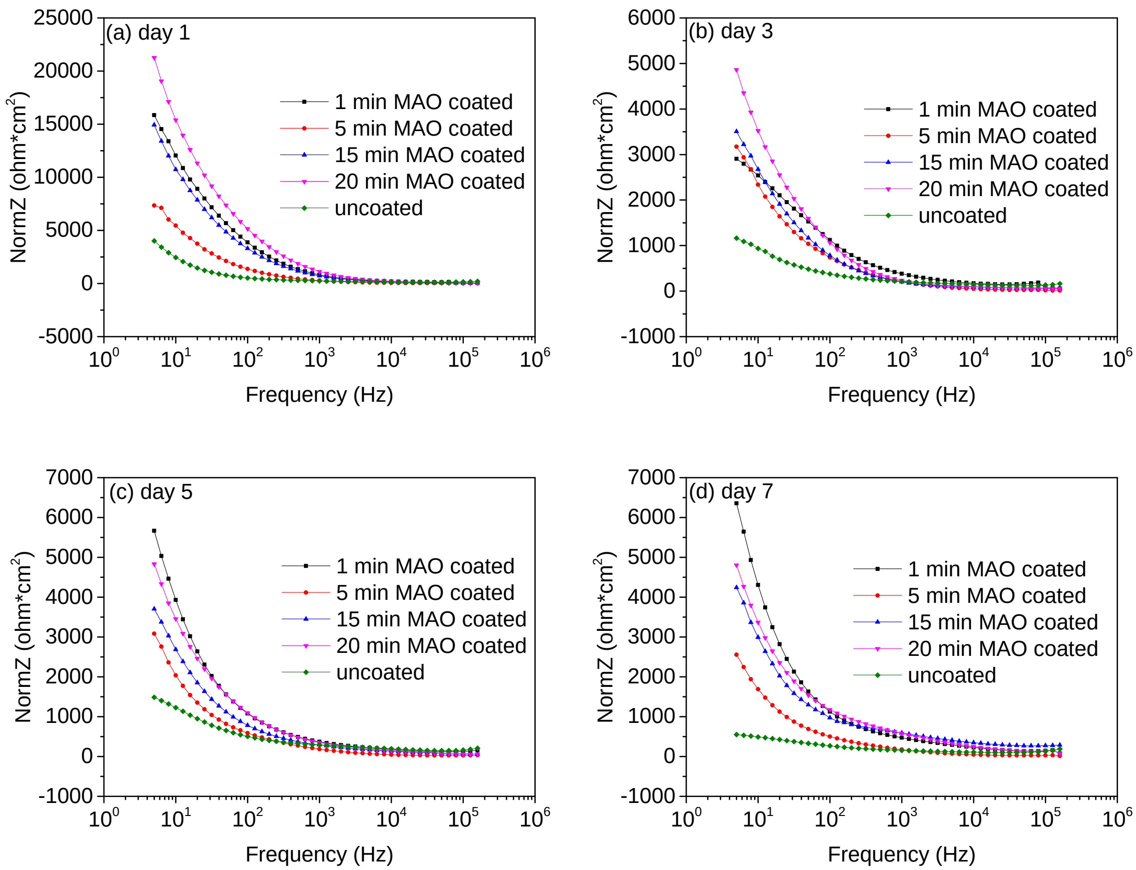


Figure 4.14. Bode plots of all samples in the cell culture medium at(a) day 1, (b) day 3, (c) day 5, and (d) day 7

## 4.3 Macroscopic and Microscopic Appearances

### 4.3.1 Macroscopic Appearances

Figure 4.16-4.19 show the changes on the macroscopic surfaces of the uncoated sample and MAO-coated samples after immersing in the cell culture medium from day 1 to day 7. The uncoated and MAO-coated AZ31 magnesium alloy samples immersed in cell culture meidum and dissolved with time. It is also determined that there are a few pits on the surface. The samples sizes remain the same with increasing immersion time, which indicates that little degree of corrosion occurred on the surface of samples in the cell culture medium. The MAO-coated and uncoated samples have much lower corrosion loss in the cell culture medium than in the simulated body fluid.

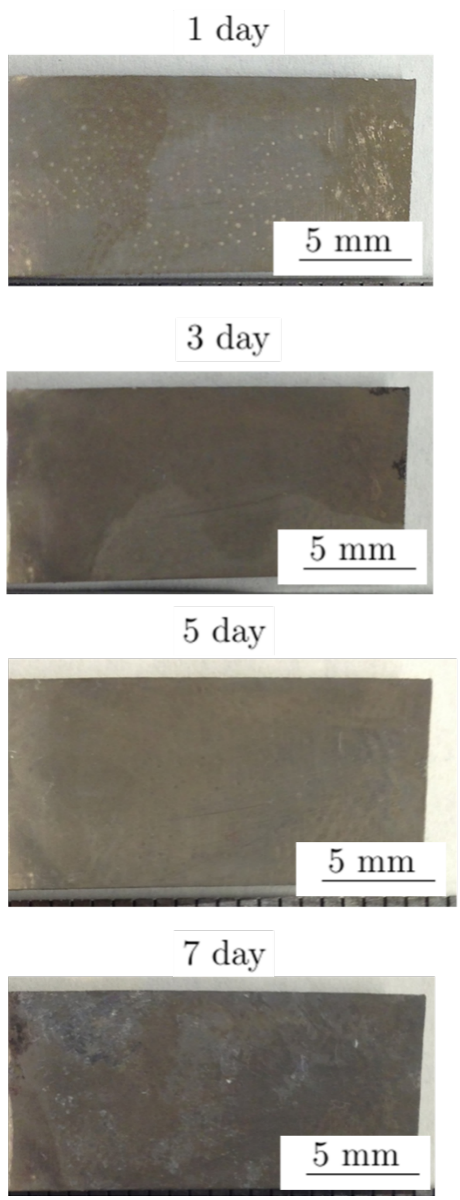


Figure 4.15. Macroscopic appearances of the uncoated AZ31 alloy after immersion in the cell culture medium

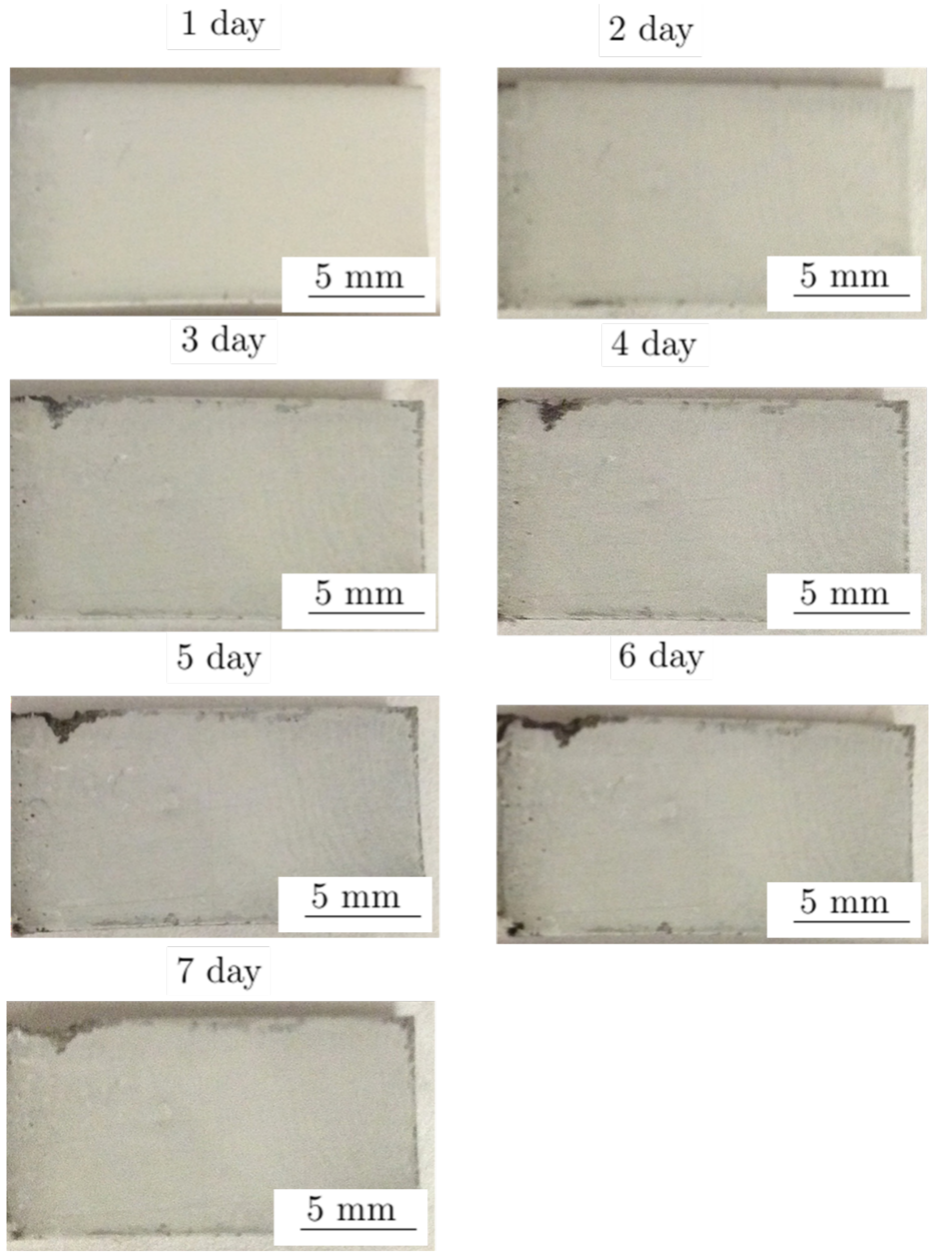


Figure 4.16. Macroscopic appearances of the 1-minute MAO-coated AZ31 alloy after immersion in the cell culture medium

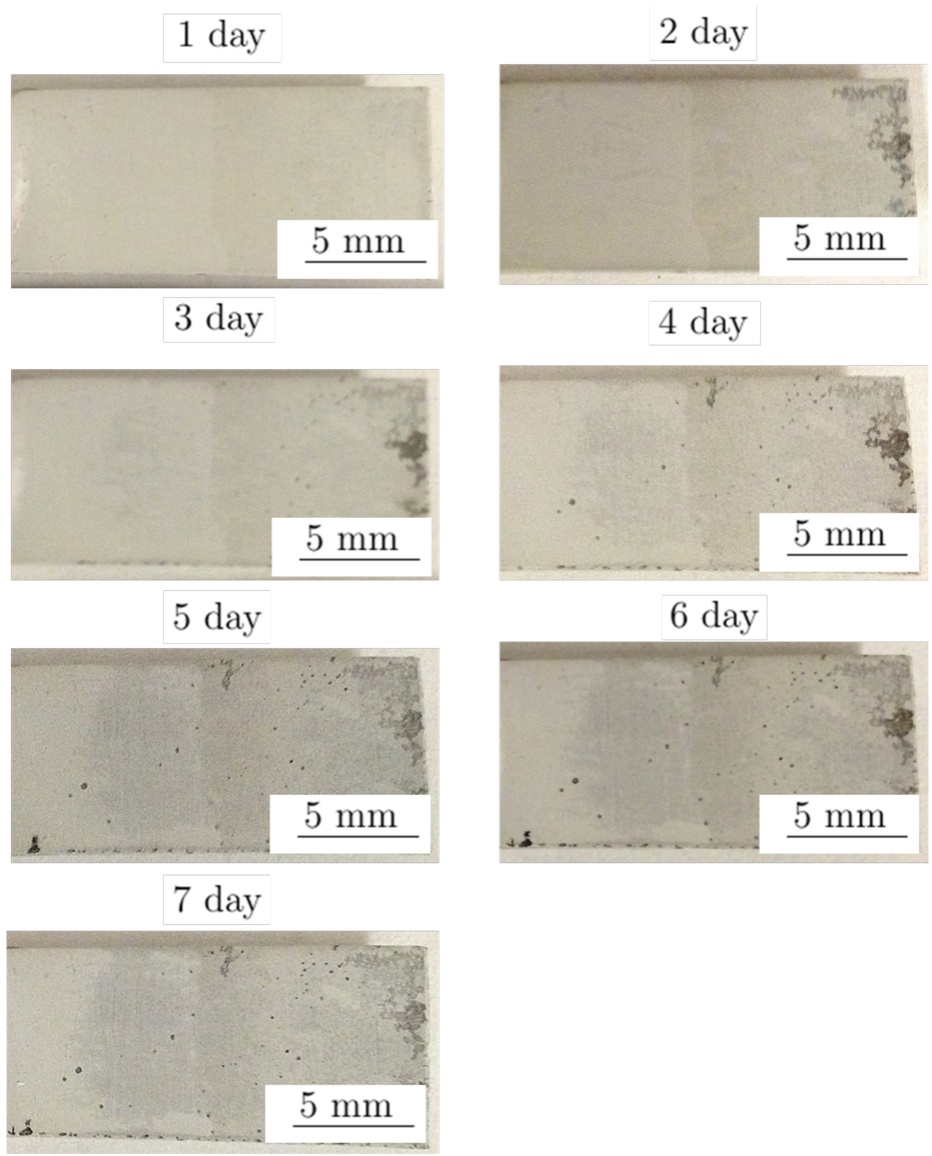


Figure 4.17. Macroscopic appearances of the 5-minute MAO-coated AZ31 alloy after immersion in the cell culture medium

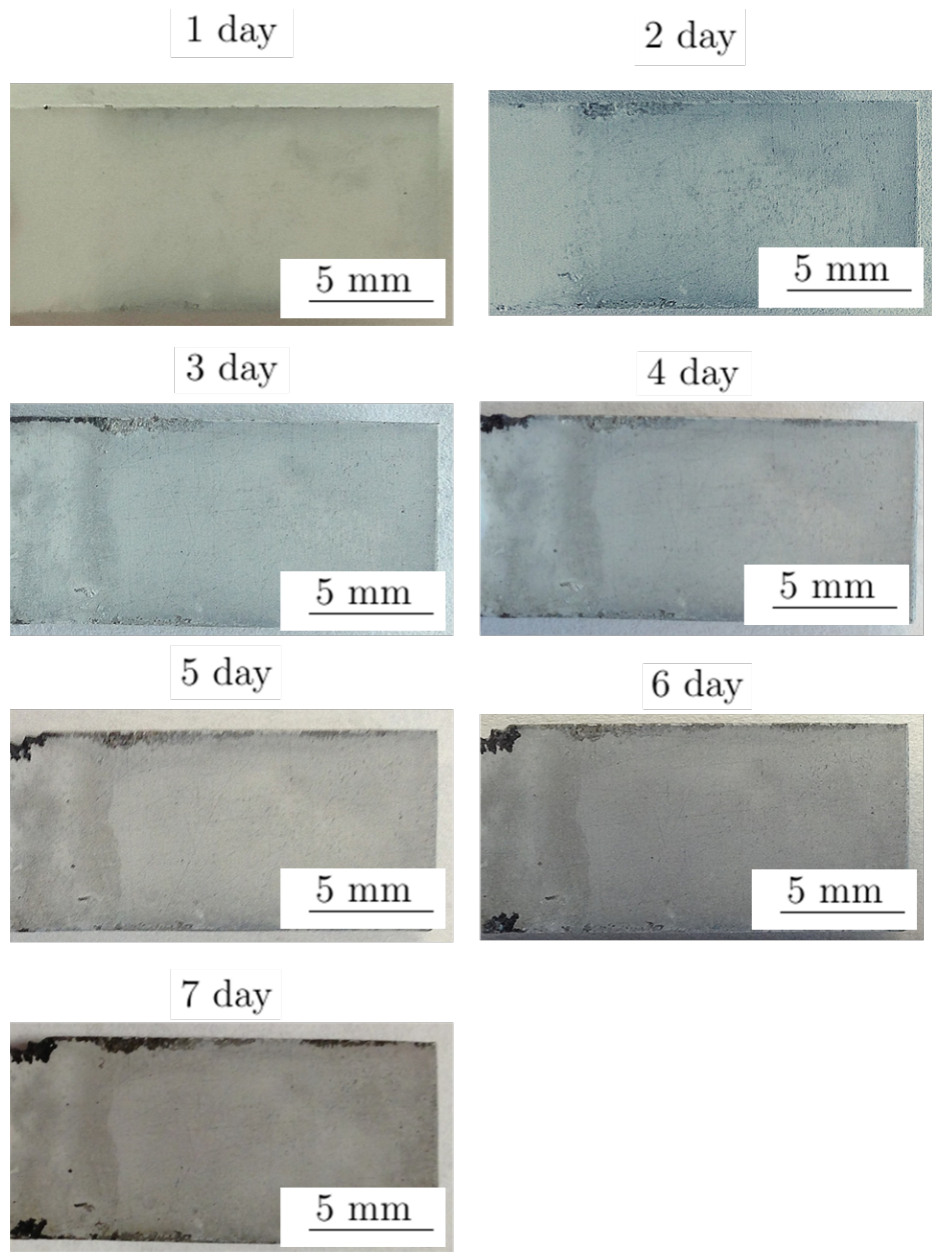


Figure 4.18. Macroscopic appearances of the 15-minute MAO-coated AZ31 alloy after immersion in the cell culture medium

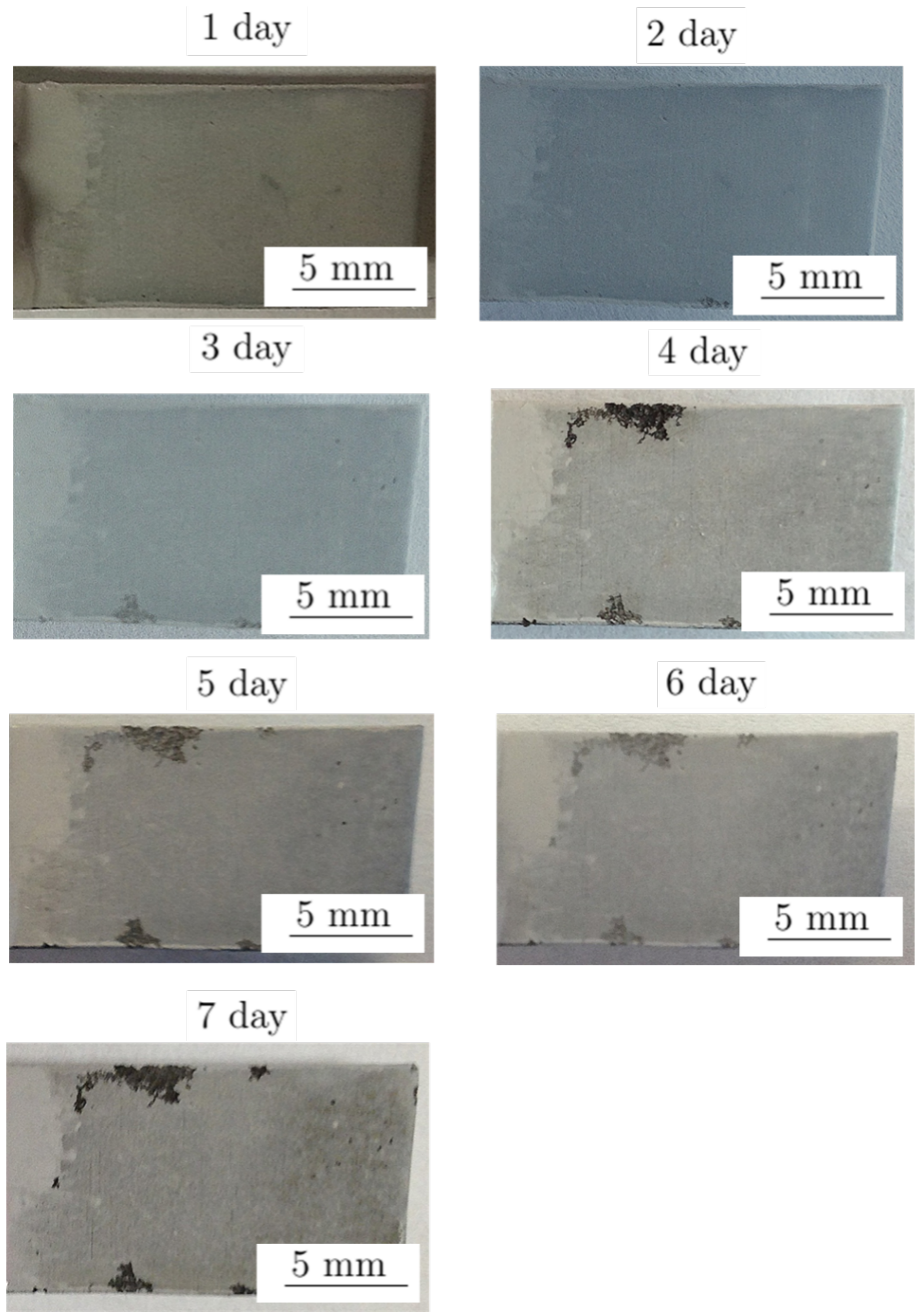


Figure 4.19. Macroscopic appearances of the 20-minute MAO-coated AZ31 alloy after immersion in the cell culture medium

### 4.3.2 Microscopic Appearances

Figure 4.20- 4.24 show the microscopic images. The surfaces of MAO-coated samples had been protected by dense coating layer in the beginning of immersion. Little microstructure change occurred after 7 days of immersion. A few pits can be observed. Those results illustrate that the MAO-coated and uncoated samples have much lower corrosion loss in the cell culture medium than in the simulated body fluid.

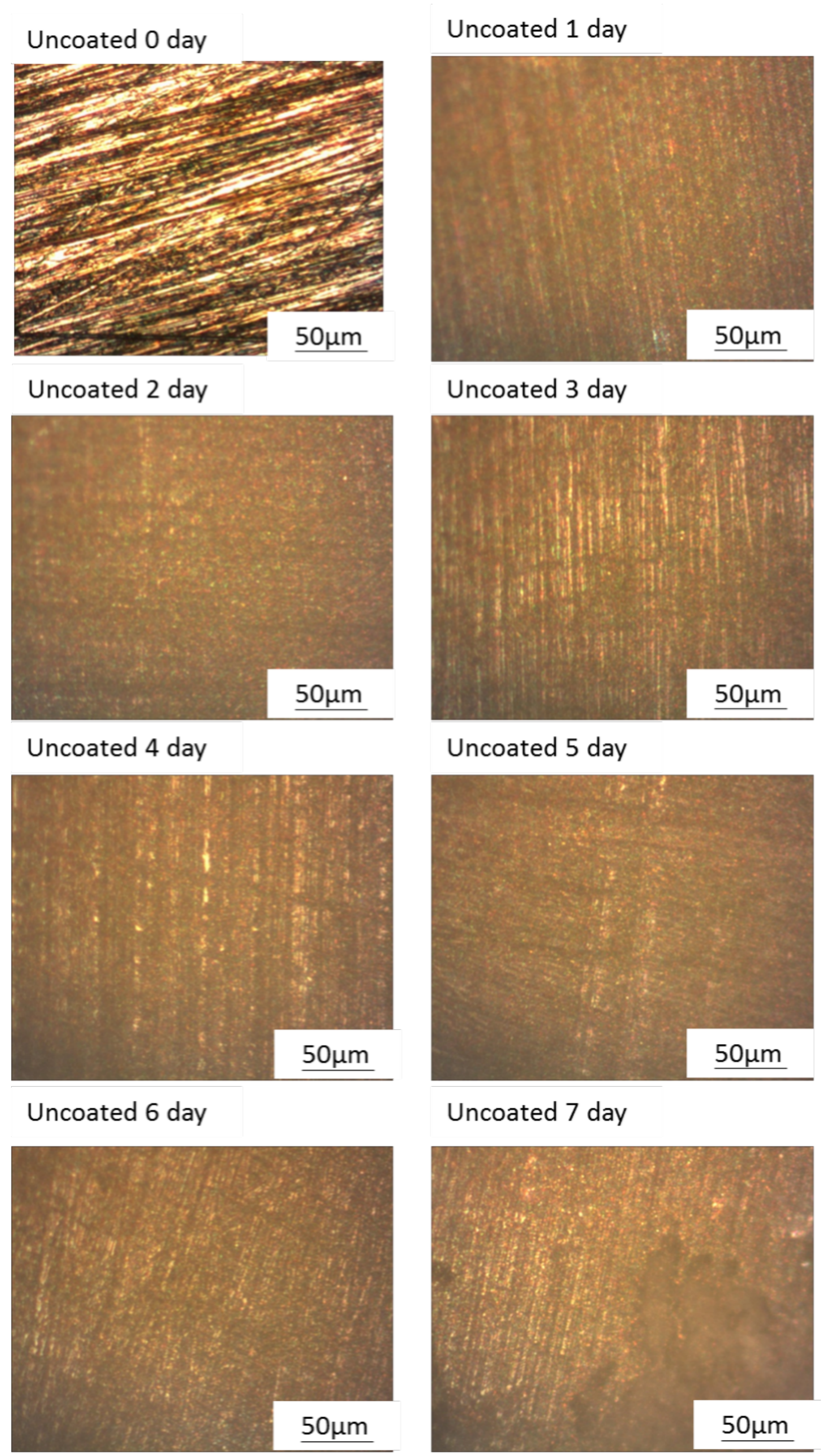


Figure 4.20. Surface microscopic images of the uncoated AZ31 magnesium alloy after immersion in the cell culture medium for various durations

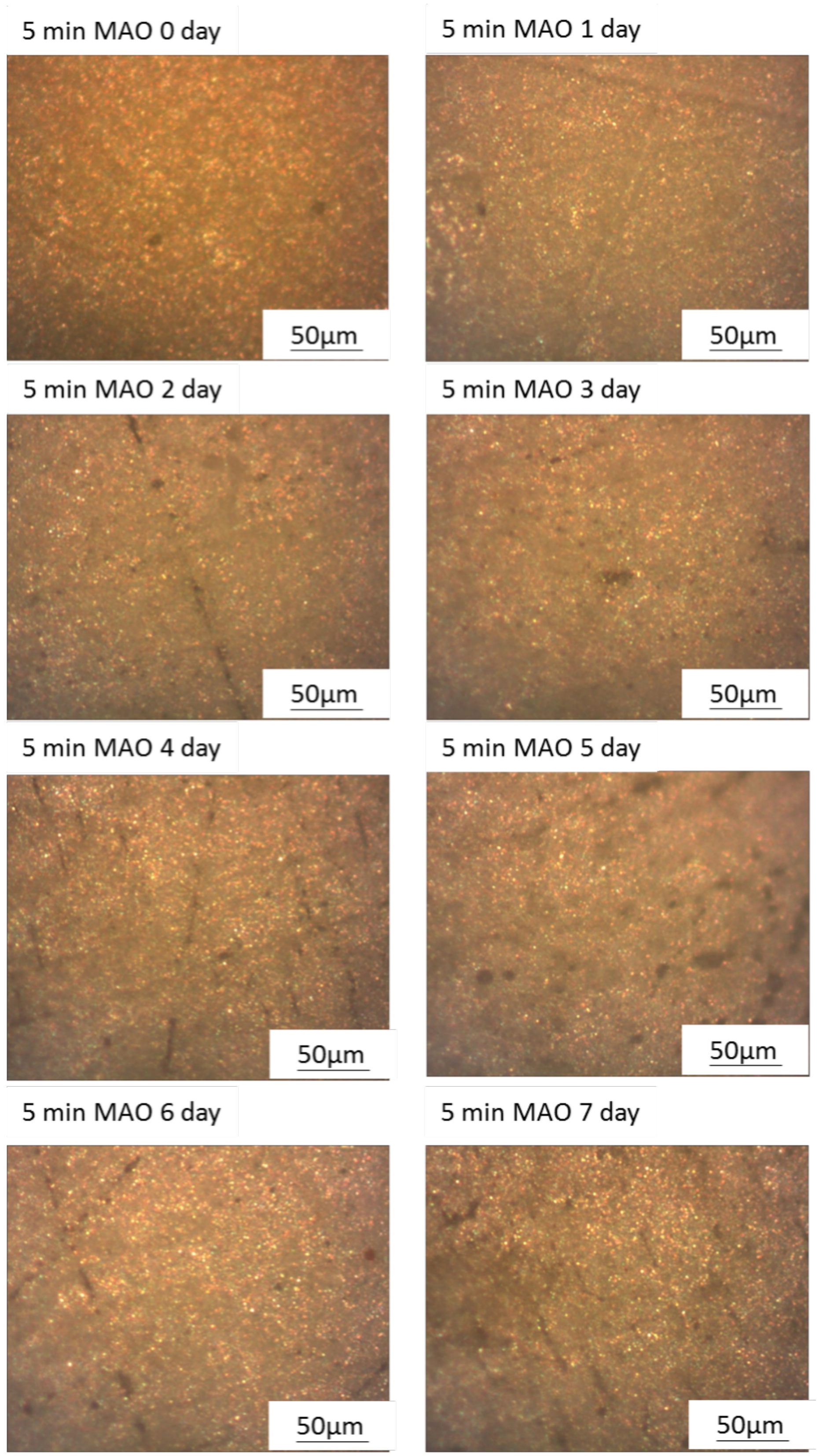


Figure 4.21. Surface microscopic images of the 1-minute MAO-coated AZ31 magnesium alloy after immersion in the cell culture medium for various durations

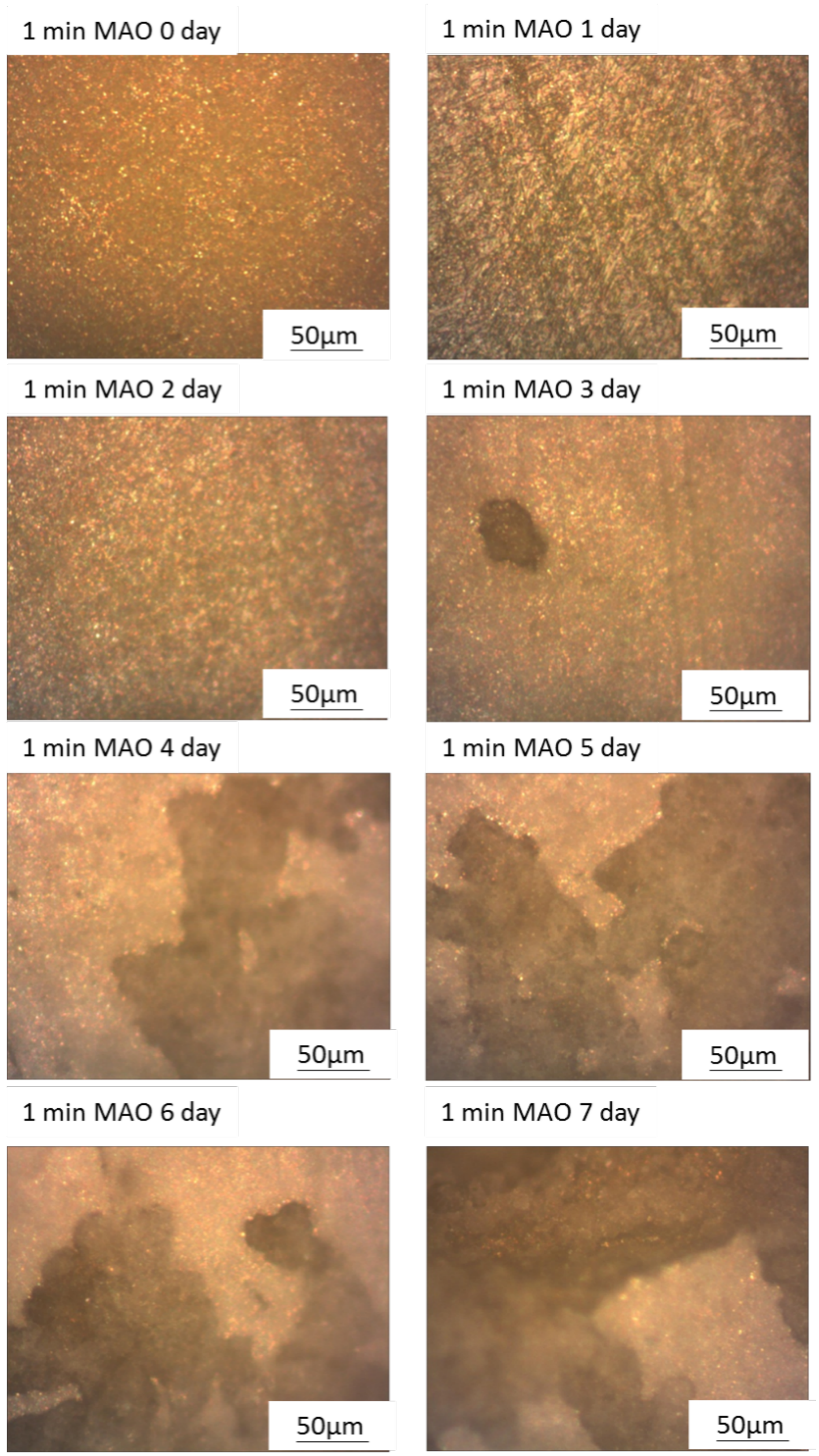


Figure 4.22. Surface microscopic images of the 5-minute MAO-coated AZ31 magnesium alloy after immersion in the cell culture medium for various durations

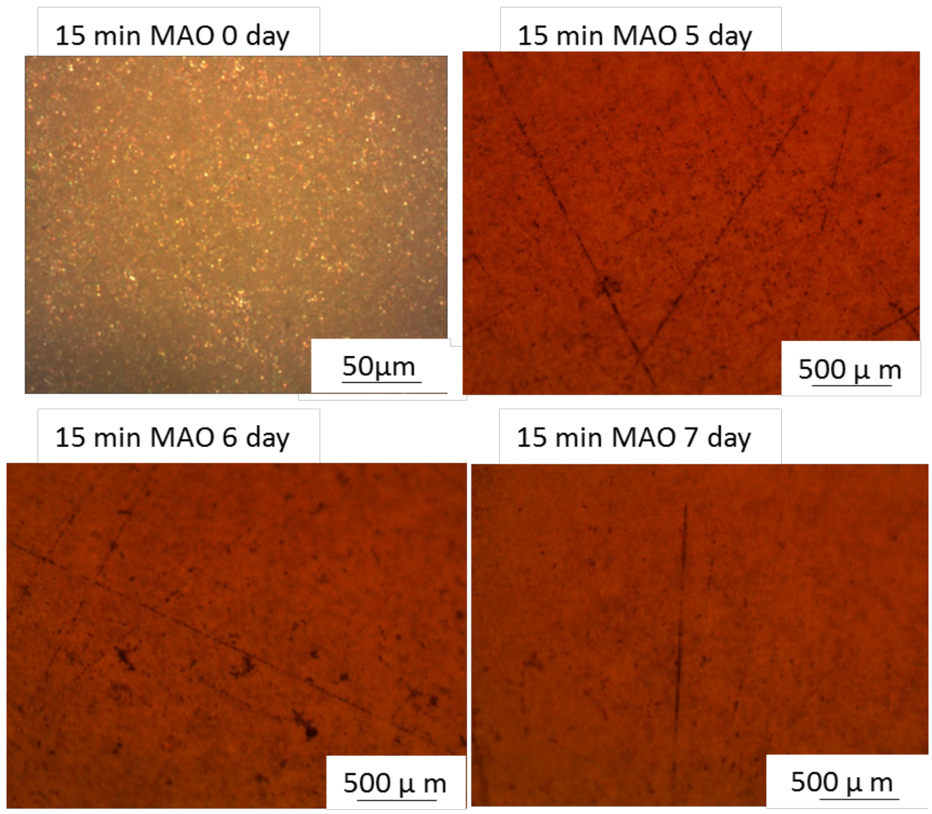


Figure 4.23. Surface microscopic images of the 15-minute MAO-coated AZ31 magnesium alloy after immersion in the cell culture medium for various durations

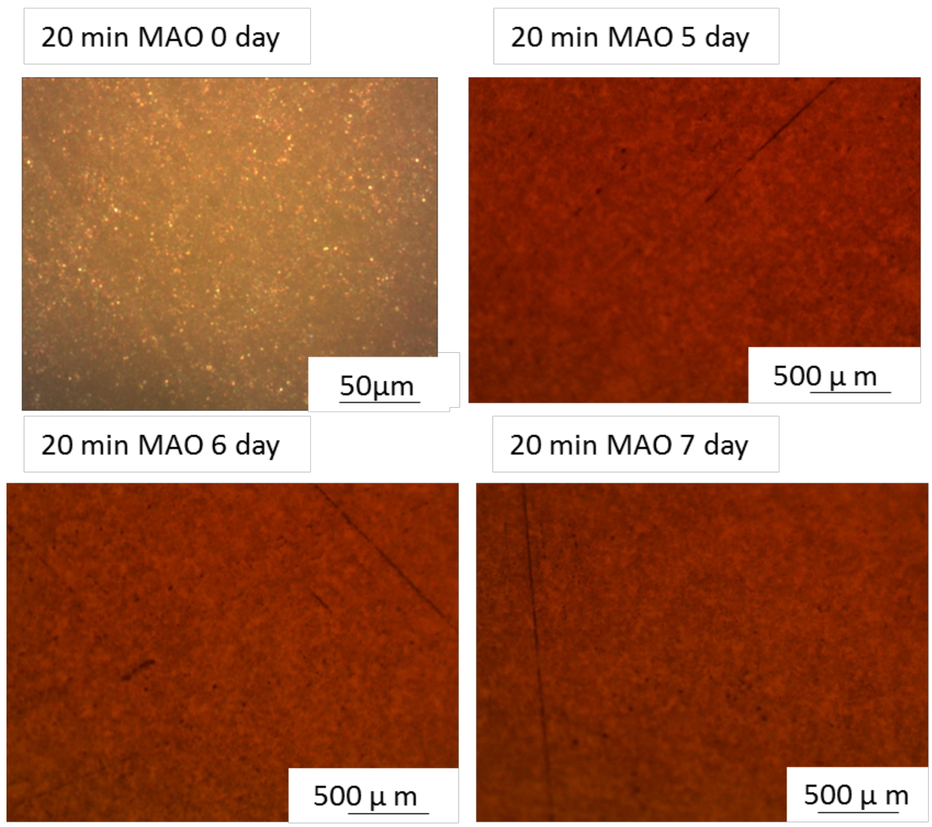


Figure 4.24. Surface microscopic images of the 20-minute MAO-coated AZ31 magnesium alloy after immersion in the cell culture medium for various durations

# 5. NUMERICAL MODELING OF CORROSION OF MAGNESIUM ALLOY

A numerical model has been developed to determine the corrosion behavior of the uncoated magnesium alloy AZ31 in simulated body fluid. The corrosion current density was calculated and compared with the experimental result.

## 5.1 Model Definition

The corrosion behavior of magnesium alloys is strongly affected by the aluminum content,including Mg phase, $Mg_{17}Al_{12}$ phase fraction, and it distribution [55,56]. The numerial model revised from a model by Deshpande [57].

The side view of the model is shown in Figure 5.1. This microstructure included the $\alpha$ phase and $\beta$ phase, which were exposed to the electrolyte solution. The width of the model is 200 $\mu$m and depth is 25 $\mu$m. Figure 5.2 shows the top view of the model, 200 $\mu$m in width and 100 $\mu$m in length. Three sides and top and bottom surfaces did not touch the electrolyte solution. Only the bottom boundary of domain was exposed to the solution.

The governing equations are based on the Nernst-Planck equation as

$$N_i = -D_i \nabla c_i - z_i F u_i c_i \nabla \phi + c_i U \tag{5.1}$$

where, $N_i$ is the flux, $D_i$ is the diffusion coefficient, $c_i$ is the concentration, $z_i$ is the charge and $u_i$ is the mobility, of species i, respectively, F is the Faradays constant, $\phi$ is the potential and U is the solvent velocity. In this equation, species flux is equated with the three additive fluxes associated with diffusion, migration and convection [57].

The following assumptions have been made in this work:

1. No concentration gradient exists in the electrolyte solution.
2. The solvent is incompressible.
3. The solution is electro neutral.

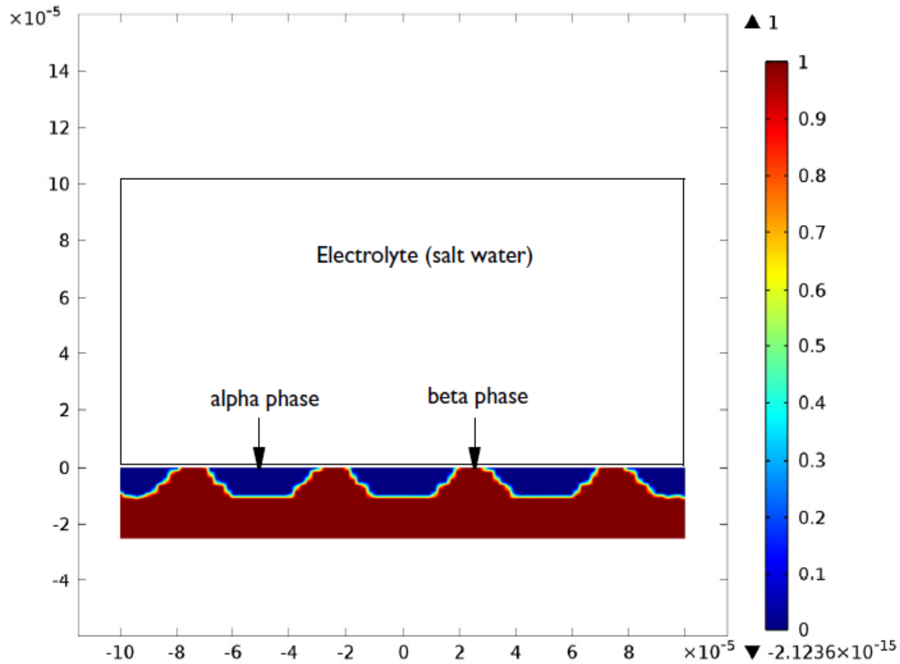


Figure 5.1. Cross-sectional view of the model and initial phase distribution

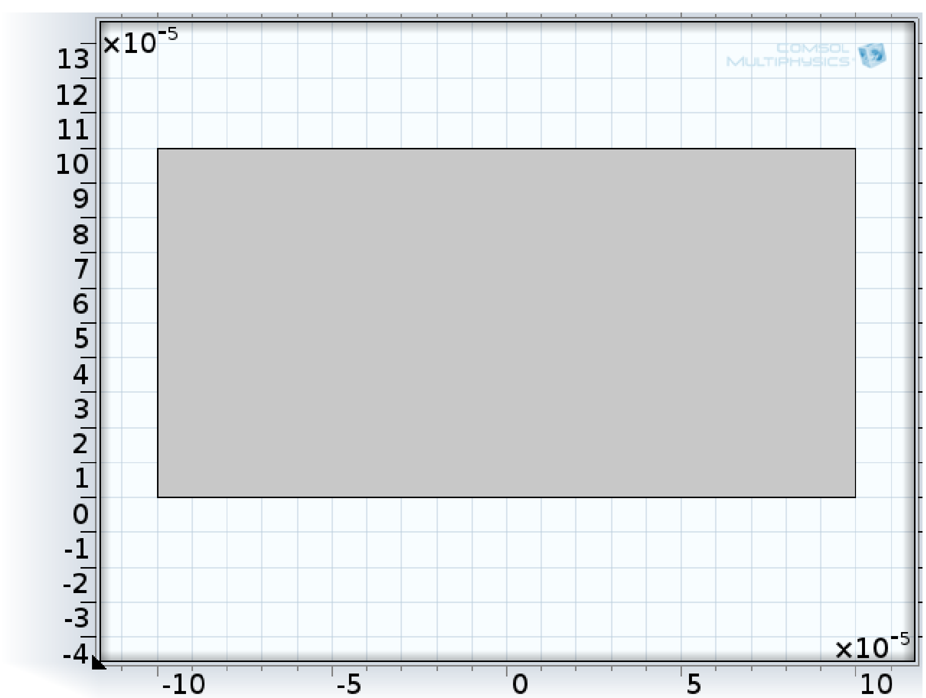


Figure 5.2. Top view of the model

4. The dissolution reaction takes place at the anode surface ($\alpha$ phase) whereas the hydrogen evolution reaction takes place at the cathode surface ($\beta$ phase). Thus, the $\alpha$ phase is assumed to be corroding while the $\beta$ phase is assumed to be non-corroding.

After estabilshing the assumptions and simplification, the equation used in this case becomes:

$$i_l = -\sigma_l \nabla \phi_l, \nabla \times i_l = 0 \tag{5.2}$$

Equation (5.2) was used to solve for the electrolyte potential, $\phi_1$(V), over the electrolyte domain, where $i_l$ (A/m$^2$) is the electrolyte current density vector and $\sigma_l$ (S/m) is the electrolyte conductivity which is assumed to be a constant of 3.5 S/m for the simulated body fluid. The conductivities were measured with an Oakton pH/Con 510 Series.

At the electrode surface, the boundary condition for the electrolyte potential follows:

$$n * i_l = \sum_m i_{loc,m} + i_{dl} \tag{5.3}$$

where $i_{loc,m}$ (A/m$^2$) is the local individual electrode reaction current density. At the surface, the dissolution velocity in the normal direction was evaluated by the following equation:

$$n \times \frac{\partial x}{\partial t} = \sum_i \frac{R_{dep,i,m} M_i}{\rho_i} \tag{5.4}$$

where M$_i$ is the molar mass which was assumed as 23.98 g/mol, and i is the density which was set as 1770 kg/m$^3$. $R_{dep,i,m}$ was evaluated using equation:

$$R_{dep,i,m} = -\frac{\upsilon_{dep,i,m} i_{loc,m}}{n_m F} \tag{5.5}$$

where $_{dep,i,m}$ is the stoichiometric coefficient and $n_m$ is the number of electrons participating in the electrode reaction.

Negative current density occurred on the cathodic reaction and a positive current density were associated with an anodic reaction [57]. The defined electrode kinetics expression was used to model the electrode reaction at the $\alpha$ phase on the electrode surface. The local current density for the $\alpha$ phase at the electrode surface was defined by the following equation, which came from the results of Deshpande's experiments [57].

$$i_\alpha = f(\phi_{s,ext} - \phi_1) * (1 - micro(x, y)) \tag{5.6}$$

The expression 1 - micro(x,y) ensures that the local current density is applied only at the $\alpha$ phase on the electrode surface. Similarly, at the $\beta$ phase on the electrode surface, the electrode kinetics was set by modeling the electrode reaction through the following expression for the local current density:

$$i_\beta = f(\phi_{s,ext} - \phi_1) * micro(x, y) \tag{5.7}$$

In this model formulation, it is assumed that there is no material loss on the $\beta$ phase. The anodic dissolution reaction takes place at the $\alpha$ phase surface and the cathodic hydrogen evolution reaction takes place at the $\beta$ phase surface. That caused only the phase surface to take a dissolution, which was shown as a movement of boundary in Figure 5.4. However, the $\beta$ phase surface is considered to remain intact.

The mesh used in the model is shown in Figure 5.3 by using a free triangular size which can provide a finer resolution at the surface of model.

All of the boundaries are set with desplacement of $U_y = 0$ except the bottom side, and all the displacement of $U_x = 0$.

Table 5.1 shows the parameters used in this model.

## 5.2 Results and Discussion

Figure 5.4 shows a surface plot of the electrolyte potential at time t = 2.11 $\times$ $10^5$ s. It can be seen that the $\alpha$ phase, being electrochemically more active, dissolved from the electrode surface whereas the $\beta$ phase, being relatively more noble, remained intact. With the preferential dissolution of the $\alpha$ phase, the underneath $\beta$ phase got exposed to the electrolyte solution resulting in an increase in the surface $\beta$ phase fraction at the electrode surface. The computations were stopped when the surface $\beta$ phase fraction reached a value of 0.95 at time t = 2.11 $\times$ $10^5$ s in this case. It can be

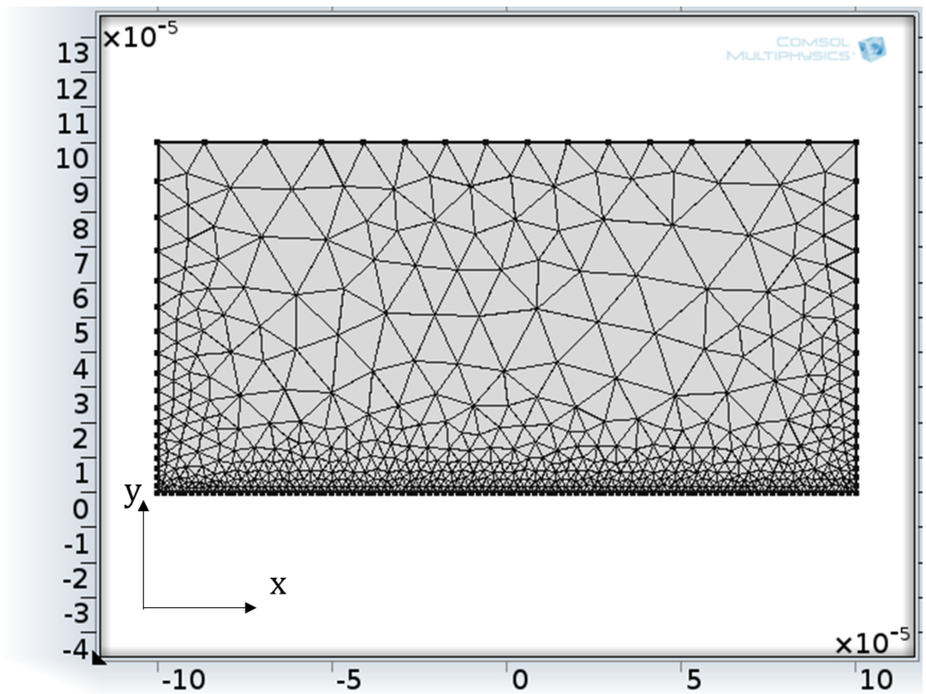


Figure 5.3. Mesh of the model

Table 5.1. Simulation parameters used in the model

| Name | Expression | Description |
|---|---|---|
| $\sigma$ | 3.5 [S/m] | Conductivity of electrolyte solution (simulated body fluid) |
| M | 23.98E-03 [kg/mol] | Atomic mass of $\alpha$ phase (AZ31) |
| Z charge | + 2 | Charge number of $\alpha$ phase (AM30) |
| $\rho$ | 1770[kg/m$^3$] | Density of $\alpha$ phase (AM30) |

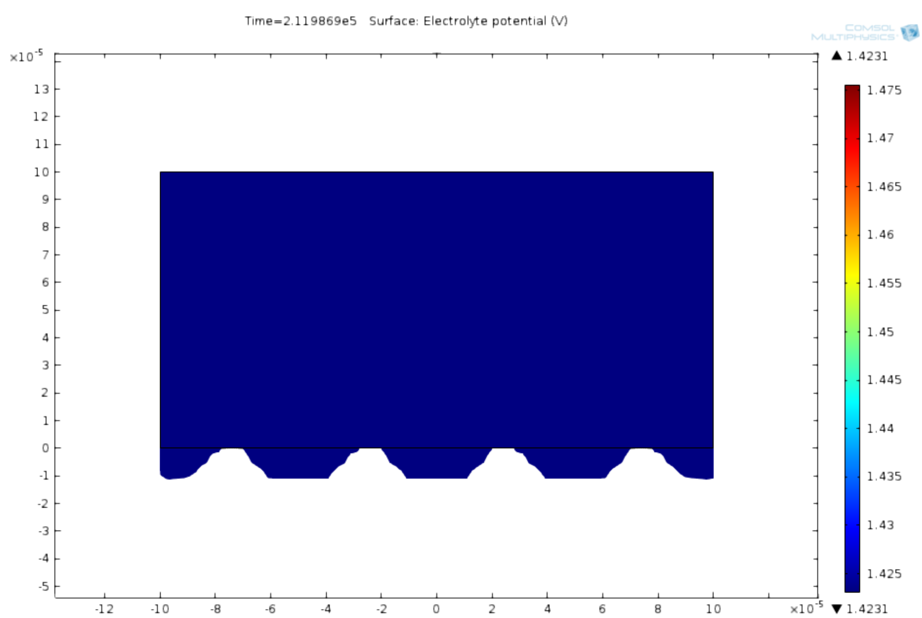


Figure 5.4. A surface plot of the electrolyte potential at time t = $2.11 \times 10^5$ s in simulated body fluid

seen in Figure 5.4 that most of the phase shown in Figure 5.1 was dissolved in the electrolyte solution at time t = $2.11 \times 10^5$ s.

Figure 5.5 shows the comparison of the corrosion current density of both simulated results and experimental data. The average current density increases very rapidly for

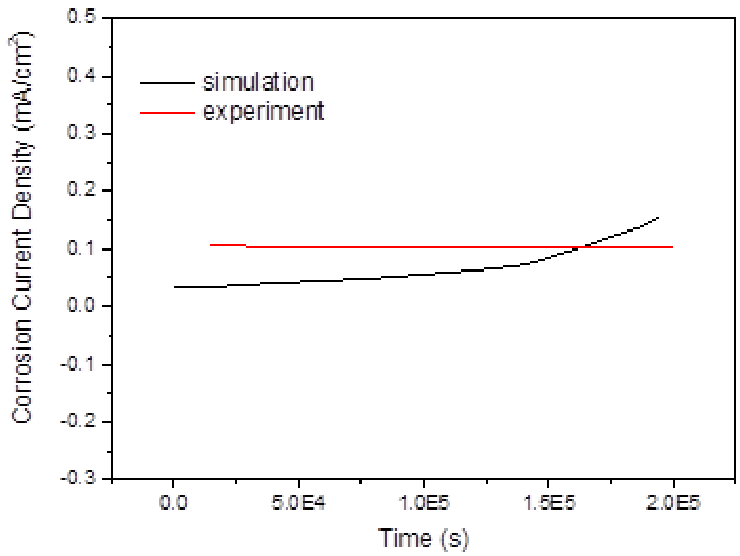


Figure 5.5. Comparison of corrosion current density of uncoated magnesium alloy immersed in the simulated body fluid at $2.11 \times 10^5$ s between simulation and experiment

the higher surface $\beta$ phase fraction which is attributed to a higher cathode to anode area ratio at the electrode surface.

According to Figure 5.5, it can be found that the simulated result is acceptable,and has a similar trend as the experimental result. The model can be revised later for more accurate prediction.

# 6. SUMMARY

## 6.1 Summary of Results

The following conclusion have been determined from this thesis work.

1. In simulated body fluid immersion tests, the MAO coated AZ31 magnesium alloys have lower corrosion current densities and higher resistances of charger transfer than the uncoated ones. That means the MAO coating can provide protection for the AZ31 substrate. Moreover, the results show that the 20-minute MAO coated sample has the best corrosion resistance among the all samples. This is due to the fact that the 20-minute MAO coated sample has the thickest coating layer and lowest porosity.

2. In contrast, in the cell culture medium immersion tests, all MAO coated AZ31 magnesium alloys demonstrate the similar behavior regardless of MAO processing time. They have much lower corrosion rates compared with simulated body fluid. It can be explained by the organic molecules in the cell culture medium and a dense passive layer formed on the samples surface, which prevent aggressive ions, such as chloride ions, from corroding the substrate.

3. A finite element model was successfully developed to simulate the corrosion process of magnesium alloy in simulated body fluid. The preliminary result shows the corrosion process of the uncoated sample. The predicted corrosion current density is in the same order of magnitude of the experimental measurements.

4. The difference between the simulated body fluid tests and the cell culture medium ones demonstrates that the composition of electrolyte solution can greatly impact the corrosion process and the MAO coating. It may also suggest that the simulated body fluid is not suitable for the experiments in biological application, because biomolecules are ignored in the simulated body fluid.

## 6.2 Contribution of this Work

1. A new electrolyte (12g/L $Na_2SiO_3$, 4 g/L NaF and 4ml/L $C_3H_8O_3$) was used in the MAO coating process to produce the coatings. This study shows that the electrochemical behaviors in simulated body fluid of the new MAO coatings are similar to electrolyte ($Na_2SO_3$, NaF and $C_3H_8O_3$) [59].

2. The new MAO coatings were also tested in a cell culture medium which has not been reported before. The composition of the cell culture medium is much close to human body fluid, thus providing a more accurate evaluation of the biological evaluation of the coating.

3. A new computational model has been developed to evaluate the corrosion behavior of AZ31 magnesium alloy immersed in simulated body fluid. The model can be applied in studying other similar alloy systems.

## 6.3 Suggested Future Work

In this work, the micro-arc oxidation processing parameter was focused on oxidation time. Future studies can focus on other control parameters, such as applied voltage and electrolyte concentration. Moreover, immersion tests (e.g., 30 days) can be used to evaluate long-term performance of the alloy. Furthermore, cell culture experiments can be conducted on the MAO coating to observe the influence of MAO coating on cell activities.

# LIST OF REFERENCES

# LIST OF REFERENCES


[1] M. P. Staiger, A. M. Pietak, J. Huadmai, and G. Dias. Magnesium and its alloys as orthopedic biomaterials: A review. *Biomaterials*, 27(9):1728–1734, 2006.

[2] Y. Xin, T. Hu, and P. K. Chu. In vitro studies of biomedical magnesium alloys in a simulated physiological environment: A review. *Acta Biomaterialia*, 7(4):1452–1459, 2011.

[3] J. J. Jacobs, J. L. Gilbert, and R. M. Urban. Corrosion of metal orthopaedic implants. *J Bone Joint Surg Am*, 80(2):268–82, 1998.

[4] D. A. Puleo and W. W. Huh. Acute toxicity of metal ions in cultures of osteogenic cells derived from bone marrow stromal cells. *J Appl Biomater*, 6(2):109–16, 1995.

[5] C. Lhotka, T. Szekeres, I. Steffan, K. Zhuber, and K. Zweymller. Four-year study of cobalt and chromium blood levels in patients managed with two different metal-on-metal total hip replacements. *Journal of Orthopaedic Research*, 21(2):189–195, 2003.

[6] J. J. Jacobs, N. J. Hallab, A. K. Skipor, and R. M. Urban. Metal degradation products: a cause for concern in metal-metal bearings? *Clin Orthop Relat Res*, (417):139–47, 2003.

[7] J. J. Jacobs, A. K. Skipor, L. M. Patterson, N. J. Hallab, W. G. Paprosky, J. Black, and J. O. Galante. Metal release in patients who have had a primary total hip arthroplasty. a prospective, controlled, longitudinal study. *J Bone Joint Surg Am*, 80(10):1447–58, 1998.

[8] J. Nagels, M. Stokdijk, and P. M. Rozing. *Stress shielding and bone resorption in shoulder arthroplasty*, volume 12.

[9] J. B. Park and Y. K. Kim. Metallic biomaterials, in biomaterials. principles and applications,. *CRC Press: Boca Raton, FL, 2003*, 2003.

[10] T. Okuma. Magnesium and bone strength. *Nutrition*, 17(7-8):679–80, 2001.

[11] N. E. Saris, E. Mervaala, H. Karppanen, J. A. Khawaja, and A. Lewenstam. Magnesium. an update on physiological, clinical and analytical aspects. *Clin Chim Acta*, 294(1-2):1–26, 2000.

[12] J. Vormann. Magnesium: nutrition and metabolism. *Mol Aspects Med*, 24(1-3):27–37, 2003.

[13] F. Witte, V. Kaese, H. Haferkamp, E. Switzer, A. Meyer-Lindenberg, C. J. Wirth, and H. Windhagen. In vivo corrosion of four magnesium alloys and the associated bone response. *Biomaterials*, 26(17):3557–3563, 2005.

[14] E. McBride. Absorbable metal in bone surgery: A further report on the use of magnesium alloys. *Journal of the American Medical Association*, 111(27):2464–2467, 1938.

[15] C. P. McCord, J. J. Prendergast, S. F. Meek, and G. C. Harrold. Chemical gas gangrene from metallic magnesium. *Indust. Med*, pages 71–75, 1942.

[16] C. Liu, Y. Xin, G. Tang, and P. K. Chu. Influence of heat treatment on degradation behavior of bio-degradable die-cast az63 magnesium alloy in simulated body fluid. *Materials Science and Engineering: A*, 456(12):350–357, 2007.

[17] F. Witte, J. Fischer, J. Nellesen, H. Crostack, V. Kaese, A. Pisch, F. Beckmann, and H. Windhagen. In vitro and in vivo corrosion measurements of magnesium alloys. *Biomaterials*, 27(7):1013–1018, 2006.

[18] L. Li, J. Gao, and Y. Wang. Evaluation of cyto-toxicity and corrosion behavior of alkali-heat-treated magnesium in simulated body fluid. *Surface and Coatings Technology*, 185(1):92–98, 2004.

[19] K. Y. Chiu, M. H. Wong, F. T. Cheng, and H. C. Man. Characterization and corrosion studies of fluoride conversion coating on degradable mg implants. *Surface and Coatings Technology*, 202(3):590–598, 2007.

[20] G. Song. Control of biodegradation of biocompatable magnesium alloys. *Corrosion Science*, 49(4):1696–1701, 2007.

[21] F. Witte, N. Hort, C. Vogt, S. Cohen, K. U. Kainer, R. Willumeit, and F. Feyerabend. Degradable biomaterials based on magnesium corrosion. *Current Opinion in Solid State and Materials Science*, 12(56):63–72, 2008.

[22] Z. Wen, C. Wu, C. Dai, and F. Yang. Corrosion behaviors of mg and its alloys with different al contents in a modified simulated body fluid. *Journal of Alloys and Compounds*, 488(1):392–399, 2009.

[23] S. Zhang, X. Zhang, C. Zhao, J. Li, Y. Song, C. Xie, H. Tao, Y. Zhang, Y. He, Y. Jiang, and Y. Bian. Research on an mgzn alloy as a degradable biomaterial. *Acta Biomaterialia*, 6(2):626–640, 2010.

[24] Y. Gu, S. Bandopadhyay, C. Chen, C. Ning, and Y. Guo. Long-term corrosion inhibition mechanism of microarc oxidation coated AZ31 mg alloys for biomedical applications. *Materials and Design*, 46(0):66–75, 2013.

[25] T. S. N. Sankara-Narayanan, I. S. Park, and M. H. Lee. Strategies to improve the corrosion resistance of microarc oxidation (MAO) coated magnesium alloys for degradable implants: Prospects and challenges. *Progress in Materials Science*, 60(0):1–71, 2014.

[26] H. M. Wong, K. W. K. Yeung, K. O. Lam, V. Tam, P. K. Chu, K. D. K. Luk, and K. M. C. Cheung. A biodegradable polymer-based coating to control the performance of magnesium alloy orthopaedic implants. *Biomaterials*, 31(8):2084–2096, 2010.

[27] M. A. Gonzalez-Nunez, C. A. Nunez-Lopez, P. Skeldon, G. E. Thompson, H. Karimzadeh, P. Lyon, and T. E. Wilks. A non-chromate conversion coating for magnesium alloys and magnesium-based metal matrix composites. *Corrosion Science*, 37(11):1763–1772, 1995.

[28] Y. Mizutani, S. J. Kim, R. Ichino, and M. Okido. Anodizing of mg alloys in alkaline solutions. *Surface and Coatings Technology*, 169170(0):143–146, 2003.

[29] T. M. Yue, A. H. Wang, and H. C. Man. Improvement in the corrosion resistance of magnesium zk60sic composite by excimer laser surface treatment. *Scripta Materialia*, 38(2):191–198, 1997.

[30] Y. K. Lee, K. Lee, and T. Jung. Study on microarc oxidation of az31b magnesium alloy in alkaline metal silicate solution. *Electrochemistry Communications*, 10(11):1716–1719, 2008.

[31] A. L. Yerokhin, X. Nie, A. Leyland, A. Matthews, and S. J. Dowey. Plasma electrolysis for surface engineering. *Surface and Coatings Technology*, 122(23):73–93, 1999.

[32] G. Sundararajan and L. Rama-Krishna. Mechanisms underlying the formation of thick alumina coatings through the mao coating technology. *Surface and Coatings Technology*, 167(23):269–277, 2003.

[33] W. Xue, Z. Deng, R. Chen, and T. Zhang. Growth regularity of ceramic coatings formed by microarc oxidation on alcumg alloy. *Thin Solid Films*, 372(12):114–117, 2000.

[34] H. M. Wang, Z. H. Chen, and L. L. Li. Corrosion resistance and microstructure characteristics of plasma electrolytic oxidation coatings formed on AZ31 magnesium alloy. *Surface Engineering*, 26(5):385–391, 2010.

[35] P. B. Srinivasan, J. Liang, R. G. Balajeee, C. Blawert, M. Strmer, and W. Dietzel. Effect of pulse frequency on the microstructure, phase composition and corrosion performance of a phosphate-based plasma electrolytic oxidation coated AM50 magnesium alloy. *Applied Surface Science*, 256(12):3928–3935, 2010.

[36] L. Wang, L. Chen, Z. Yan, and W. Fu. Optical emission spectroscopy studies of discharge mechanism and plasma characteristics during plasma electrolytic oxidation of magnesium in different electrolytes. *Surface and Coatings Technology*, 205(6):1651–1658, 2010.

[37] T. Kokubo and H. Takadama. How useful is sbf in predicting in vivo bone bioactivity. *Biomaterials*, 27(15):2907–2915, 2006.

[38] Y. W. Song, D. Y. Shan, R. S. Chen, F. Zhang, and E. H. Han. Biodegradable behaviors of az31 magnesium alloy in simulated body fluid. *Materials Science and Engineering C-Biomimetic and Supramolecular Systems*, 29(3):1039–1045, 2009.

[39] Y. Wang, M. Wei, J. Gao, J. Hu, and Y. Zhang. Corrosion process of pure magnesium in simulated body fluid. *Materials Letters*, 62(14):2181–2184, 2008.

[40] M. Laleh, A. Sabour Rouhaghdam, T. Shahrabi, and A. Shanghi. Effect of alumina sol addition to micro-arc oxidation electrolyte on the properties of mao coatings formed on magnesium alloy AZ91D. *Journal of Alloys and Compounds*, 496(12):548–552, 2010.

[41] C. Liu, Q. Bi, A. Leyland, and A. Matthews. An electrochemical impedance spectroscopy study of the corrosion behaviour of pvd coated steels in 0.5 n nacl aqueous solution: Part ii.: Eis interpretation of corrosion behaviour. *Corrosion Science*, 45(6):1257–1273, 2003.

[42] D.A. Jones. *Principles and prevention of corrosion*. Prentice Hall, 1996.

[43] N. Dinodi and A. Nityananda-Shetty. Electrochemical investigations on the corrosion behaviour of magnesium alloy ze41 in a combined medium of chloride and sulphate. *Journal of Magnesium and Alloys*, 1(3):201–209, 2013.

[44] R. Ambat, N. N. Aung, and W. Zhou. Studies on the influence of chloride ion and ph on the corrosion and electrochemical behaviour of az91d magnesium alloy. *Journal of Applied Electrochemistry*, 30(7):865–874, 2000.

[45] S. H. Ahn, J. H. Lee, H. G. Kim, and J. G. Kim. A study on the quantitative determination of through-coating porosity in pvd-grown coatings. *Applied Surface Science*, 233(14):105–114, 2004.

[46] A. Ghasemi, V. S. Raja, C. Blawert, W. Dietzel, and K. U. Kainer. Study of the structure and corrosion behavior of peo coatings on am50 magnesium alloy by electrochemical impedance spectroscopy. *Surface and Coatings Technology*, 202(15):3513–3518, 2008.

[47] J. Liang, P. Bala Srinivasan, C. Blawert, M. Strmer, and W. Dietzel. Electrochemical corrosion behaviour of plasma electrolytic oxidation coatings on am50 magnesium alloy formed in silicate and phosphate based electrolytes. *Electrochimica Acta*, 54(14):3842–3850, 2009.

[48] C. Liu, Q. Bi, A. Leyland, and A. Matthews. An electrochemical impedance spectroscopy study of the corrosion behaviour of pvd coated steels in 0.5 n nacl aqueous solution: Part ii.: Eis interpretation of corrosion behaviour. *Corrosion Science*, 45(6):1257–1273, 2003.

[49] W. Lee and S. Pyun. Role of prior cathodic polarization in the pitting corrosion of pure aluminium in acidic chloride solution. *Materials Science and Engineering: A*, 279(12):130–137, 2000.

[50] Y. Xin, C. Liu, X. Zhang, G. Tang, X. Tian, and P. K. Chu. Corrosion behavior of biomedical AZ91 magnesium alloy in simulated body fluids. *Journal of Materials Research*, 22(07):2004–2011, 2007.

[51] L. Xu, G. Yu, E. Zhang, F. Pan, and K. Yang. In vivo corrosion behavior of mg-mn-zn alloy for bone implant application. *Journal of Biomedical Materials Research Part A*, 83A(3):703–711, 2007.

[52] M. Carboneras, M. C. Garca-Alonso, and M. L. Escudero. Biodegradation kinetics of modified magnesium-based materials in cell culture medium. *Corrosion Science*, 53(4):1433–1439, 2011.

[53] W. D. Mueller, M. F. de Mele, M. L. Nascimento, and M. Zeddies. Degradation of magnesium and its alloys: dependence on the composition of the synthetic biological media. *J Biomed Mater Res A*, 90(2):487–95, 2009.

[54] Y. Xin, K. Huo, H. Tao, G. Tang, and P. K. Chu. Influence of aggressive ions on the degradation behavior of biomedical magnesium alloy in physiological environment. *Acta Biomater*, 4(6):2008–15, 2008.

[55] R. Ambat, N. N. Aung, and W. Zhou. Evaluation of microstructural effects on corrosion behaviour of AZ91D magnesium alloy. *Corrosion Science*, 42(8):1433–1455, 2000.

[56] M. Marya, L. G. Hector, R. Verma, and W. Tong. Microstructural effects of az31 magnesium alloy on its tensile deformation and failure behaviors. *Materials Science and Engineering: A*, 418(12):341–356, 2006.

[57] K. B. Deshpande. Numerical modeling of micro-galvanic corrosion. *Electrochimica Acta*, 56, 2011.

[58] COMSOL Multiphysics 4.3b. Localized corrosion. 2013.

[59] Y. H. Gu, S. Bandopadhyay, C. F. Chen, Y. J. Guo, and C. Y. Ning. Effect of oxidation time on the corrosion behavior of micro-arc oxidation produced AZ31 magnesium alloys in simulated body fluid. *Journal of Alloys and Compounds*, 543:109–117, 2003.